Universidade de Aveiro Departamento de Ciências Médicas
2021

ANDRÉ RICARDO BARBOSA GÓIS

Remodelação do lipidoma de células epiteliais mamárias pela SETD7 e a sua significância para cancro da mama: abordagem lipidómica

Remodeling of the mammary epithelial cell lipidome by SETD7 and its significance to breast cancer: a lipidomic approach

Universidade de Aveiro Departamento de Ciências Médicas
2021

ANDRÉ RICARDO BARBOSA GÓIS

Remodelação do lipidoma de células epiteliais mamárias pela SETD7 e a sua significância para cancro da mama: abordagem lipidómica

Remodeling of the mammary epithelial cell lipidome by SETD7 and its significance to breast cancer: a lipidomic approach

Dissertação apresentada à Universidade de Aveiro para cumprimento dos requisitos necessários à obtenção do grau de Mestre em Biomedicina Molecular, realizada sob a orientação científica da Professora Doutora Luisa Helguero, Professora Auxiliar do Departamento de Ciências Médicas da Universidade de Aveiro, e coorientação da Professora Doutora Maria do Rosário Domingues, Professora Associada com agregação do Departamento de Química da Universidade de Aveiro.

This work was supported by iBiMED research unit through national funds: UIDB/04501/2020, UIDP/04501/2020; MEDISIS (CENTRO-01-0246-FEDER-000018) supported by Comissão de Coordenação e Desenvolvimento Regional do Centro; Bolsa de Investigação em Oncologia Dr. Rocha Alves 2020 by Liga Portuguesa contra o Cancro - Núcleo Regional do Centro.

Dedico este trabalho aos meus pais e à minha Maria pelo amor e apoio incondicionais.

o júri

presidente

Professora Doutora Ana Margarida Domingos Tavares de Sousa
Professora Auxiliar em Regime Laboral do Departamento de Ciências Médicas da Universidade de Aveiro

vogal

Doutora Maria Luísa Mouta Faria Lima Dória
Investigadora (Metabolista) na Bial

vogal

Professora Doutora Luisa Alejandra Helguero
Professora Auxiliar do Departamento de Ciências Médicas da Universidade de Aveiro

agradecimentos

Gostaria de expressar a minha gratidão às minhas orientadoras, Professora Doutora Luisa Helguero e Professora Doutora Rosário Domingues, não só pela orientação científica, pelo acompanhamento, pela disponibilidade e pelo seu profundo conhecimento, que me permitiu ver muitas vezes a luz quando nada parecia fazer sentido, mas pela paciência, pela compreensão, pelo apoio moral e pelo esforço que fizeram desde o primeiro dia para me integrar nos seus grupos de trabalho, e por proporcionarem as condições para tornar possível este trabalho.

Agradeço também à Liliana Monteiro, pela paciência interminável, pelas horas que dedicou a dar-me as ferramentas necessárias para que pudesse desenvolver o meu trabalho de forma autónoma, pela disponibilidade constante, por toda a colaboração, por todas as conversas e pela amizade.

Agradeço ainda a todo o grupo do Laboratório de Lipidómica, pelo espírito de cooperação e por todo o apoio. Agradeço em particular à Doutora Tânia Melo pelo esclarecimento das minhas infindáveis dúvidas, pelo acompanhamento e presença, e ao Tiago Conde e à Bruna Neves pelo acompanhamento desde o primeiro dia. À Inês Guerra, à Joana Fernandes, à Diana Lopes e a todos os restantes membros do grupo que tantas vezes me apoiaram, o meu muito obrigado. Foram muitas vezes a diferença para o sucesso de cada etapa do meu trabalho.

Por fim, agradeço à minha família e amigos pelo amor, apoio, carinho, pelo orgulho que têm em mim e por motivarem cada passo da minha vida.

palavras-chave

Diferenciação, glândula mamária, lípidos, metabolismo, SET7, cancro da mama, lipidómica, fosfolipidoma, LC-MS

resumo

Lípidos são componentes estruturais das membranas celulares e importantes mediadores de sinalização. A composição lipídica da membrana celular determina a sua fluidez, e consequentemente, o seu potencial proliferativo, migratório e secretor. Quando a lactação é induzida na glândula mamária, células epiteliais mamárias diferenciam-se e adquirem uma função secretora. Como tal, o seu lipidoma acompanha esta transição, a fim de suportar as necessidades lipídicas da lactação. Sabe-se que o lipidoma de células de cancro da mama com um prognóstico da doença mais negativo é semelhante àquele apresentado por células epiteliais mamárias proliferativas e indiferenciadas. Assim, é imperativo estudar os mecanismos que controlam o metabolismo lipídico nestas células, e os fatores envolvidos na transição do fenótipo lipídico de um estádio proliferativo para um diferenciado e funcional. A SETD7 é uma metiltransferase que modula a expressão de vários fatores de transcrição relacionados com processos biológicos de relevância para o cancro, incluído a proliferação celular e remodelação da cromatina. Resultados anteriores demonstraram que a inibição da SETD7 em células epiteliais mamárias HC11 levou a um fenótipo anormal em células diferenciadas, semelhante ao apresentado por células indiferenciadas, sugerindo assim um papel da SETD7 na diferenciação epitelial. Sabe-se que a SETD7 atua sobre alguns dos reguladores principais do metabolismo lipídico, como XBP1 e RORα2. Assim, neste estudo, foi inibida a atividade da SETD7 em células HC11, a fim de estudar o efeito desta inibição no lipidoma, e relacioná-lo com as alterações sofridas ao longo da diferenciação. Foram aplicadas espectrometria de massa e cromatografia em camada fina para avaliar o lipidoma destas células. Uma redução na quantidade de fosfatidilcolina, e promoção da síntese de fosfatidiletanolamina, e de ácidos gordos mais longos e insaturados, foram alterações observadas durante a diferenciação, a fim de facilitar a função secretora. Estas adaptações pareceram ser prejudicadas pela inibição de SETD7. Esta inibição levou a um perfil lipídico sugestivo de um maior potencial proliferativo, característico de células indiferenciadas e cancerígenas com potencial metastático. Quando combinados com observações anteriores, estes resultados sugerem que a SETD7 não só tem uma importante função moduladora na diferenciação de células epiteliais mamárias, mas que a sua atividade é importante para a homeostasia lipídica, e adaptação às necessidades da lactação.

Keywords Differentiation, mammary gland, lipids, metabolism, SETD7, breast cancer, lipidomics, phospholipidome, LC-MS

abstract

Lipids are structural components of cell membranes, as well as important signaling mediators. The membrane's lipid composition dictates its fluidity, and consequently the cell's proliferative, migratory, and secretory potential. When lactation is induced on the mammary gland, mammary epithelial cells differentiate into a specialized secretory state, and their lipidome accompanies this transition, to cope with the increased lipidic demand for lactation. It has been reported that the lipidome of breast cancer cells with a worse disease prognosis is resemblant to that of proliferative undifferentiated mammary epithelial cells. Therefore, it is imperative to study the mechanisms controlling the lipid metabolism on these cells and the factors involved in the transition from a proliferative to a functionally differentiated lipidomic phenotype. SETD7 is a methyltransferase that modulates the expression of several transcription factors related to biological processes with relevance for cancer, including cell proliferation and chromatin remodelling. Previous results showed that inhibition of SETD7 on HC11 mammary epithelial cells led to an abnormal phenotype on differentiated cells, resembling that of undifferentiated cells, suggesting a role for SETD7 in epithelial differentiation as well. SETD7 is also known to target key players of lipid metabolism like XBP1 and RORα2. In this study, we inhibited the activity of SETD7 on HC11 mammary epithelial cells to study the effect of this shut down on the lipidome and relate the differences to the profile presented during differentiation. Mass spectrometry and thin-layer chromatography were used to study the lipidome of these cells. A decrease in phosphatidylcholine and synthesis of phosphatidylethanolamine, longer and more unsaturated fatty acids, are observed during differentiation to facilitate secretion. These adaptations seemed to be impaired by the inhibition of SETD7. This inhibition led to a lipid profile suggestive of higher proliferative potential, characteristic of undifferentiated cells and cancer cells with metastatic potential. In sum, when combined with previous observations, these results suggest not only that SETD7 has an important modulating role in the differentiation of MEC, but that its activity is important for lipid homeostasis and the adaptation to the demands of lactation.

Contents

List of Figures

List of Tables

List of Abbreviations, symbols and acronyms

Acox1/3	Acyl-Coa Oxidase 1/3
AKT1	RAC-Alpha Serine/Threonine-Protein Kinase
ANOVA	Analysis of Variance
ARA	Arachidonic Acid
BC	Breast Cancer
C/Ebpβ	CCAAT Enhancer Binding Protein Beta
Cdipt	CDP-Diacylglycerol-Inositol 3-Phosphatidyltransferase
CDP	Cytidine Diphosphate
CDP-DG	Cytidine Diphosphate Diacylglycerol
Cds1	CDP-Diacylglycerol Synthase 1
Chka	Choline Kinase Alpha
Chpt1	Choline Phosphotransferase 1
CL	Cardiolipins
Crls1	Cardiolipin Synthase 1
Csn2	Casein Beta
CTE-1	Acyl-Coa Thioesterase 1
DESI	Desorption Electrospray Ionization
Dgat2	Diacylglycerol O-Acyltransferase 2
DIF	Differentiated Cells
DMSO	Dimethyl Sulfoxide
EGF	Epidermal Growth Factor
EGFR	Epidermal Growth Factor Receptor
Elovl5/6	Elongation of Very Long Chain Fatty Acids Protein 5/6
EMT	Epithelial-Mesenchymal Transition
ER	Endoplasmic Reticulum
Erα	Estrogen Receptor Alpha
Etnk1	Ethanolamine Kinase 1
Fads1	Fatty Acid Desaturase 1

Fames	Fatty Acid Methyl-Esters
FASN	Fatty Acid Synthase
Gpdl1	Glycerophosphodiester Phosphodiesterase
HDAC3	Histone Deacetylase 3
HILIC	Hydrophilic Interaction Liquid Chromatography
IC_{50}	Half Maximal Inhibitory Concentration
Jak/Stat	Janus Kinase/Signal Transducer and Activator of Transcription
LD	Lipid Droplet
LXR/RXR	Liver X Receptor/Retinoid X Receptor
MALDI	Matrix Assisted Laser Desorption Ionization
MAPK	Mitogen-Activated Protein Kinase
Mecs	Mammary Epithelial Cells
MPIS	Multiple Precursor Ion Scanning
NF-Kb	Nuclear Factor Kappa-Light-Chain-Enhancer Of Activated B Cells
P53	Tumor Protein P53
PC	Phosphatidylcholine
PCA	Principal Component Analysis
Pcyt2	Phosphate Cytidylyltransferase 2, Ethanolamine
PD	Pre-Differentiated Cells
PE	Phosphatidylethanolamine
PG	Phosphatidylglycerol
Pgs1	Phosphatidylglycerophosphate Synthase 1
PI	Phosphatidylinositol
PI3K	Phosphoinositide 3-Kinases
PIP_2	Phosphatidylinositol 4,5-Bisphosphate
PL	Phospholipids
PLA2	Phospholipase A2
PLS-DA	Partial-Least Squares Discriminant Analysis
PPAR	Peroxisome Proliferator-Activated Receptor

PRLR	Prolactin Receptor
PS	Phosphatidylserine
Ptdss1	Phosphatidylserine Synthase 1
Rorα2	Retinoid Acid-Related Orphan Receptor A
Scd1	Stearoyl-Coa Desaturase-1
Sgms2	Sphingomyelin Synthase 2
SLC	Stem-Like Cells
Smad	Mothers Against Decapentaplegic Homolog
SREBP-1c	Sterol Regulatory Element-Binding Protein 1
STAT3/5	Signal Transducers and Activators Of Transcription 3/5
TAG	Triacylglycerol
TEII	Thioesterase
TGF-B	Transforming Growth Factor Beta
TLC	Thin Layer Chromatography
UHPLC	Ultra High-Performance Liquid Chromatography
UPR	Unfolded Protein Response
Wap	Whey Acidic Protein
XBP1	X-Box-Binding Protein 1

1 Introduction

1.1 Development of the Mammary Gland

The mammary gland epithelium is composed of two main cellular lineages. Luminal cells form the lumen of the gland's ducts and myoepithelial cells lying along the basement membrane. These two cell types establish a branching ductal tree which connects to the many secretory alveoli, during pregnancy. A stromal matrix composed by endothelial cells, adipocytes, fibroblasts, and immune cells surrounds this tree-like structure. Different stimuli, mainly systemic endocrine signals brought up by the menstrual and reproductive cycles throughout the lifetime of a female, lead to profound changes on the architecture of the mammary gland tissue [1,2]. In the mouse embryo, mammary buds develop from placodes and penetrate the mesenchyme, to later establish a lumen, arborize and grow into the maturing fat pad[2]. Significant changes occur again during puberty, where estrogen, progesterone and prolactin induce branching and development of alveoli on the tips of the mammary ducts[3]. During pregnancy and lactation, prolactin induces functional differentiation and thus the secretory state, after which the gland undergoes involution[4]. Usually, prolactin in circulation is synthesized on the adenohypophysis. However, in the mammary gland, prolactin is produced by mammary epithelial cells and exerts its action mainly as an autocrine/paracrine effect. Prolactin synergizes with estrogen and progesterone to promote growth and differentiation of the alveoli[3] and regulates the ovarian production of progesterone during pregnancy as well[5]. In the mammary alveolar cells, prolactin binds to the prolactin receptor (PRLR), a class I cytokine receptor, activating multiple signalling cascades: MAPK, PI3K and Jak/Stat. Activation of STAT5 leads to the expression of milk protein genes Csn2 and Wap[5]. Given the dynamic nature and continuous remodelling of the mammary tissue, the research on mammary gland development has included the study of mechanisms regulating cell differentiation, branching morphogenesis, development of polarity and involution of the gland[1]. Interestingly, dysregulated mechanisms observed in breast cancer (BC) progression often resemble those occurring during the normal development of the mammary gland[1].

Early pregnancy and breastfeeding are protective factors against the development of hormone responsive BC. This effect is attributed to the decrease on circulating hormones, particularly estrogen, and the increased differentiation state of epithelial cells[6]. Another

central aspect in the development of BC is the involvement of stem cells, which are unspecialized cells with the ability to self-renew virtually unlimitedly and to differentiate into multiple cell types within a tissue[6,7]. The presence of a population of stem cells within the mammary gland is responsible for the dynamism involved on the proliferation and differentiation of mammary epithelial cells (MECs), and the ability to renew alveoli and regenerate the gland with each successive cycle of pregnancy[7,8]. These undifferentiated estrogen receptor–negative mammary stem cells give rise to myoepithelial progenitor cells, which then differentiate into myoepithelial cells, and luminal progenitors which originate alveolar and ductal cells[9]. Considering this, it is clear how important these cells are in the development of the mammary gland. However, in previous studies comparing the transcriptome of these stem cells and that of specific subtypes of BC, it was reported that BC subtypes with a gene expression profile more closely related to that of stem-like cells yield a more aggressive cancer[8,10,11]. Additionally, lineage regulators that maintain the normal activity of stem or progenitor cells are usually abnormally enhanced in tumor cells and thus increase tumor plasticity and metastasis. Also, factors which promote differentiation are downregulated, leading to a stem-like cell profile, promoting tumours' progression[10,12]. Thus, studying these stem cells as well as understanding their similarities to cancer cells becomes quite relevant considering this connexion.

HC11 cells are an epithelial cell line with origin on mid-pregnancy BALB/c mice which closely resemble stem cells[8]. These cells possess the ability to self-renew and to differentiate into a functional state and secrete milk proteins *in vitro*, and are able to reconstitute the mammary gland *in vivo*[8]. The gene expression profile of HC11 mammary stem-like cells overlapped with that of breast tumours with poor prognosis, which is according to previous observations[8,13].

1.2 Lipids and the cell membrane

Lipids are molecules typically characterized as poorly soluble in aqueous environments, and their biological function varies according to their structure. Fatty acids, oxidized in the mitochondria for energy production, are stored and transported as triglycerides and esterified phospholipids, the main structural components of cellular membranes[14]. Lipids also mediate

signalling between cells and within them. Cholesterol, another membrane component, can be converted into steroid hormones and other bioactive lipids important for cell signalling, as well as the fat-soluble vitamins A, D, E and K[14]. Lipids also have important roles as enzyme cofactors, hydrophobic anchors of proteins, emulsifying agents and electron carriers[15]. Overall, most lipids can be classified as storage, structural or signalling lipids.

Storage lipids are mostly comprised of fatty acids, ranging from 12 to 24 carbon chains, frequently with *cis* double bonds. Three fatty acids can assemble into triacylglycerols by an esterification reaction with the hydroxyl groups of a glycerol molecule[15].

Structural lipids, contrarily, are usually polar. The most abundant are glycerophospholipids, the main components of membranes, which are formed by two fatty acids esterified to two hydroxyl groups of glycerol, and a head group, esterified to the remaining hydroxyl of glycerol via a phosphodiester bond[15]. This head group is variable and determines the class of the phospholipid. Phosphatidylethanolamine (PE), phosphatidylcholine (PC), phosphatidylinositol (PI), phosphatidylglycerol (PG) and phosphatidylserine (PS) are phospholipid classes characterized by specific head groups. This group bears charge which is dependent on the pH, and these charges contribute to the surface properties of membranes. In cardiolipins (CL), a phospholipid specific of mitochondria, two phosphatidic acids are linked to a single glycerol and thus CL have 4 acyl chains. Therefore, at pH 7, cardiolipins bear a double negative net charge. An ether linkage may also connect the acyl chain to glycerol, instead of the ester bond, giving rise to an ether-lipid. These can be either plasmanyl- or plasmenyl-phospholipids, depending on whether the ether bond in position sn-1 of glycerol connects to an alkyl (prefix O-) or an alkenyl (prefix P-) group, respectively. These ether lipids are mainly found in PC and PE classes. Sphingolipids are another group of lipids which contain no glycerol, but contain a sphingosine backbone, a long-chain aliphatic amino alcohol[15]. Sphingomyelin contains a phosphoric acid moiety, a choline group and two hydrocarbon chains, one from the sphingosine and another from a fatty acid. Other sphingolipids may contain sugar moieties, such as gangliosides and cerebrosides. Ceramides are sphingolipids containing a sphingosine with a fatty acyl chain, and no head group. Finally, sterols have four rings and a hydroxyl group, and are structural components of membranes as well as precursors of a wide range of signalling molecules, such as steroids. They can be found free or esterified to a fatty acid.

Lipids that act as signalling molecules or as cofactors are usually present in smaller amounts. However, these play crucial roles in several mechanisms. An important lipid signalling molecule is PI4,5-biphosphate (PIP_2), that can be hydrolysed to yield diacylglycerol and inositol 1,4,5-triphosphate, both central intracellular messengers, with the latter being a crucial nucleation point for the formation of supramolecular protein complexes involved in signalling[15]. Fatty acids esterified to PL can also be hydrolysed by PLA2 and released, such as arachidonic acid (C20:4 ω6). This fatty acid is a precursor of prostaglandins, thromboxanes and leukotrienes, which are important hormones and players in inflammation. Steroid hormones, oxidized derivatives from sterols, are also powerful signalling molecules which trigger responses even at very low concentrations, such is the case of the sex hormones[15].

Lipids and proteins compose the membranes of cells, defining their spatial identity and separating intracellular from extracellular spaces. Amphipathicity drives the organization of lipids into a bilayered structure, with hydrophobic moieties self-associating and hydrophilic moieties interacting with the surrounding aqueous environments. Most organelles themselves are surrounded by membranes, structured under a similar architecture, and all of these assure signalling and the compartmentalization of biological processes. Approximately one third of the genome encodes membrane proteins, while many others interact with this structure directly during their lifetime[16], which reflects the major importance of cell membranes. This extremely dynamic structure is dependent on its lipid constitution, as the shape of lipid molecules determines the form of the overall supramolecular structure. For instance, PC (cylindrical molecular shape), assemble stable flat bilayers under physiological conditions, while other phospholipids like PE and PS (conic) or lyso-PC (LPC, inverted conic shape) destabilize them to favour membrane bending and contribute to the morphological plasticity of the lipid bilayer [16–18]. So, the ratio between differently shaped phospholipids dictates the membrane curvature and thus cell morphology[17]. The acyl chain length, however, determines the membrane rigidity and thickness, and the number of *cis* double bonds reduces phospholipid rotation and movement, as well as increases polarity[17]. Additionally, specific classes such as sphingolipids contribute to the formation of microdomains, presenting thus a functional role, rather than a structural one[17].

The synthesis of glycerophospholipids (Figure 1) occurs among the endoplasmic reticulum (ER), the mitochondria and the Golgi apparatus. Glycerol-3-P is the main precursor of this

synthetic pathway, which is turned into phosphatidic acid (PA) in the ER, before being turned into diacylglycerol or CDP-diacylglycerol. The latter is then used to form PI (and phosphoinositides), PG and CL. Diacylglycerol is converted into PC or PE, which can both be used to produce PS. These three PL classes are interconvertible, since PE can be turned into PC, PC into PS, and PS into PE. Ceramides are also synthesized in the ER from palmitate, serine residues and acylCoA. These can be turned into SM in the Golgi lumen, or HexCer in the ER or the cytosolic side of the Golgi apparatus, depending on the sugar moiety that is coupled to the ceramide[19]. The composition of the cell membrane dictates its characteristics. Curvature of the membrane depends on the sizes of polar head groups and phospholipid's nonpolar tails. Longer tails and larger head groups form a cylindrical shape, and smaller head groups are cone shaped. Therefore, bilayers of cylindrical phospholipids are flatter, while those composed by cone-shaped lipids form curved structures. This curvature determines the formation of membrane blebs and pits, membrane vesicles and other structures[14].

The cell membrane is more than an inert envelope that surrounds the contents of the cell. It is highly dynamic, and its plasticity allows it to perform vital functional tasks, including the transport of ions, small molecules, proteins, and other soluble macromolecules from the extracellular milieu. This inwards transport happens via endocytosis, in which an invagination of the plasma membrane occurs, surrounding the extracellular molecule and delivering it to its intracellular destination[14]. Some membrane components are recycled back to the membrane, while others are transported to other structures inside the cell in a continuous flow of membrane components between all bilayer structures inside the cell. Other integral membrane proteins, like integrins and cadherins, are dependent on the membrane fluidity and therefore on its composition. Cell migration and cell-cell adhesion are mediated by cadherines[14], while integrins modulate adhesive interactions and serve as cell signalling receptors, mediating interactions between the extracellular environment and the actin cytoskeleton which allow cell migration[14].

In sum, the cell membrane is a very dynamic structure, crucial to the maintenance of homeostasis, transport, signalling and motility of cells. Its biochemical properties depend on its lipid composition and their interaction with the membrane proteins. These conditions are then adapted and combined according to the functions or needs of the cell. Secretory function, for instance, is facilitated by a more fluid membrane. In MECs, this takes place

upon lactation, through the secretion of milk fat globules. These structures are formed in the ER, through the release of triacylglyceride droplets, which are surrounded by a single layer of ER phospholipids. The globule then migrates to the apical pole of the cell, fuses with the cell membrane, and is released into the alveolar lumen via pinocytosis. Almost 1/3 of this portion of the cell membrane surrounding the globule consists of glycerophospholipids[20]. Considering the vast amount of lipids necessary for lactation, it is predictable that the metabolic framework of MECs must adapt to cope with lipid biosynthesis and secretory demands.

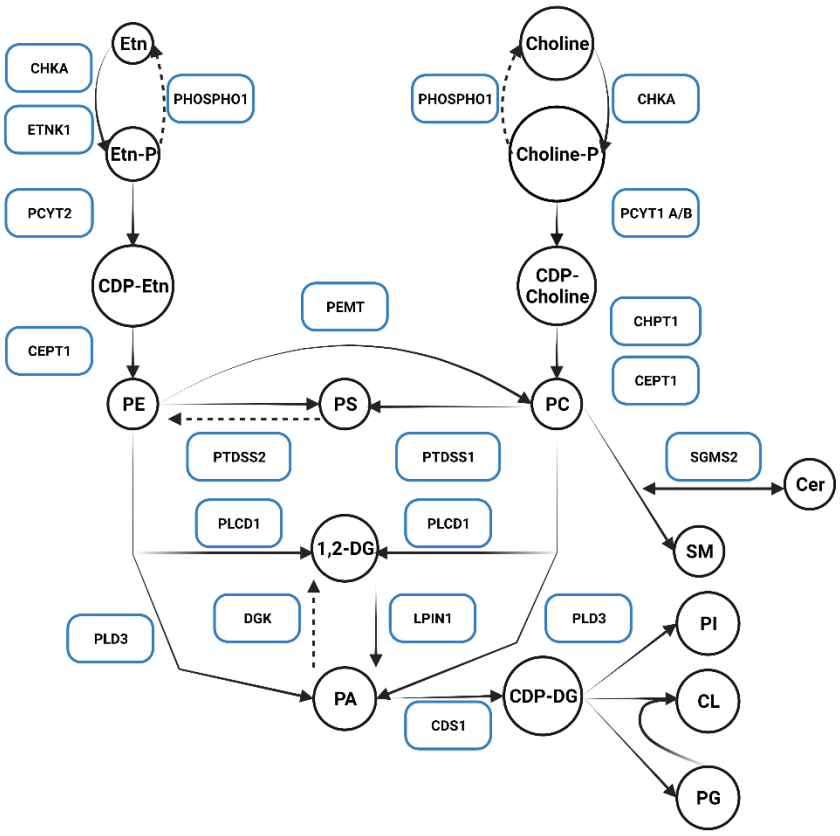

Figure 1. Schematic representation of phospholipid biosynthetic pathways regulated in HC11 cell differentiation. Etn, ethanolamine; Chka, choline kinase; Etnk1, ethanolamine kinase 1; Pcyt2, phosphate cytidylyltransferase 2, ethanolamine; Pcyt1A/B, phosphate cytidylyltransferase 1, choline isoform; Cept1, transcript variant 2, choline/ethanolaminephosphotransferase 1; Chpt1, choline phosphotransferase 1; Pemt, phosphatidylethanolamine N-methyltransferase; Ptdss1, phosphatidylserine synthase 1; Ptdss2, phosphatidylserine synthase 2; Smgs2, phosphatidylcholine:ceramide cholinephosphotransferase 2; Plcd1, phospholipase 1; Plcd3, phospholipase D3; Lpin1, phosphatidate phosphatase; Dgk, diacylglycerol kinase; Gpd1l, glycerol-3-phosphate dehydrogenase 1-like; Cds1, CDP-diacylglycerol synthase 1. Black circles, lipid classes/intermediate molecules; Blue boxes, enzymes from the

phospholipid biosynthetic pathway, responsible for the catalysation of the step represented by the corresponding black arrow. (Adapted from Kyoto Encyclopedia of Genes and Genomes (KEGG) and Dória et al.[17])

1.3 Lipid metabolism on the mammary gland

Several metabolomic changes occur in the mammary gland during the transition between pregnancy and lactation, which is triggered by a drop in progesterone levels. In mice, this happens with a sharp decrease at the 18th day of pregnancy while in humans the progesterone level decreases approximately 10-fold during the first 4 days after birth[21,22]. To cope with the large demand of lipids for lactation and for the maintenance of apical-basal polarity, an adaptation and integration of PL and FA synthesis and transport is necessary[23]. During lactation, the endoplasmic reticulum and Golgi expand with alveolar cell differentiation, in line with the changes in phospholipid synthesis and unidirectional transport[23]. The secretion of lipids occurs through lipid droplets, that is, envelopment of the secreted substances with a coating derived from the cell membrane[24]. In this period, the RNA expression of glucose, amino acid and fatty acid membrane transporters is significantly upregulated. Lactose synthesis is increased through the rise in RNA levels of the cofactor α-lactalbumin. Fatty acid synthesis is also increased, likely following an increase in the activity of the transcription factor that regulates lipid biosynthesis, SREBP-1c. AKT1, STAT5a, STAT5b, SREBP-1c and C/EBPβ regulate lactose and lipid synthesis, while PPAR, LXRβ, and fatty acids generated by CTE-1 act as inhibitors[22].

In humans, all aspects of lipid metabolism and milk fatty acid production increase immediately postpartum, including de novo FA synthesis, elongation, and desaturation[25]. Accordingly, the mammary gland comprises one of the three sources of FA for milk triglycerides, along with maternal fat stores and maternal dietary lipids. During secretory activation, the expression of rate-limiting enzymes ACACA and FASN is upregulated. The expression of genes from the TCA cycle, responsible for the supply of substrates for FA synthesis is increased at this stage as well. It is noteworthy that the mammary gland synthesizes shorter FA, with a length of 8-16 carbons, due to activity of a unique enzyme, TEII, present in MECs[25]. Milk from mice contains 15-40% of these medium-chain fatty acids, depending on diet and strain[26]. Furthermore, it was shown in a previous study that the deletion of FASN not only negatively affects the FA content of milk, but also induces

premature involution and lack of functional competence on the lactating mammary gland, suggesting FA synthesis is required for normal mammary cell development during lactation, and not only milk production[27]. The 2014 study by Dória *et al.* reported the changes to the lipid metabolism with lactogenic differentiation in HC11 mammary epithelial cell lines[17]. It was found that an increase in fatty acid elongases and desaturases occurred, as well as an increase in PE during differentiation, thus increasing the cylindrical/conic-shaped PL ratio and membrane fluidity, which can be related to the secretory activity in the lactating gland. Fatty acyl chains on PL increased length and saturation, due to the increased activity of enzymes from FA-synthetic pathways, and the regulation of sphingolipid metabolism also varied according to the proliferative and migratory characteristic[17].

1.4 Lipidomics of Breast Cancer cells

In Portugal alone, from a population of 5 million women, 7,000 new cases of BC (BC) were registered, and 1,800 women died with this disease in 2020[28]. Given the struggle with lowering the prevalence of risk factors for BC, a secondary approach based on preventive diagnosis and medical screening is being developed[28]. In this sense, better knowledge regarding processes related to the biology of normal mammary cells and their relation to BC development is always helpful to build solid diagnostic tools and prevent disease progression.

Inhibition of apoptosis, cell proliferation and the acquisition of invasive ability are hallmarks of tumor development and progression. These processes involve functional and morphological changes that occur in the cell membrane[29]. Furthermore, cellular biomembranes have a critical role on signalling, and thus on the regulation of cellular functions as well[30]. Phospholipids, as primary constituents of these structures, have an inherent influence on this interplay. As discussed previously, the changes on the lipid environment determine membrane fluidity and the availability of membrane-bound proteins, as well as cell polarity[29]. Accordingly, previous studies from our group have identified differences in the relative level of phospholipid classes from mammary epithelial cell lines compared with BC cell lines with different levels of aggressiveness (metastatic and not metastatic) [30]. Lower PC and higher LPC levels were observed in more aggressive BC cells.

SM were more abundant on cancer cells, and PS were relatively constant among non-malignant mammary epithelial and BC cells. Additionally, PI containing saturated fatty acid chains were found to be increased in BC cells when compared with epithelial cells, which presented unsaturated fatty acid chains. On the contrary, C20 fatty acids were lower in BC cells[30]. Other results pointed to a possible association between alkylacyl PC species and malignant progression, and variations on the profile of certain PI species were reported on cancer cells, specifically the lower ratio of PI(20:3/18:0), the most abundant species in this class, and PI(18:0/18:1)[29]. Differences in lipid species were reported between non cancer mammary and BC cells (decrease in PC(14:0/18:1-16:0/16:1), PI(16:0/18:1-16:1/18:0) and PI(18:0/18:1)), between metastatic and non-metastatic BC cells (increased PC(O-16:0/18:1), PC(O-16:0/20:1) and PI(22:5/18:0)) and between cells with migratory potential and epithelial cells (epithelial cells presented lower PC(18:0/18:1), SM(18:1/24:0), SM(18:1/22:0), SM(18:1/24:1), CL(18:1/18:2/18:2/20:3-18:2/18:2/18:2/20:2), increased PE(16:1/18:0-16:0/18:1) and (18:1/18:1-18:0/18:2), and CL(16:1/18:1/18:1/18:2)[29]. Shorter and more saturated aliphatic PC and SM chains were also associated with a less migratory profile in human cells[29].

1.5 SETD7 and its role in breast cancer and the lipidome

The methyltransferase SETD7 (Su(var)3-9, Enhancer of zeste and Trithorax Domain-containing 7) is canonically responsible for the monomethylation of the Lys-4 residue of the H3 histone (and is thus classified as an H3-K4-HMTase). It is therefore known to be involved on the regulation of gene expression through epigenetic modulation[31,32]. Additionally, its SET domain is responsible for the transfer of a methyl group to a lysine residue of not only histone H3 but also numerous non histone substrates. Accordingly, SETD7 has been found to influence the regulation of the cell cycle, processes related to cellular differentiation, repairing of DNA, gene transcription, chromatin modulation and cellular proliferation[31–34], as well as pro-inflammatory regulation and mitochondrial function[35]. For instance, the expression of SETD7 increases throughout cardiomyocyte lineage commitment[32,36] and during the differentiation of human embryonic stem cells[37,38], due to its canonical methyltransferase activity and role in chromatin remodelling. Studies have identified a role

for SETD7 in a wide variety of signalling pathways, including those regulated by transcription factors NF-κB, p53, STAT3 and ERα[31,39].

Research on the transcription of genes dependent on SETD7 activity and mechanisms of regulation is important considering its role in pathological processes related to cancer, diabetes, inflammatory diseases or mental illnesses[31]. Its selective inhibition with (R)-PFI-2 is a common approach to perform studies aiming to understand SETD7 role[39], and was applied in the present work. (R)-PFI-2 exhibits a cofactor-dependent (S-adenosylmethionine) and substrate-competitive inhibitory mechanism, through which it occupies the SETD7 substrate binding groove, and directly contacts the cofactor's donor methyl group[39]. It has been shown to be highly selective in nM concentrations, with an IC_{50} value of 2.0 ± 0.2 nM[39].

Different studies in BC have proposed that SETD7 may either stimulate or inhibit both differentiation and proliferation, depending on the active signalling pathways, type of tissue and pathological condition at any given moment[31]. Therefore, the molecular environment and physiological context may determine its role. A study showed that SETD7 inhibited epithelial to mesenchymal transition (EMT) of metastatic BC cells, through down-regulation of Vimentin and EGFR and up-regulation of cadherin-1[40]. In another BC cell line, SETD7 knock-down led to the dedifferentiation of mammospheres (discrete clusters of cells capable of surviving and proliferating in non-adherent non-differentiating culture conditions) likely due to lack of cadherin-1. This evidence suggests that changes to cell membrane may occur under the absence or inhibition of SETD7[40]. Other published data associate the over-expression of SETD7 with reduced viability, colony formation and mitosis, while its down-regulation led to increased migration and invasion[40,41], thus suggesting a tumour-supressing role of SETD7. Overall, results tend to suggest that the lack of SETD7's function is connected with the progression of BC. However, SETD7 has also been associated with a poorer prognosis of BC, with a lower overall survival of patients with higher SETD7 expression, although not as an independent prognostic factor[42].

SETD7 has also been correlated with the mitigation of stress or disfunction of the endoplasmic reticulum. The ER regulates a number of cellular processes including lipid and protein metabolism, calcium homeostasis, and protein trafficking and posttranslational modification. Several events can provoke a disruption of ER homeostasis, referred to as ER stress, often causing a decrease in Ca^{2+} concentration, which in turn negatively affects

chaperones and other enzymes responsible for posttranslational protein modifications, ultimately leading to the accumulation of unfolded or misfolded proteins in the ER lumen. This triggers a series of signalling pathways that tend to maintain ER function. Known as unfolded protein response (UPR), this is a controlled process since prolonged or excessive UPR activation may lead to apoptosis. The UPR leads to an increase in the synthesis of protein and lipid components that compensate for the impaired ER function[43]. XBP1 is one of the transcription factors activated by the UPR, and was shown to directly regulate lipogenic genes in the liver, including *Dgat2*, *Scd1*, and *Acc2*[43], fatty acid synthesis under normal conditions and the regulation of lipid homeostasis[44]. SETD7 mRNA and protein expression were increased during ER stress in the kidneys of diabetic mice, due to the recruitment of XBP1[44]. Given the link of XBP1 to lipogenesis under ER stress, and that activation of XBP-1 signalling in lactation is necessary to prepare the cells for secretory activation, this raises the question of whether SETD7 is also involved in this process and the mitigation of ER stress.

RORα2 is another direct substrate for SETD7 linked to the regulation of lipid metabolism. It was reported that the lysine methylation of RORα2 by SETD7 is responsible for the transcriptional regulatory function of RORα2 and the expression of tumorigenic genes in prostate cancer cells, by binding to the pontin/Tip60 complex[45]. In other settings, RORα2 was linked to hepatic fatty acid and glucose metabolism, through the repression of PPARγ signalling by association with HDAC3[46]. In this study, RORα2 was shown to maintain lipid homeostasis in response to excess of dietary lipid intake[46]. Furthermore, another study reported that RORα2 has a role in the regulation of lipid absorption, lipogenesis and β-oxidation, cholesterol efflux and energy expenditure on muscle cells, through SREBP-1c and its downstream enzymes FAS, SCD-1, and -2[47]. Taken together, these evidences make the regulation of the MEC lipidome by SETD7 very interesting in the sense that lipid metabolism and the composition of the cell membrane are both a consequence and a defining factor of cell state and homeostasis, and SETD7 is involved in the regulation of a number of processes that tend to compensate these imbalances.

1.6 Lipidomics approach and Mass spectrometry

In order to unravel the role of lipids in homeostasis or in disease, like cancer, lipidomics has been used as a powerful analytical approach, aiming to identify the adaptation of lipidome and lipid metabolism. The lipidome comprises the whole set of lipid species in a cell or tissue. Lipidomics focuses on the description of the lipidome, its variation according to external stimuli or natural processes.

Mass spectrometry is the most widespread analytical tool for lipidomics. The lipidomics approach starts with extraction of lipids from the biological matrix, and analysis of this extract by mass spectrometry approaches, coupled or not with liquid chromatography (LC). Ionization of lipids can be done using techniques such as electrospray ionization (ESI), matrix assisted laser desorption ionization (MALDI) or desorption electrospray ionization (DESI). Identification of lipids can be accompanied by MS or MS/MS spectra. LC-MS data allows for peak identification and integration, and thus semi-quantification of the detected lipid species.

Different separation methods are available, depending on the desired lipids species to analyse. Gas chromatography (GC) is a method in which the stationary phase is a liquid adsorbed onto the surface of an inert solid. The sample is vaporized and elutes in a gaseous mobile phase, usually He or N_2, under high pressure. In this work, fatty acids were analysed using GC-MS, and were previously derivatised to methyl-esters (FAMEs), to increase their volatility and allow the analysis[48]. Hydrophilic interaction liquid chromatography (HILIC) is a variant of normal-phase liquid chromatography where hydrophilic stationary phases with reversed-phase type eluents are employed to separate polar analytes[49]. Alternatively, reverse-phase chromatography uses a hydrophobic stationary phase, frequently an octadecyl carbon chain (C18)-bonded silica can also be used to LC-MS analysis of lipids. Since phospholipids are amphipathic molecules, their elution and separation are possible on both normal and reverse phases, although with differing results regarding the retention times of species and the resolution of the separation of different molecular species from the same lipid species. An HILIC approach separates phospholipids according to the polarity of their head group, while a C18 column would separate them mostly based on the characteristics of the fatty acyl chains.

The lipidomics of BC have been extensively studied[50] for the assessment of its prognosis value and potential as tool for patient management[51]. As mentioned previously, the lipidome is modulated according to the needs and functions of the cell, and upon cancer proliferation. PL and other lipids from BC cell lines were analysed by LC and the multiple precursor ion scanning (MPIS) method by Sevinsky and coworkers[52]. The remodelling of the lipidome has also been related to metastasis progression in mice using targeted LC-MS/MS[53]. In a very interesting study, Chagovets et al.[54] used spray ionization and quadrupole time-of-flight mass spectrometry to determine the intraoperative molecular fingerprint of very small ($1mm^3$) BC tissue samples and identify tumor margins and reduce surgical intervention. The blood lipidome is one of targets of lipidomics, since it needs a minimally invasive sample collection and promotes the continuous monitoring of biomarkers. Wolrab et al.[55] used ultrahigh-performance supercritical fluid chromatography and mass spectrometry to determine the lipid profile of plasma from patients with breast, kidney, and prostate cancers, although no association of statistical models with tumor stage were observed, and another group applied triple quadrupole liquid chromatography electrospray ionization tandem mass spectrometry to plasma samples, with some success[56]. Lipids with potential for an early diagnosis of BC have been identified in urine, plasma, serum, and tissue, with multiple combinations of ionization, analysis and detection methods, including Nano-Scale Liquid Chromatography, Ultra Performance Liquid Chromatography, Hydrophilic interaction chromatography, Ion-mobility spectrometry, Quadrupole Time-of-flight, Matrix-assisted laser desorption/ionization and Electrospray ionization[50].

1.7 Objectives

This work aims at describing the effects of SETD7 inactivation via treatment with (R)-PFI-2 on the lipidome of the mouse MEC cell line HC11. These cells can reproduce, *in vitro*, the process of lactogenic differentiation, starting from stem-like cells all the way to a functionally differentiated stage. Accordingly, the plasticity of the lipidome will be analysed by integration with the changes in the context of epithelial cell differentiation in the mammary gland. Given the role of the cell membrane and lipid metabolism in several cellular processes, particularly in lactation and proliferation, the deeper understanding of the

regulation of these mechanisms is important. Therefore, the specific objectives of this study were the following:

1.1. To characterize differences in the lipidome of MECs at different differentiation stages and the changes provoked by the inhibition of SETD7 activity;

1.2. To integrate these observations with previous literature and knowledge on lipid metabolism, to predict possible previously undescribed regulatory mechanisms of SETD7 over MEC lipid metabolism and the relationship to phenotypes associated with BC;

1.3. To analyse the expression level of genes associated with the regulation of lipid metabolism and their significance under the inhibition of SETD7 activity.

1.4. To conclude on the phenotypic effect of SETD7 inhibition on mammary epithelial cell lines and propose possible functions of this protein in the modulation of the lipidome throughout epithelial and lactogenic differentiation.

2 Materials and Methods

2.1 Cell culture

HC11 mammary epithelial cells were grown on 100mm plates in complete medium (RPMI 1640, L-glutamine, 5 µg/mL insulin, 10 ng/mL EGF, 10% FBS and 50 µg/mL gentamicin). Stem-like cells (S-LC) were obtained under these conditions before confluence was attained. When cells reached confluence of 80%, EGF was removed from the culture medium to initiate differentiation and a medium composed of RPMI 1640, L-glutamine, 5 ug/mL insulin, 2% FBS and 50 ug/mL gentamicin was used. Pre-differentiated (PD) cells were collected after 48h under these conditions. Functionally differentiated (DIF) cells were obtained after treatment with 100 nM dexamethasone and 1 ug/ml prolactin for 72h at full confluence. For each stage, (R)-PFI-2 8nM and DMSO (1:1000) were applied 24h before the collection of cells, and three replicates of each experimental group were produced. To further study the inhibition of SETD7 with (R)-PFI-2 8nM, a second cell culture was performed, where cells cultured in medium containing the lactogenic hormones were treated with (R)-PFI-2 8nM and DMSO (1:1000) 48h before collection.

2.2 Lipid Extraction

Total lipids were extracted according to the method of Bligh & Dyer (1959)[57]. In detail, the pelleted cells were resuspended in 1mL of miliQ water, after which 3.75mL of a mixture of chloroform and methanol (1:2, v:v) were added, and set in ice for 30min. Next, 1.25mL of chloroform and 1.25mL of miliQ water were added, with 1min of vortexing between each step. After centrifugation, the organic phase was collected, and three washes were performed with 1.88mL of chloroform to further remove any lipidic components remaining. Finally, the collected organic fractions were evaporated under nitrogen stream and redissolved in 300µL of chloroform, stirred and evaporated again. Samples were stored at -20°C until further analysis.

2.3 Quantification of phospholipids by phosphorus assay

Phospholipids in the lipid extract were quantified according to the method of Bartlett and Lewis (1970)[58]. A volume of 10µL of samples in chloroform were dried under nitrogen steam, 0.125mL of 70% perchloric acid was added and then set for 60min at 180°C. After incubation, 825µL of miliQ water, 125µL of 2.5% of ammonium molybdate and 125µL of 10% ascorbic acid were added, with vortexing after each addition, and finally incubated at 100°C for 10min. The same procedure was applied to standards of phosphate prepared from sodium dihydrogen phosphate dihydrate. Absorbance was measured at 797nm.

2.4 Fatty acid analysis by gas chromatography mass spectrometry

FAMEs were obtained by base-catalyzed transmethylation of 10µg of each dried lipid extract, to which 1 mL of internal standard (1.08 µg mL^{-1} of methyl nonadecanoate in n-hexane) and 200 µL of a methanolic solution of potassium hydroxide (2 M) were added. After 2 min vortexing, 2 mL of an aqueous solution of sodium chloride (10 mg mL^{-1}) was added and the sample was centrifuged for 5 min at 626× g. The upper organic phase (600 µL) was collected and completely dried under a nitrogen stream. FAMEs were then redissolved in 30 µL of n-hexane and 3 µL were used for GC–MS analysis. GC–MS analyses were performed on an Agilent 6890 N gas chromatograph interfaced with an Agilent 5973 mass spectrometer (Agilent, Santa Clara, CA, USA) with electron impact ionization (70 eV). A DB-FFAP capillary column (30 m × 0.32 mm, 0.25 µm film thickness (J&W Scientific, Folsom, CA, USA)) was used. The following conditions were used: helium as carrier gas (constant flow 1.4 mL min^{-1}), inlet temperature 220 °C, detector temperature 280 °C, injection volume 2 µL (splitless). The oven temperature was programmed as follows: 80 °C for 3 min, 25 °C min^{-1} to 160 °C, 2 °C min^{-1} to 210 °C, 30 °C min^{-1} to 250 °C (held for 10 min). The fatty acids were identified by comparing their retention times with those of commercial standards (Supelco 37 Component Fame Mix, Sigma-Aldrich), and by matching their mass spectral fragmentation patterns with

the standards and corresponding data (Wiley 275 library and AOCS lipid library). The relative abundance (RA) of fatty acids was calculated by the percent area method without using correction factors. The RA of fatty acids was calculated by integrating the area under the peak and dividing the results by the sum of all areas of the identified fatty acids. The results were expressed as mean ± standard deviation.

2.5 Separation of phospholipid classes by thin layer chromatography

TLC silica gel plates were used to separate phospholipid classes from the total lipid extract. Plates were pre-washed with chloroform/methanol (1:1, v/v), followed by treatment with 2.3% boric acid in ethanol. The application of boric acid was removed for the analysis of lipid extracts from cells treated for 48h. Thirty µL (30 µg) of lipid extract dissolved in dichloromethane were seeded in the plate. The TLC spots were developed in solvent mixture chloroform/ethanol/water/triethylamine (30:35:7:35, v/v/v/v). Lipid spots were observed by exposure to primuline (50mg/100 mL acetone:water, 80:20, v/v), and visualized under a UV lamp at 254 nm. PL standards for different classes were ran on the same plate as the samples. The spots for each class were scraped off the plate and quantified using phosphorus assay. Before absorbance was measured, PLs were separated from the silica by centrifugation. The relative abundance of each phospholipid class was calculated by relating the amount of phosphorus in each spot to that of the total. Two different cultures for each cell type were analysed.

2.6 Ultra High-Performance Liquid Chromatography-Mass Spectrometry

For the analysis of the lipid extracts of cells treated for 24 hours, a Ultimate 3000 Dionex ultra high-performance liquid chromatography (UHPLC) system (Thermo Fisher Scientific, Bremen, Germany) was used, with an autosampler coupled online to the Q-

Exactive mass spectrometer with Orbitrap technology (Thermo Fisher Scientific, Bremen, Germany). The solvent system consisted of two mobile phases as follows: mobile phase A (acetonitrile:methanol:water 50:25:25 (per volume) with 5 mM ammonium acetate) and mobile phase B (acetonitrile:methanol 60:40 (per volume) with 5 mM ammonium acetate). Initially, 5% of mobile phase A was held isocratically for 2 min, followed by a linear increase to 48% of A within 8 min. A new linear increase to 65% A within in 5 min was followed by a maintenance period of 2 min, returning to the initial conditions in 3 min and held for more 10 min. A volume of 5 µL of each sample containing an amount equivalent to 10 µg of lipid extract, a volume of 8 µL of phospholipid standards mix (dMPC—0.02 µg, dMPE—0.02 µg, SM (d18:1/17:0)—0.02 µg, 19 Lyso PC—0.02 µg, dPPI—0.08 µg, CL(14:0)4—0.08 µg, dMPG—0.012 µg, dMPA—0.08 µg, Cer (d18:1/17:0)—0.04 µg, dMPS—0.04 µg) and 82 µL of starting eluent (5% of mobile phase A; final volume of 100 µL) was introduced into a microbore Ascentis® Si column (10 cm × 2.1 mm, 2.7 µm, Sigma–Aldrich) with a flow rate of 200 µL min–1 and at 35 °C. The mass spectrometer was operated using a positive/negative switching toggles between positive (electrospray voltage 3.0 kV) and negative (electrospray voltage -2.7 kV) ion modes with a capillary temperature of 250 °C and a sheath gas flow of 20 U. In MS experiments, a resolution of 70,000, an automatic gain control (AGC) target of 1 x 10^6 and maximum injection time (IT) of 100 ms were used. In MS/MS experiments, a resolution of 17,500, AGC target of 1×10^5, and maximum IT of 50 ms were used. Cycles consisted of one full-scan mass spectrum and ten data-dependent MS/MS scans were repeated continuously throughout the experiments with the dynamic exclusion of 60 s and intensity threshold of 2 × 104. Normalized collision energy™ (CE) ranged between 25, 30, and 35 eV. Data acquisition was carried out using the Xcalibur data system (V3.3, Thermo Fisher Scientific, USA). The identification of lipid species was performed using LC-MS typical retention time and accurate mass measurements (≤ 5 ppm) were employed to confirm the elemental composition. Analysis of the LC-MS/MS spectra was used to confirm molecular composition of lipid species by identifying the polar head group and the fatty acyl chains. MS data was acquired in positive ion mode for ceramide (Cer), hexosylceramide (HexCer), PC, LPC, PE, LPE and sphingomyeline (SM) classes, identified as [M + H]+ ions. The MS was acquired in

negative ion mode for cardiolipin (CL), PE, LPE, phosphatidylglycerol (PG), lyso-phosphatidylglycerol (LPG) and phosphatidylinositol (PI) classes, identified as $[M - H]^-$ ions, while PC and LPC were seen in negative mode, identified as $[M + CH3COO]^-$ ions and SM as $[M + OAc]^-$.

The analysis of lipids extracts from cells treated for 48 hours was performed in the same Ultimate 3000 Dionex (Thermo Fisher Scientific, Bremen, Germany), however, using an Ascentis® Express C18 column (Sigma-Aldrich®, 2.1 x 100 mm, 2.7 µm) coupled to the Q-Exactive® hybrid quadrupole Orbitrap mass spectrometer (Thermo Fisher, Scientific, Bremen, Germany). The extracts were analysed in two mobile phases, as follows: mobile phase A was composed of water/acetonitrile (40/60%) with 10 mM ammonium formate and 0.1% formic acid; mobile phase B was composed of isopropanol/acetonitrile (90/10%) with 10 mM ammonium formate and 0.1% formic acid. The gradient was composed of 32% B at 0 min, 45% B at 1.5 min, 52% B at 4 min, 58% B at 5 min, 66% B at 8 min, 70% B at 11 min, 85% B at 14 min, 97% B at 18 min, 97% B at 25 min, 32% B at 25.01 min and 32% B at 33 min. A volume of 5 µL of each sample, containing 10 µg of lipid extract (in 10 µL of dichloromethane), 82 µL of a solvent system consisting of isopropanol/methanol (1:1), and 8 µL of phospholipid standards mixture was loaded into the column at 55 °C and at a flow-rate of 260 µL min^{-1}. The standard mixture was composed by the following: dMPC - 0.04 µg, SM d18:1/17:0 - 0.04 µg, dMPE - 0.04 µg, LPC - 0.04 µg, dPPI - 0.08 µg, $CL(14:0)_4$ - 0.16 µg; dMPG - 0.024 µg, Cer(17:0/d18:1) - 0.08 µg, dMPS - 0.08 µg; dMPA-0.16 µg. The mass spectrometer operated in simultaneous positive (ESI 3.0 kV) and negative (ESI −2.7 kV) modes as previously described. The capillary temperature was 320 °C and a sheath gas flow was 35 U. Data was acquired at full scan mode with a high resolution of 70,000, automatic gain control (AGC) target of 3×10^6, in a *m/z* range of 300-1600, 2 microscans, and maximum inject time (IT) of 100 ms. The tandem mass spectra (MS/MS) were obtained with a resolution of 17,500, AGC target of $1x10^5$, 1 microscan, maximiun IT of 100 ms. The cycles consisted of one full-scan mass spectrum and ten data-dependent MS/MS scans, which were repeated continuously throughout the experiments with a dynamic exclusion of 30 s and intensity threshold of 8×10^4. Normalized collision energy™ (CE) ranged between 20, 24 and 28 eV in the negative mode and 25 and 30 eV in positive

mode. Data acquisition was performed using the Xcalibur data system (V3.3, Thermo Fisher Scientific, Bremen, Germany).

The quantification of molecular and lipid species was performed in the bioinformatic tool MZmine 2.53[59]. The MS raw data were pre-processed by filtering and smoothing, peak detection, peak processing, and assignment against an in-house lipid database for data from HILIC-MS. Peak assignment in data from C18-MS was performed using the bioinformatic tool MSDial 4.70[60]. Only molecular species with detectable MS/MS data from PE, PC and SM classes was considered. The previous features assured the exclusion of peaks with raw intensity lower than 10^4 and a mass tolerance of 5 ppm was also used. Integrated peak area values from lipid species were exported in the comma separated values (.csv) format, and the normalization of the data proceeded by dividing the values of each molecular species of each lipid class with the value of internal standard selected for each class.

2.7 Polymerase Chain Reaction

Isolation of RNA from pelleted cells was performed using NZYol, followed by treatment with DNAse. cDNA (1000ng) was then synthesized, using NZY First-Strand cDNA Synthesis Kit. Amplification was performed using a Biorad SsoAdvanced SYBR Green Supermix on a CFX connect Real-Time PCR System (Biorad). The primers utilized were the following:

Table 1. Primers used in RT-PCR

	Forward	**Reverse**
Fasn	GGAGGTGGTGATAGCCGGTAT	TGGGTAATCCATAGAGCCCAG
Elovl5	TTCGATGCGTCACTCAGTACCT	TGTCCAGGAGGAACCATCCTT
Elovl6	CCGAACTAGGTGACACGATATT	TGTAGGAGTACCAGGAGTACA
Fads1	CCAGCTTTGAACCCACCAA	CATGAGGCCCATTCGCTCTA
Acox1	GGATGGTAGTCCGGAGAACA	AGTCTGGATCGTTCAGAATCAAG
Acox3	CTTCTGAGAAACGGGGACAA	GCTCGGTAGGCACTAAGAGG

Melt-curve analysis was applied to assess the amplification after 3 replicates. The ΔΔCt method was used to evaluate differential expression from Ct values obtained from the linear phase of logarithmic amplification. RNA18S was used as housekeeping reference for gene expression.

2.8 Statistical analysis

Univariate data analysis was performed using GraphPad Prism version 9 (GraphPad Software, San Diego, CA) to obtain barplots and boxplots. Kruskal-Wallis and Mann-Whitney tests were applied to data from 24h treatments, and t-tests to the data from 48h treatments. Multivariate analysis of data from C18-MS (normalized peak areas of lipid species) and TLC (in relative amount of total) was performed using online tool Metaboanalyst, where data was log-transformed and scaled to unit variance (auto-scaling). Principal Component Analysis (PCA) and Partial-least Squares Discriminant Analysis (PLS-DA) were performed, and illustrated in scores scatter plots, VIP plots of the most discriminating variables, and cross-validation plots. Correlation analysis, heatmaps and data clustering was also performed. A p-value under 0.05 was considered significant.

2. Methods

3 Results

3.1 The Lipidome of HC11 Mammary epithelial Stem Cells Changes with Differentiation

3.1.1 Phospholipid Classes

To determine the PL class profile of HC11 cells under normal conditions and establish a comparison point to study the effect exerted by inhibition of SETD7 in a later stage of this study, the lipid extract of cells from the three differentiation states, treated with DMSO for 24h, were collected. Thin layer chromatography (TLC) was used to separate and quantify the relative amounts of SM, PC, PI, PS, PE, PG, PA, and CL classes (Figure 2). The elution process did not allow for a clear distinction between PE and PG, and therefore these classes were quantified together. It is expected, however, that PG accounted for a minor quantity. Although it wasn't possible to quantify PE independently, an upregulation on PE biosynthesis appears highly likely in differentiated cells, as suggested by the increase in PE+PG in previous data of the same cell stages but without DMSO[17]. A reduction on PC and PS was also observed, and CL was increased in differentiated cells (Figure 3). It seems therefore that with differentiation, these cells tend to promote the synthesis of PE (conical), and lower that of PC (cylindrical). Thus, the ratio of cylindrical/conic-shaped PL (mainly PC/PE) is lowered with differentiation, promoting membrane curvature and vesicle budding (Figure 4), which are needed to sustain the secretory phenotype of differentiated cells.

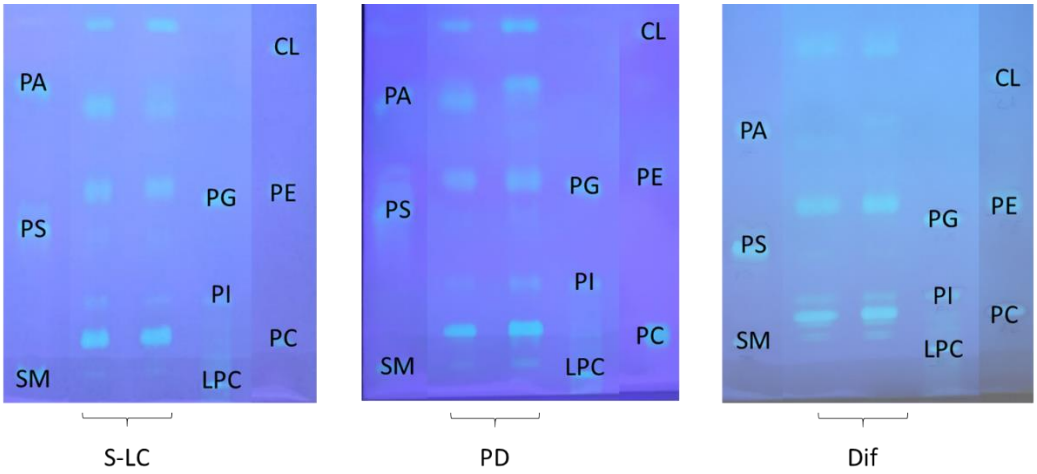

Figure 2. Thin layer chromatography plates with the separation of the lipid extracts from HC11 cells treated with DMSO for 24 hours. The plates were previously sprinkled with 2,3% boric acid.

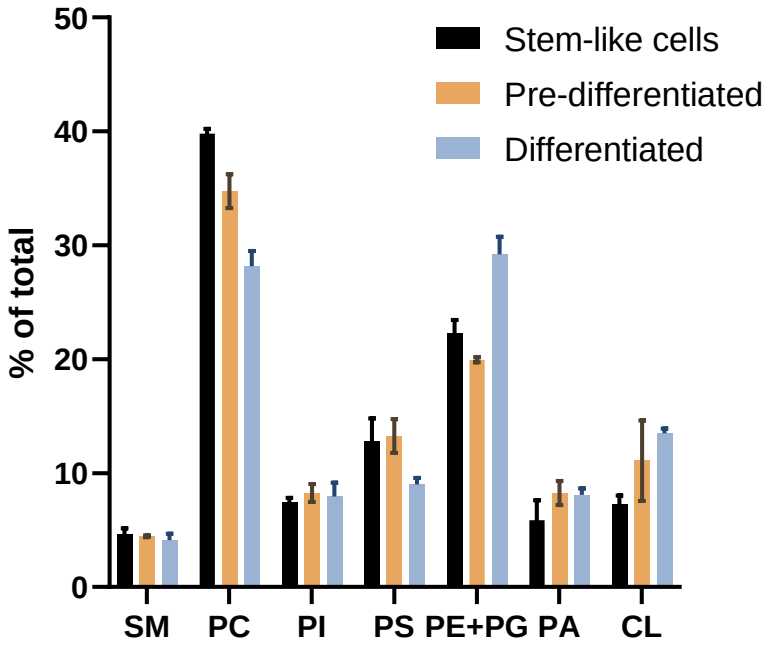

Figure 3. Lipid class profile of HC11 cells, quantified by thin layer chromatography. Variation of lipid classes across differentiation states of HC11 cells (black: stem-like cells; brown: pre-differentiated cells; blue: differentiated cells) is shown as % of total phospholipid content. Error bars represented as mean±SD. (n=2)

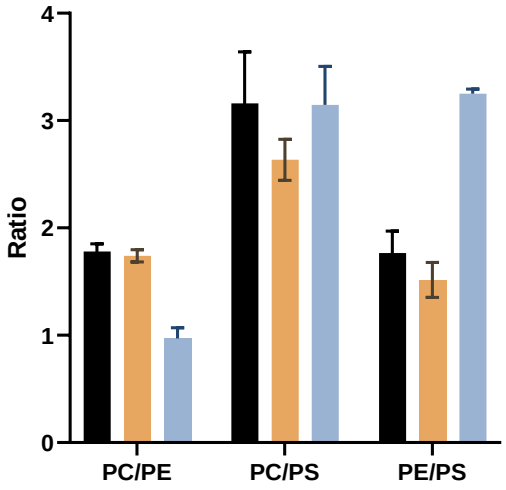

Figure 4. Ratio between PL species known to be in high proportion in the plasma membrane and metabolically interconverted on DMSO-treated control cells (24h). (black: stem-like cells; brown: pre-differentiated cells; blue: differentiated cells). Error bars represented as mean±SD. (n=2)

3.1.2 Lipidomics analysis with LC-MS

The identification and quantification of lipid species from the lipid extracts of HC11 cells were achieved through interpretation of data from high resolution LC-MS. Lipid species from the same class present a similar retention time (RT) when analysed under HILIC, and thus a typical RT range can be assigned for the lipid species of each class. Figure 5 illustrates a TIC from HILIC-MS, showing the different elution times of the different PL classes identified. Additionally, a reconstructed ion chromatogram (RIC) can be obtained, for each ion of each lipid species, allowing a representation of the relative abundance of PL species.

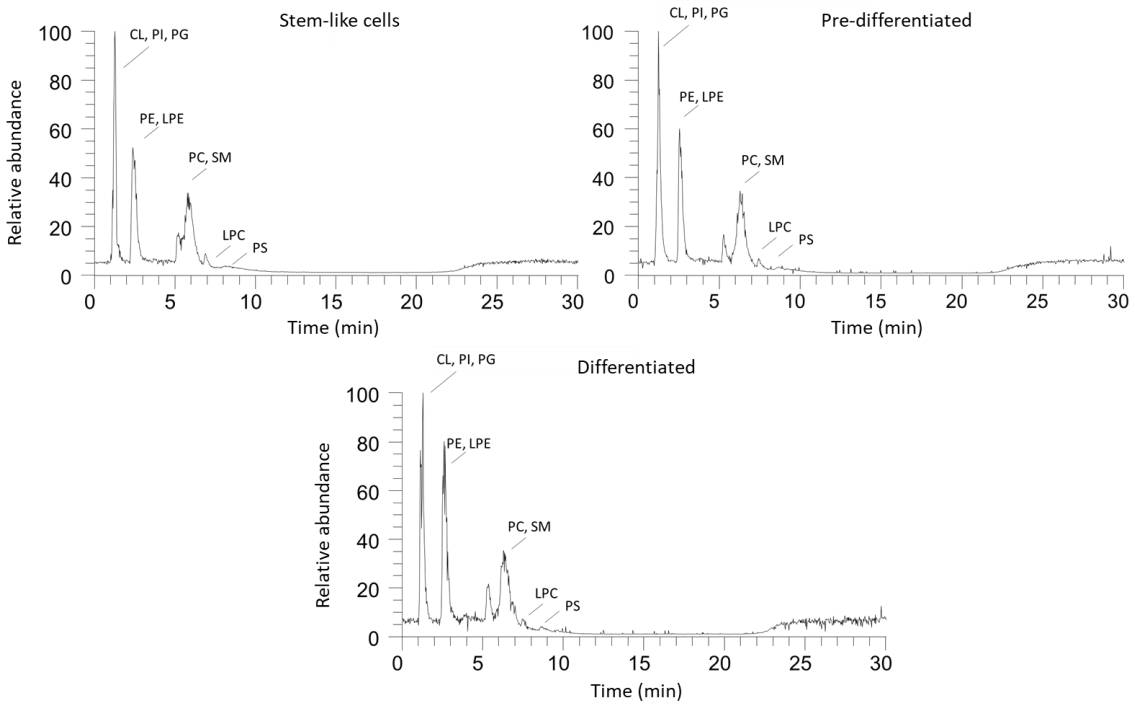

Figure 5. Total ion chromatogram of the HILIC-MS data obtained in negative mode of DMSO-treated (24h) (control) HC11 cells.

The identification of each individual lipid species was possible through the interpretation of MS and MS/MS data, in negative and positive ionization modes. Exact mass of the lipid species, the retention time and characteristic fragment ions and neutral losses of each class found on MS/MS spectra allowed for the identification of each lipid species. Fatty acyl chains were identified by the interpretation of MS/MS data, specifically, the presence of carboxylate anions on the negative mode.

3.1.3 Class Identification on hydrophilic interaction liquid chromatography (HILIC)-MS

The identification of PC was performed in positive ion mode as [M+H]+ ions, with PC(36:2) as the most abundant molecular specie at *m/z* 786.6000 (Figure 6). It was also possible to

identify PCs as [M+CH3COOH]- ions in negative ion mode, such as PC(36:2) at *m/z* 844.6065 (Figure 7). MS/MS data of the [M+H]+ ions showed the characteristic fragment ion at *m/z* 184.0730 allowing the confirmation of this identification (Figure 8). MS/MS spectrum of the [M+CH3COOH]- ions showed a fragment ion at *m/z* 281.2482, which was attributed to a carboxylate anion (RCOO-) of fatty acyl chain 18:1 (Figure 9). Therefore, this PC was identified as PC(36:2) [PC(18:1/18:1)]. All shown MS data is from control (DMSO) differentiated cells. All identified species are presented in Tables 2-11

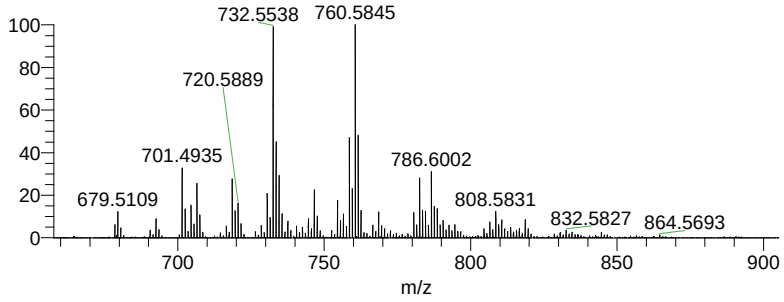

Figure 6. LC-MS spectrum in positive ion mode of *m/z* interval corresponding to phosphatidylcholines. Retention time interval: 5.22-6.73 minutes.

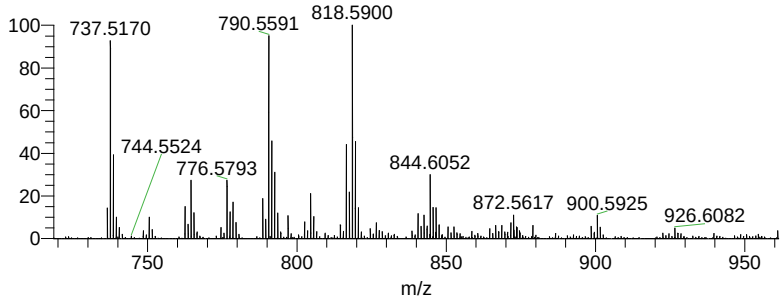

Figure 7. LC-MS spectrum in negative ion mode of *m/z* interval corresponding to phosphatidylcholines. Retention time interval: 4.98-6.71 minutes.

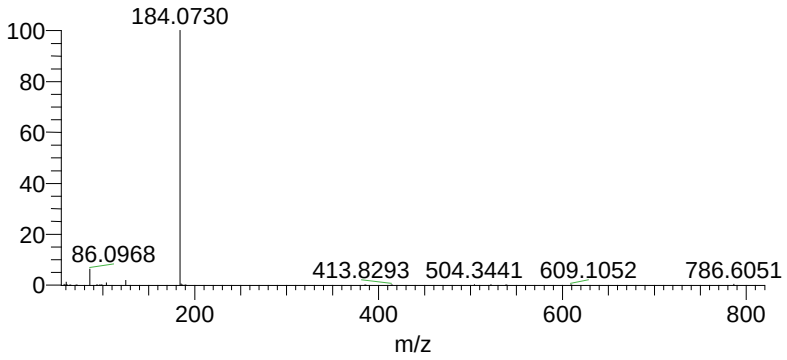

Figure 8. LC-MS/MS of the [M+H]+ ion of PC(36:2) at *m/z* 786.6006. Retention time: 6.10 minutes.

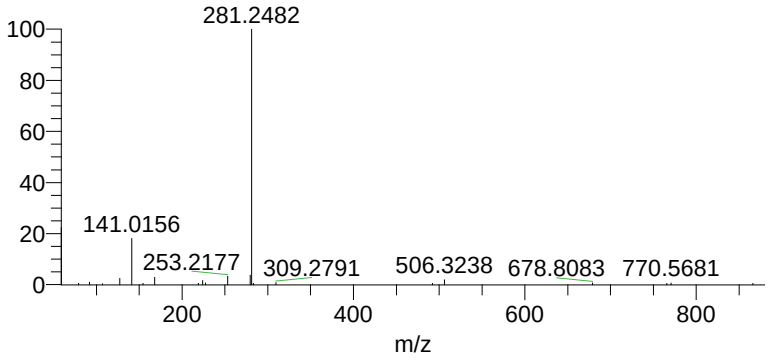

Figure 9. LC-MS/MS of the [M+CH3COOH]- ion of PC(36:2) at *m/z* 844.5328. Retention time: 6.47 minutes.

LPC were identified as PCs, in positive and negative ions modes. LPC(16:0) was the most abundant LPC, detected as [M+H]+ in positive ion mode at *m/z* 496.3397, and as [M+CH3COOH]- in negative ion mode at *m/z* 554.3459 (Figure 10). For LPC(16:0), an MS/MS spectrum in negative ion mode was obtained, containing a fragment ion at *m/z* 255.2326 and a characteristic neutral loss of 74 attributed to the loss of the methyl acetate group (Figure 11). A positive ion mode MS/MS showed the characteristic fragment ion at *m/z* 184 (Figure 12).

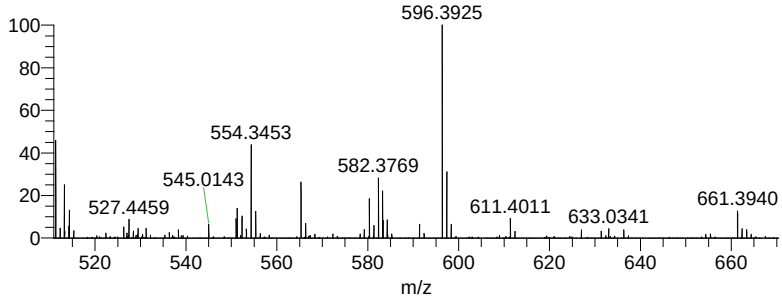

Figure 10. LC-MS spectrum in negative ion mode of *m/z* interval corresponding to lysophosphatidylcholines. Retention time interval: 7.90-8.54 minutes.

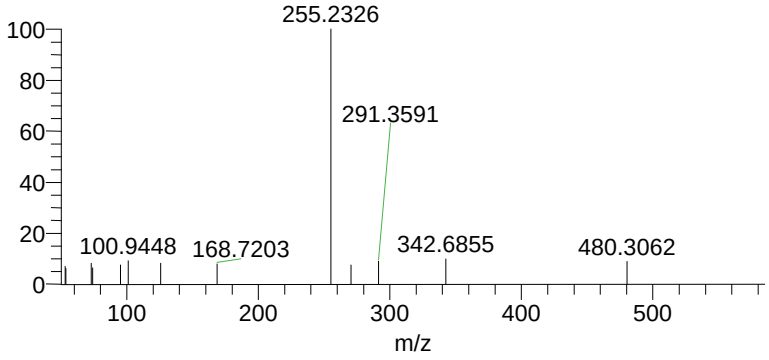

Figure 11. LC-MS/MS of the [M+CH3COOH]- ion of LPC(16:0) at *m/z* 554.3456. Retention time: 8.55 minutes.

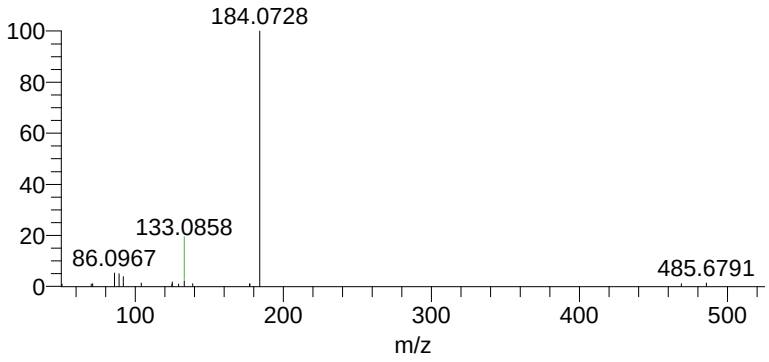

Figure 12. LC-MS/MS of the [M+H]+ ion of LPC(16:0) at *m/z* 496.3396. Retention time: 8.67 minutes.

Identification of PE was achieved in both positive and negative ion modes and PE molecular species identified respectively, as [M+H]+ and [M-H]- ions. PE(38:4) was the most abundant. In positive ion mode, PE(38:4) was identified at *m/z* 764.5222 (Figure 13). The MS/MS spectrum of the M+H ion showed the typical neutral loss of 141, attributed to the PE polar head group (Figure 15). In negative ion mode, PE(38:4) was identified at *m/z*

766.5384 (Figure 14). Data from MS/MS of the M-H ion showed the carboxylate anions of fatty acyl chains 18:0 (R1COO-) at *m/z* 283.2637, 18:1 (R1COO-) at *m/z* 281.2478, 20:3 (R2COO-) at *m/z* 305.2480 and 20:4 (R2COO-) at *m/z* 303.2321, allow for the identification of PE(38:4) as either [PE(18:0/20:4)] or [PE(18:1/20:3)] (Figure 17).

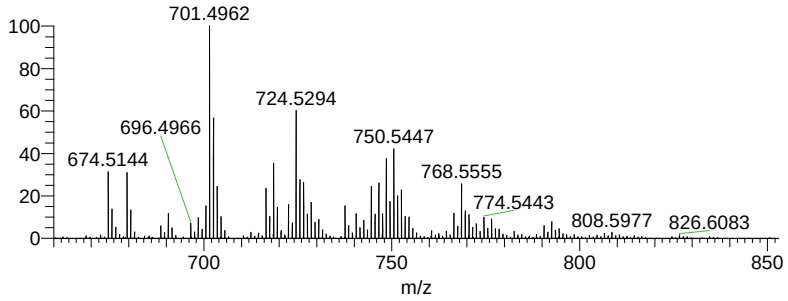

Figure 13. LC-MS spectrum in positive ion mode of *m/z* interval corresponding to Phosphatidylethanolamines. Retention time interval: 2.38-3.40 minutes.

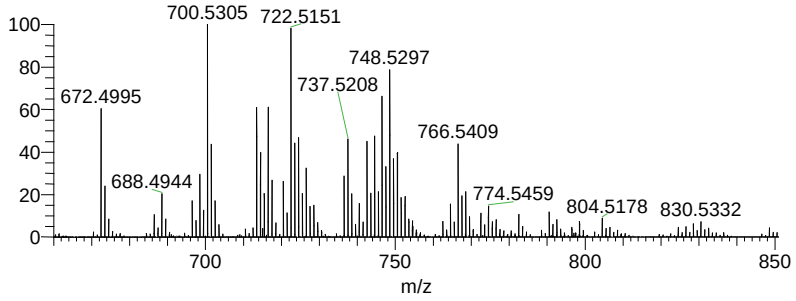

Figure 14. LC-MS spectrum in negative ion mode of *m/z* interval corresponding to Phosphatidylethanolamines. Retention time interval: 2.38-3.40 minutes.

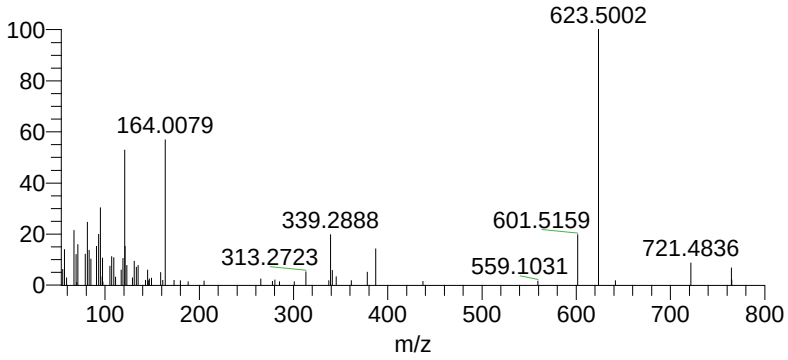

Figure 15. LC-MS/MS of the [M+H]+ ion of PE(38:4) at *m/z* 764.5209. Retention time: 2.59 minutes.

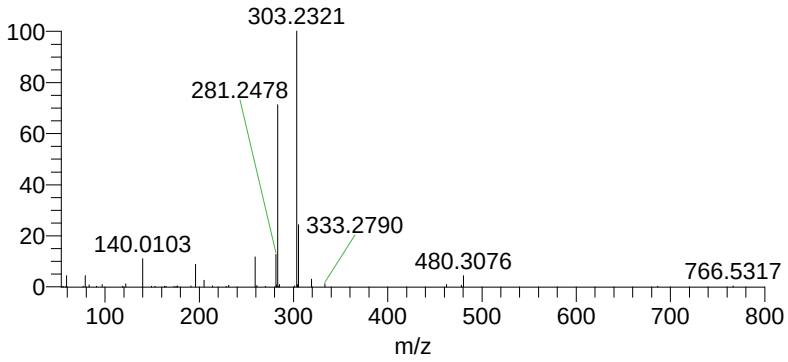

Figure 16. LC-MS/MS of the [M-H]- ion of PE(38:4) at *m/z* 766.5372. Retention time: 2.49 minutes.

Identification of LPE followed the same criteria as PE. LPE(18:1) was the most abundantly, detected at *m/z* 480.3084 as [M+H]+ ion in the positive mode and at *m/z* 478.2936 as [M-H]- ion in negative mode. MS/MS data, besides showing neutral loss of 141 in positive mode, presented a single fragment ion corresponding to a carboxylate anion of fatty acyl chain 18:1 (RCOO-) at *m/z* 281.2479, thus confirming the identification of this LPE as LPE(18:1) (Figure 17).

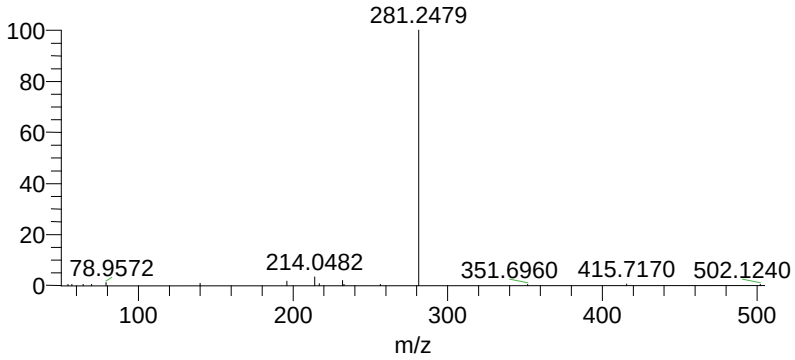

Figure 17. LC-MS/MS of the [M-H]- ion of LPE(18:1) at *m/z* 478.2930. Retention time: 3.96 minutes.

SM lipid species were identified as [M+H]+ ions, with SM(d34:1) at *m/z* 703.5753 as the most abundant lipid species (Figure 18). Information from MS/MS spectra showed a fragment ion at *m/z* 184.0730, attributed to the phosphocholine polar head, and fragment ions of sphingoid base d18:1 at 264.2673 (Figure 20). Thus, this SM was identified as

SM(d34:1) [SM(d18:1/16:0)]. Additionally, in negative ion mode, SMs were identified as [M+CH3COOH]- ions. SM(d34:1) at *m/z* 761.5808 was the most abundant lipid specie as well (Figure 19), and MS/MS data contained peaks at *m/z* 78.9574 (phosphonate group), *m/z* 168,0419 (phosphocholine) and a neutral loss of 74, due to the loss of the methyl acetate group (Figure 21).

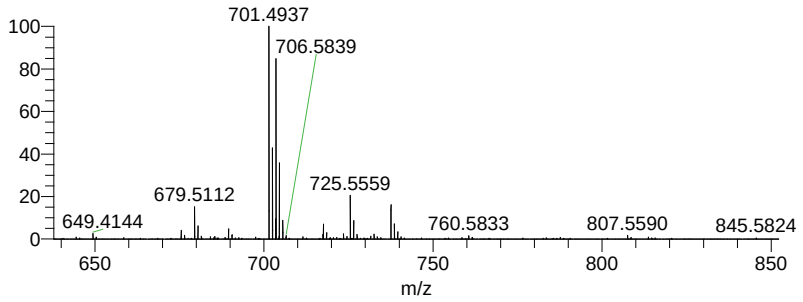

Figure 18. LC-MS spectrum in positive ion mode of *m/z* interval corresponding to sphingomyelins. Retention time interval: 6.73-7.40 minutes.

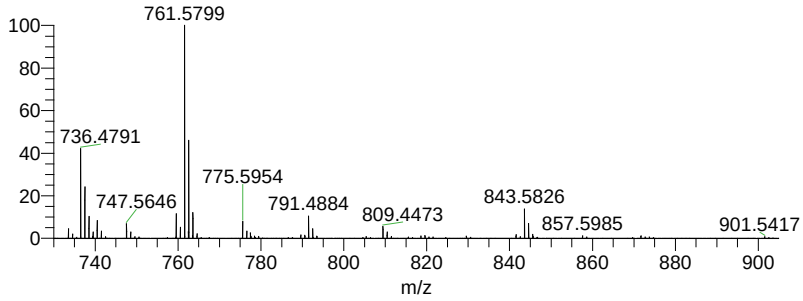

Figure 19. LC-MS spectrum in negative ion mode of *m/z* interval corresponding to sphingomyelins. Retention time interval: 6.71-7.40 minutes.

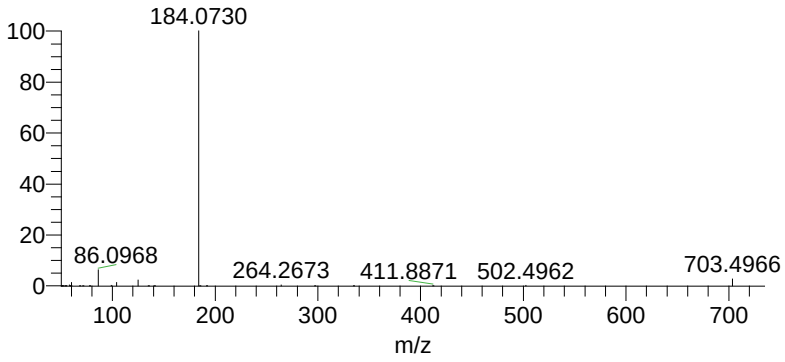

Figure 20. LC-MS/MS of the [M+H]+ ion of SM(d34:1) at *m/z* 703.5030. Retention time: 7.30 minutes.

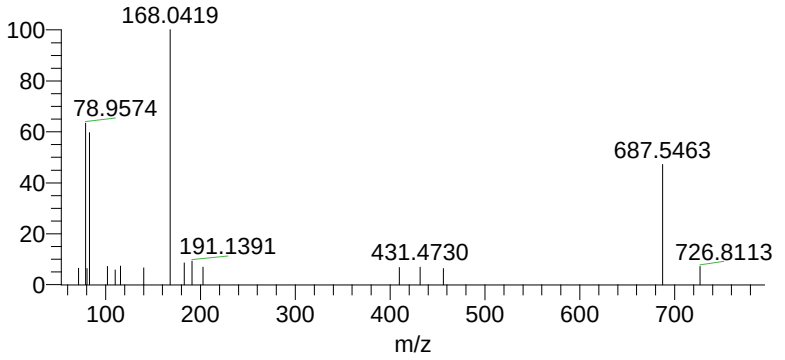

Figure 21. LC-MS/MS of the [M+CH3COOH]- ion of SM(d34:1) at *m/z* 761.5793. Retention time: 7.30 minutes.

CL were identified in negative ion mode, as $[M-H]^-$ or $[M-2H]^{2-}$ ions. CL(68:4) was the most abundant molecular species in this class and was detected at *m/z* 1399.9616 and 699.4780, respectively (Figure 22). MS/MS data showed the presence of carboxylate anions of fatty acyl chains 18:1 (RCOO-) at *m/z* 281.2483 and 16:1 (RCOO-) at *m/z* 253.2165 (Figure 23). Thus, the exemplified molecular species was identified as CL(68:4) [CL(16:1/18:1/16:1/18:1].

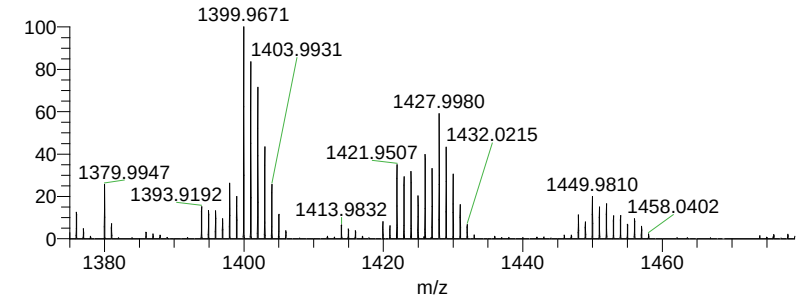

Figure 22. LC-MS spectrum in negative ion mode of *m/z* interval corresponding to Cardiolipins. Retention time interval: 1.21-2.38 minutes.

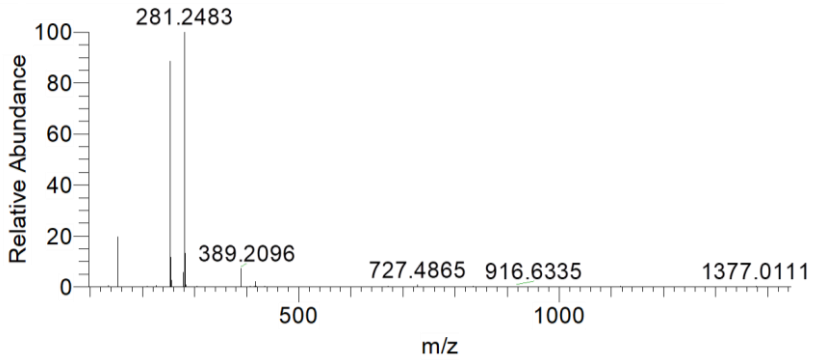

Figure 23. LC-MS/MS of the $[M-2H]^{2-}$ ion of CL(68:4) at *m/z* 699.4780. Retention time: 1.44 minutes.

PG were detected in the negative mode as [M-H]- ions, with PG(36:2) as the most abundant species, at *m/z* 773.5339 (Figure 24). A fragment ion from carboxylate anions of fatty acyl chains was detected, namely corresponding to 18:1 at 281.2483 (Figure 25). Therefore, this PG species was identified as PG(36:2) [PG(18:1/18:1)].

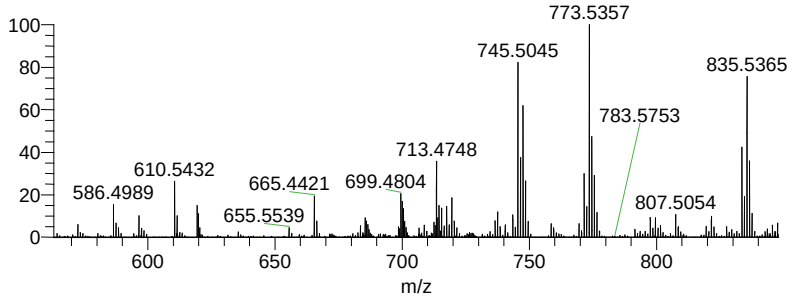

Figure 24. LC-MS in negative ion mode of *m/z* interval corresponding to Phosphatidylglycerols. Retention time interval: 1.10-1.51 minutes.

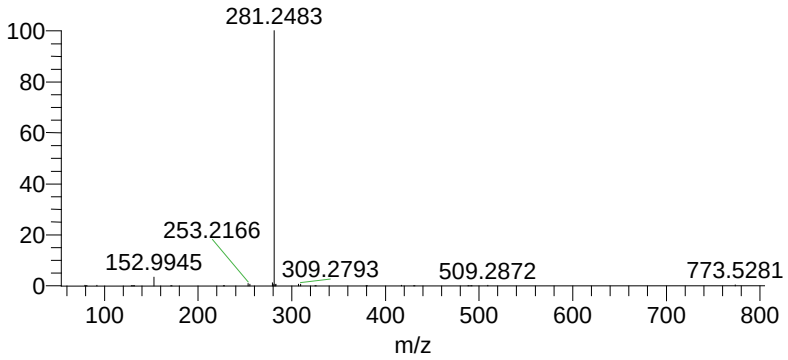

Figure 25. LC-MS/MS of the [M-H]- ion of PG(36:2) at *m/z* 773.5325. Retention time: 1.21 minutes.

The identification of PI was performed in negative ion mode, as [M-H]- ions. PI(36:2), the most abundant lipid specie in this class, was detected at *m/z* 861.5488 (Figure 26). The MS/MS spectra revealed a characteristic fragment ion at *m/z* 241.0110 due to the polar head group (Figure 27). A fragment ion at *m/z* 281.2479 was attributed to a carboxylate anion of fatty acyl chain 18:1. Therefore, this PI specie was identified as PI(36:2) [PI(18:1/18:1)].

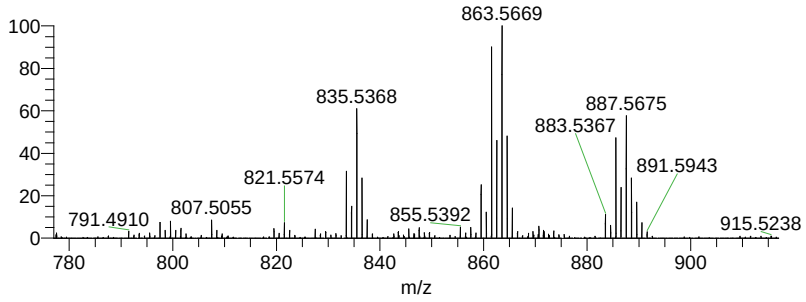

Figure 26. LC-MS spectrum in negative ion mode of *m/z* interval corresponding to phosphatidylinositols. Retention time interval: 1.01-1.40 minutes.

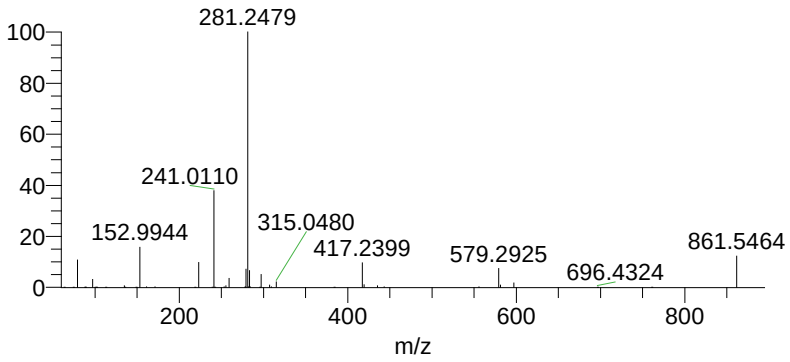

Figure 27. LC-MS/MS of the [M-H]- ion of PI(36:2) at *m/z* 861.5475. Retention time: 1.33 minutes.

PS were identified in negative ion mode as [M-H]- ions, with the characteristic neutral loss of 87, attributed to the polar head group (Figure 28). PS(34:1) was the most abundant molecular specie in this class and was detected at *m/z* 760.5123. Fragment ions correspondent to the carboxylate anions of fatty acyl chains were found at *m/z* 283.2639 and *m/z* 253.2169, thus identifying this PS as PS(34:1) [PS(16:1/18:0)].

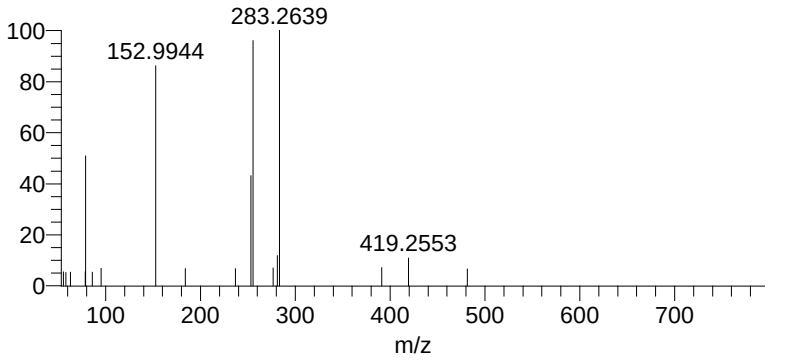

Figure 28. LC-MS/MS of the [M-H]- ion of PS(34:1) at *m/z* 760.5125. Retention time: 9.29 minutes.

Cer were identified as [M+H]+ ions in positive ion mode. Cer(d42:1) was the most abundant Cer specie, detected at *m/z* 650.6448 (Figure 29). Further identification was possible using data from MS/MS, namely fragment ions attributed to sphingosine d18:1 at *m/z* 264.2679 (Figure 30). Thus, this specie was identified as Cer(d42:1) [Cer(d18:1/24:0)]. Hexosylceramides were also detected in a similar fashion, with GlcCer(d18:1/24:0)/GalCer(d18:1/24:0) as the most abundant species, at *m/z* 812.6964. The same characteristic peak at *m/z* 264.2677 confirmed these species' identification (Figure 31).

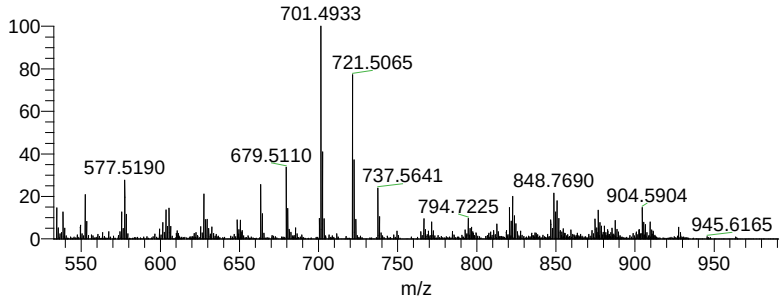

Figure 29. LC-MS in positive ion mode of *m/z* interval corresponding to ceramides. Retention time interval: 1.05-1.36 minutes.

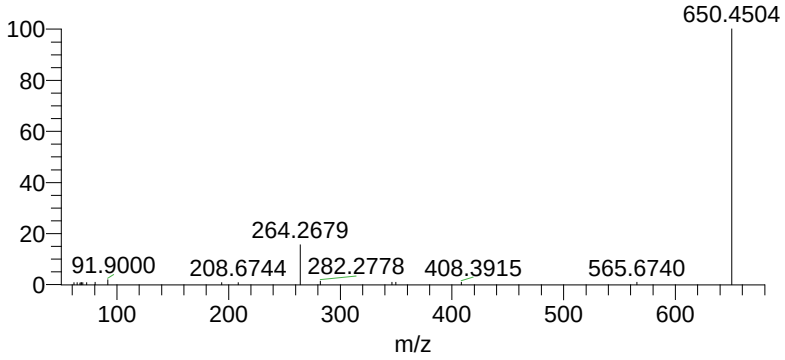

Figure 30. LC-MS/MS of the [M+H]+ ion of Cer(d42:1) at *m/z* 650.4186. Retention time: 1.61 minutes.

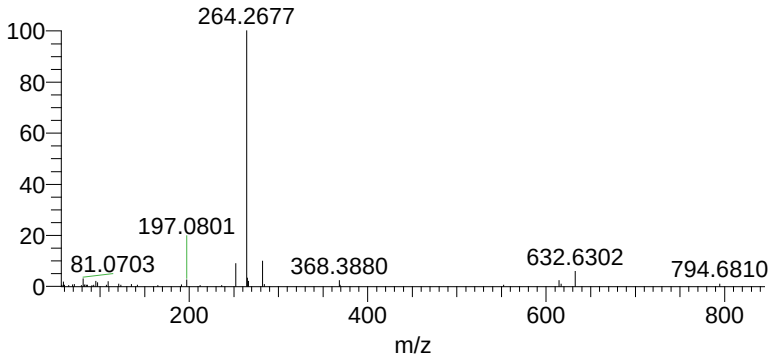

Figure 31. LC-MS/MS of the [M+H]+ ion of GlcCer(d18:1/24:0)/GalCer(d18:1/24:0) at *m/z* 812.6960. Retention time: 1.35 minutes.

Table 2. LPC molecular species identified in HC11 cells.

Lipid Species (C:N)	Calculated m/z	Observed m/z	Error (ppm)	Formula
LPC(14:0)	468.3090	468.3084	**-1.2316**	C22H47NO7P
LPC(16:0)	496.3403	496.3397	**-1.2687**	C24H51NO7P
LPC(16:1)	494.3247	494.3242	**-0.9491**	C24H49NO7P
LPC(18:0)	524.3716	524.3713	**-0.6672**	C26H55NO7P
LPC(18:1)	522.3560	522.3555	**-0.9406**	C26H53NO7P
LPC(18:2)	520.3403	520.3397	**-1.1022**	C26H51NO7P
LPC(20:0)	552.4029	552.4028	**-0.2251**	C28H59NO7P
LPC(20:1)	550.3873	550.3870	**-0.4880**	C28H57NO7P
LPC(20:4)	544.3403	544.3402	**-0.2873**	C28H51NO7P
LPC(20:5)	542.3247	542.3233	**-2.5815**	C28H49NO7P
LPC(22:1)	578.4186	578.4190	**0.7927**	C30H61NO7P
LPC(22:4)	572.3716	572.3693	**-4.0935**	C30H55NO7P
LPC(22:6)	568.3403	568.3399	**-0.7954**	C30H51NO7P
LPC(O-14:0)	454.3298	454.3290	**-1.6561**	C22H49NO6P
LPC(O-16:0)	482.3611	482.3607	**-0.7705**	C24H53NO6P
LPC(O-16:1)/LPC(P-16:0)	480.3454	480.3451	**-0.6031**	C24H51NO6P
LPC(O-18:0)	510.3924	510.3923	**-0.0951**	C26H57NO6P
LPC(O-18:1)/LPC(P-18:0)	508.3767	508.3765	**-0.4501**	C26H55NO6P
LPC(O-20:0)	538.4237	538.4224	**-2.4024**	C28H61NO6P
LPC(P-18:1)	506.3611	506.3612	**0.2124**	C26H53NO6P

Table 3. PC lipid species identified in HC11 cells.

Lipid Species (C:N)	Calculated m/z	Observed m/z	Error (ppm)	Fatty acyl chains (C:N)	Formula
PC(30:0)	706.5387	706.5385	**-0.2350**	**PC(14:0/16:0)**	C38H77NO8P
PC(30:1)	704.5230	704.5220	**-1.4295**	**PC(14:0/16:1)**	C38H75NO8P
PC(32:0)	734.5700	734.5694	**-0.8068**	**PC(16:0/16:6)**	C40H81NO8P
PC(32:1)	732.5543	732.5532	**-1.5509**	**PC(16:0/16:1)**	C40H79NO8P
PC(32:2)	730.5387	730.5383	**-0.5368**	**PC(16:1/16:1)**	C40H77NO8P
PC(34:1)	760.5856	760.5850	**-0.8896**	**PC(16:0/18:1)**	C42H83NO8P
PC(34:2)	758.5700	758.5700	**-0.0324**	**PC(16:0/18:2), PC(16:1/18:1)**	C42H81NO8P
PC(34:3)	756.5543	756.5533	**-1.3091**	**PC(16:1/18:2), PC(16:0/18:3), PC(14:0/20:3)**	C42H79NO8P
PC(34:4)	754.5387	754.5385	**-0.2287**	**PC(16:1/18:3)**	C42H77NO8P
PC(36:1)	788.6169	788.6156	**-1.7235**	**PC(18:0/18:1)**	C44H87NO8P
PC(36:2)	786.6013	786.6000	**-1.6167**	**PC(18:1/18:1)**	C44H85NO8P
PC(36:4)	782.5700	782.5670	**-3.8177**	**PC(18:1/18:3), PC(16:1/20:3), PC(16:0/20:4)**	C44H81NO8P

PC(36:5)	780.5543	780.5547	**0.4862**	**PC(18:2/18:3), PC(16:1/20:4)**	C44H79NO8P
PC(36:6)	778.5387	778.5379	**-1.0526**	**PC(16:1/20:5), PC(14:0/22:6)**	C44H77NO8P
PC(36:7)	776.5230	776.5222	**-1.1165**		C44H75NO8P
PC(38:2)	814.6326	814.6308	**-2.2465**	**PC(18:1/20:1)**	C46H89NO8P
PC(38:3)	812.6169	812.6159	**-1.3073**	**PC(18:1/20:2)**	C46H87NO8P
PC(38:4)	810.6013	810.5997	**-1.9358**	**PC(18:1/20:3)**	C46H85NO8P
PC(38:5)	808.5856	808.5826	**-3.7841**	**PC(18:1/20:4)**	C46H83NO8P
PC(38:6)	806.5700	806.5700	**0.0257**	**PC(18:1/20:5), PC(16:0/22:6)**	C46H81NO8P
PC(38:7)	804.5543	804.5538	**-0.6681**	**PC(16:1/22:6)**	C46H79NO8P
PC(38:8)	802.5387	802.5388	**0.1581**		C46H77NO8P
PC(40:1)	844.6795	844.6772	**-2.7555**	**PC(18:1/22:0)**	C48H95NO8P
PC(40:10)	826.5387	826.5387	**0.0548**		C48H77NO8P
PC(40:2)	842.6639	842.6631	**-0.9288**	**PC(18:1/22:1)**	C48H93NO8P
PC(40:3)	840.6482	840.6465	**-2.0703**	**PC(18:1/22:2)**	C48H91NO8P
PC(40:4)	838.6326	838.6324	**-0.1774**	**PC(18:1/22:3)**	C48H89NO8P
PC(40:6)	834.6013	834.5985	**-3.3005**	**PC(18:0/22:6), PC(18:1/22:5)**	C48H85NO8P
PC(40:7)	832.5856	832.5848	**-1.0309**	**PC(18:1/22:6)**	C48H83NO8P
PC(40:8)	830.5699	830.5699	**-0.0385**	**PC(18:2/22:6)**	C48H81NO8P
PC(40:9)	828.5543	828.5543	**0.0101**		C48H79NO8P
PC(42:1)	872.7108	872.7104	**-0.4570**	**PC(18:1/24:0)**	C50H99NO8P
PC(42:10)	854.5700	854.5673	**-3.0902**		C50H81NO8P
PC(42:11)	852.5543	852.5541	**-0.2689**	**PC(20:5/22:6)**	C50H79NO8P
PC(42:2)	870.6952	870.6947	**-0.5179**	**PC(18:1/24:1)**	C50H97NO8P
PC(42:3)	868.6795	868.6794	**-0.1412**		C50H95NO8P
PC(42:4)	866.6639	866.6626	**-1.4307**	**PC(20:3/22:1)**	C50H93NO8P
PC(42:5)	864.6482	864.6483	**0.0808**	**PC(20:3/22:4)**	C50H91NO8P
PC(42:7)	860.6169	860.6148	**-2.4520**	**PC(20:1/22:6)**	C50H87NO8P
PC(42:8)	858.6013	858.6011	**-0.1567**		C50H85NO8P
PC(42:9)	856.5856	856.5835	**-2.5424**	**PC(20:4/22:5)**	C50H83NO8P
PC(44:1)	900.7421	900.7430	**0.9629**		C52H103NO8P
PC(44:10)	882.6013	882.6010	**-0.2970**		C52H85NO8P
PC(44:2)	898.7265	898.7278	**1.4416**		C52H101NO8P
PC(44:3)	896.7108	896.7098	**-1.2060**		C52H99NO8P
PC(44:4)	894.6952	894.6939	**-1.4066**		C52H97NO8P
PC(44:5)	892.6795	892.6790	**-0.5655**		C52H95NO8P
PC(44:6)	890.6639	890.6632	**-0.7494**		C52H93NO8P
PC(O-28:0)	664.5281	664.5280	**-0.2368**		C36H75NO7P
PC(O-30:0)	692.5594	692.5592	**-0.3460**		C38H79NO7P
PC(O-30:1)/PC(P-30:0)	690.5438	690.5435	**-0.4474**		C38H77NO7P
PC(O-32:0)	720.5907	720.5895	**-1.7161**		C40H83NO7P

PC(O-32:1)/PC(P-32:0)	718.5751	718.5740	**-1.4874**	C40H81NO7P
PC(O-34:1)/PC(P-34:0)	746.6064	746.6056	**-1.0396**	C42H85NO7P
PC(O-34:2)/PC(P-34:1)	744.5907	744.5902	**-0.6921**	C42H83NO7P
PC(O-34:3)/PC(P-34:2)	742.5751	742.5742	**-1.2266**	C42H81NO7P
PC(O-34:4)/PC(P-34:3)	740.5599	740.5605	**0.7943**	C42H79NO7P
PC(O-36:1)/PC(P-36:0)	774.6377	774.6375	**-0.2325**	C44H89NO7P
PC(O-36:2)/PC(P-36:1)	772.6220	772.6206	**-1.8113**	C44H87NO7P
PC(O-36:3)/PC(P-36:2)	770.6064	770.6050	**-1.8295**	C44H85NO7P
PC(O-36:4)/PC(P-36:3)	768.5907	768.5882	**-3.3292**	C44H83NO7P
PC(O-36:5)/PC(P-36:4)	766.5751	766.5737	**-1.8267**	C44H81NO7P
PC(O-38:1)/PC(P-38:0)	802.6690	802.6683	**-0.8324**	C46H93NO7P
PC(O-38:2)/PC(P-38:1)	800.6533	800.6519	**-1.8150**	C46H91NO7P
PC(O-38:3)/PC(P-38:2)	798.6377	798.6355	**-2.7418**	C46H89NO7P
PC(O-38:4)/PC(P-38:3)	796.6220	796.6202	**-2.3313**	C46H87NO7P
PC(O-38:5)/PC(P-38:4)	794.6064	794.6042	**-2.6702**	C46H85NO7P
PC(O-38:6)/PC(P-38:5)	792.5907	792.5896	**-1.4032**	C46H83NO7P
PC(O-40:1)/PC(P-40:0)	830.7003	830.7002	**-0.1146**	C48H97NO7P
PC(O-40:2)/PC(P-40:1)	828.6846	828.6850	**0.4827**	C48H95NO7P
PC(O-40:3)/PC(P-40:2)	826.6690	826.6705	**1.8039**	C48H93NO7P
PC(O-40:4)/PC(P-40:3)	824.6533	824.6529	**-0.4650**	C48H91NO7P
PC(O-40:5)/PC(P-40:4)	822.6377	822.6351	**-3.0952**	C48H89NO7P
PC(O-40:6)/PC(P-40:5)	820.6220	820.6199	**-2.5587**	C48H87NO7P
PC(O-42:2)/PC(P-42:1)	856.7159	856.7165	**0.7380**	C50H99NO7P
PC(O-42:3)/PC(P-42:2)	854.7003	854.7009	**0.7371**	C50H97NO7P
PC(O-42:4)/PC(P-42:3)	852.6846	852.6844	**-0.2975**	C50H95NO7P
PC(O-42:5)/PC(P-42:4)	850.6690	850.6689	**-0.1183**	C50H93NO7P
PC(O-42:6)/PC(P-42:5)	848.6533	848.6542	**1.0800**	C50H91NO7P
PC(P-28:0)	662.5125	662.5120	**-0.6332**	C36H73NO7P
PC(P-30:1)	688.5281	688.5260	**-3.0072**	C38H75NO7P
PC(P-32:1)	716.5594	716.5588	**-0.8610**	C40H79NO7P
PC(P-36:5)	764.5594	764.5592	**-0.3398**	C44H79NO7P
PC(P-38:6)	790.5751	790.5766	**1.9573**	C46H81NO7P
PC(P-40:6)	818.6064	818.6043	**-2.5207**	C48H85NO7P
PC(P-42:6)	846.6377	846.6371	**-0.6378**	C50H89NO7P
PC(P-44:6)	874.6690	874.6681	**-1.0185**	C52H93NO7P

Table 4. LPE lipid species identified in HC11 cells.

Lipid Species (C:N)	Calculated m/z	Observed m/z	Error (ppm)	Formula
LPE(14:0)	424.2464	424.2468	**0.9374**	C19H39NO7P
LPE(16:0)	452.2777	452.2781	**0.9184**	C21H43NO7P
LPE(16:1)	450.2621	450.2625	**0.8871**	C21H41NO7P
LPE(18:0)	480.3090	480.3090	**-0.0298**	C23H47NO7P
LPE(18:1)	478.2934	478.2936	**0.4899**	C23H45NO7P

LPE(18:2)	476.2777	476.2779	**0.4558**	C23H43NO7P
LPE(18:3)	474.2621	474.2622	**0.1880**	C23H41NO7P
LPE(20:1)	506.3247	506.3247	**0.1047**	C25H49NO7P
LPE(20:3)	502.2934	502.2943	**1.8418**	C25H45NO7P
LPE(20:4)	500.2777	500.2781	**0.8594**	C25H43NO7P
LPE(20:5)	498.2621	498.2624	**0.5956**	C25H41NO7P
LPE(22:1)	534.3560	534.3561	**0.3270**	C27H53NO7P
LPE(22:2)	532.3403	532.3405	**0.3526**	C27H51NO7P
LPE(22:4)	528.3090	528.3100	**1.8077**	C27H47NO7P
LPE(22:5)	526.2934	526.2932	**-0.2559**	C27H45NO7P
LPE(22:6)	524.2777	524.2779	**0.3060**	C27H43NO7P
LPE(O-16:0)	438.2985	438.2987	**0.5385**	C21H45NO6P
LPE(O-18:0)	466.3298	466.3298	**0.1922**	C23H49NO6P
LPE(P-16:0)	436.2828	436.2830	**0.5156**	C21H43NO6P
LPE(P-18:0)/LPE(O-18:1)	464.3141	464.3143	**0.3469**	C23H47NO6P
LPE(P-20:0)	492.3454	492.3454	**0.0207**	C25H51NO6P

Table 5. PE lipid species identified in HC11 cells.

Lipid Species (C:N)	Calculated m/z	Observed m/z	Error (ppm)	Fatty acyl chains (C:N)	Formula
PE(30:0)	662.4760	662.4761	**0.1569**	**PE(14:0/16:0)**	C35H69NO8P
PE(30:1)	660.4600	660.4608	**1.2262**	**PE(14:0/16:1)**	C35H67NO8P
PE(32:2)	686.4760	686.4762	**0.3183**	**PE(16:0/16:2), PE(16:1/16:1)**	C37H69O8NP
PE(32:3)	684.4600	684.4600	**0.0157**	**PE(16:1/16:2)**	C37H67NO8P
PE(34:1)	716.5230	716.5230	**-0.0012**	**PE(16:0/18:1), PE(16:1/18:0)**	C39H75NO8P
PE(34:2)	714.5070	714.5066	**-0.5286**	**PE(16:1/18:1), PE(16:0/18:2)**	C39H73NO8P
PE(34:3)	712.4920	712.4918	**-0.2197**	**PE(16:1/18:2), PE(16:0/18:3)**	C39H71O8NP
PE(34:4)	710.4700	710.4701	**0.0843**	**PE(16:1/18:3)**	C39H69NO8P
PE(36:3)	740.5230	740.5229	**-0.1173**	**PE(16:1/20:2), PE(16:0/20:3), PE(18:0/18:3), PE(18:2/18:1)**	C41H75NO8P
PE(36:6)	734.4760	734.4770	**1.4202**	**PE(16:1/20:5), PE(16:2/20:4), PE(14:1/22:5)**	C41H69NO8P
PE(38:1)	772.5860	772.5862	**0.2173**	**PE(16:1/22:0), PE(16:0/22:1), PE(18:0/20:1), PE(18:1/20:0)**	C43H83O8NP

PE(38:3)	768.5540	768.5524	**-2.0176**	**PE(18:1/20:2), PE(18:0/20:3)**	C43H79NO8P
PE(38:4)	766.5390	766.5384	**-0.7980**	**PE(18:0/20:4), PE(18:1/20:3)**	C43H77O8NP
PE(38:5)	764.5230	764.5226	**-0.4620**	**PE(16:0/22:5), PE(14:0/24:5)**	C43H75NO8P
PE(38:7)	760.4920	760.4915	**-0.6217**	**PE(16:1/22:6)**	C43H71NO8P
PE(40:1)	800.6170	800.6174	**0.4793**	**PE(18:1/22:0)**	C45H87NO8P
PE(40:2)	798.6010	798.6012	**0.2933**	**PE(18:1/22:1)**	C45H85NO8P
PE(40:3)	796.5800	796.5821	**2.6102**	**PE(18:1/22:2), PE(18:0/22:3)**	C45H83O8NP
PE(40:4)	794.5700	794.5671	**-3.6913**	**PE(18:0/22:4)**	C45H81NO8P
PE(40:5)	792.5540	792.5531	**-1.0753**	**PE(18:0/22:5)**	C45H79O8NP
PE(40:7)	788.5230	788.5227	**-0.4092**	**PE(18:1/22:6)**	C45H75NO8P
PE(40:8)	786.5070	786.5076	**0.7842**	**PE(18:2/22:6)**	C45H73O8NP
PE(42:2)	826.6330	826.6326	**-0.4999**	**PE(18:1/24:1)**	C47H89O8NP
PE(42:3)	824.6170	824.6154	**-1.9827**	**PE(18:1/24:2)**	C47H87O8NP
PE(42:4)	822.6010	822.6009	**-0.0838**	**PE(22:1/20:3)**	C47H85O8NP
PE(42:5)	820.5860	820.5847	**-1.5235**		C47H83O8NP
PE(42:8)	814.5390	814.5364	**-3.1328**		C47H77NO8P
PE(42:9)	812.5230	812.5235	**0.6320**		C47H75O8NP
PE(44:4)	850.6330	850.6320	**-1.1704**	**PE(24:1/20:3)**	C49H89NO8P
PE(44:5)	848.6170	848.6164	**-0.6604**	**PE(24:1/20:4)**	C49H87NO8P
PE(O-28:0)	620.4660	620.4654	**-1.0043**		C33H67NO7P
PE(O-30:0)	648.4970	648.4964	**-0.9746**		C35H71NO7P
PE(O-34:5)/PE(P-34:4)	694.4810	694.4810	**0.0295**		C47H83NO7P
PE(O-38:3)/PE(P-38:2)	754.5750	754.5721	**-3.8921**		C35H69NO7P
PE(O-40:6)/PE(P-40:5)	776.5590	776.5580	**-1.3341**		C35H67NO7P
PE(O-40:9)/PE(P-40:8)	770.5130	770.5131	**0.1644**		C37H73NO7P
PE(O-42:6)/PE(P-42:5)	804.5910	804.5908	**-0.2043**		C37H71NO7P
PE(O-30:1)/PE(P-30:0)	646.4810	646.4816	**0.8862**		C39H77NO7P
PE(O-30:2)/PE(P-30:1)	644.4660	644.4656	**-0.6490**		C39H75NO7P
PE(O-32:1)/PE(P-32:0)	674.5130	674.5107	**-3.3919**		C39H73NO7P
PE(O-32:2)/PE(P-32:1)	672.4970	672.4971	**0.1128**		C39H71NO7P
PE(O-34:1)/PE(P-34:0)	702.5440	702.5409	**-4.3685**		C41H81NO7P
PE(O-34:2)/PE(P-34:1)	700.5280	700.5280	**0.0612**		C41H79NO7P
PE(O-34:3)/PE(P-34:2)	698.5130	698.5125	**-0.7142**		C41H77NO7P
PE(O-34:4)/PE(P-34:3)	696.4970	696.4968	**-0.2297**		C41H73NO7P
PE(O-34:6)/PE(P-34:5)	692.4660	692.4658	**-0.2726**		C41H71NO7P
PE(O-36:1)/PE(P-36:0)	730.5750	730.5745	**-0.6911**		C43H85NO7P
PE(O-36:2)/PE(P-36:1)	728.5590	728.5582	**-1.1098**		C43H83NO7P
PE(O-36:3)/PE(P-36:2)	726.5440	726.5434	**-0.8542**		C43H79NO7P
PE(O-36:5)/PE(P-36:4)	722.5130	722.5125	**-0.7558**		C43H77NO7P
PE(O-36:6)/PE(P-36:5)	720.4970	720.4969	**-0.1565**		C43H73NO7P

PE(O-36:7)/PE(P-36:6)	718.4810	718.4800	**-1.4538**	C45H87NO7P
PE(O-38:1)/PE(P-38:0)	758.6060	758.6049	**-1.4711**	C45H85NO7P
PE(O-38:2)/PE(P-38:1)	756.5910	756.5889	**-2.7456**	C45H83NO7P
PE(O-38:4)/PE(P-38:3)	752.5590	752.5578	**-1.5462**	C45H81NO7P
PE(O-38:5)/PE(P-38:4)	750.5440	750.5423	**-2.2648**	C45H77NO7P
PE(O-38:7)/PE(P-38:6)	746.5130	746.5126	**-0.5011**	C45H75NO7P
PE(O-40:2)/PE(P-40:1)	784.6220	784.6190	**-3.8165**	C39H69O7NP
PE(O-40:3)/PE(P-40:2)	782.6060	782.6046	**-1.7788**	C43H81O7NP
PE(O-40:4)/PE(P-40:3)	780.5910	780.5893	**-2.1256**	C45H77O7NP
PE(O-40:5)/PE(P-40:4)	778.5750	778.5729	**-2.6818**	C45H73O7NP
PE(O-40:7)/PE(P-40:6)	774.5440	774.5430	**-1.3028**	C39H67O7NP
PE(O-40:8)/PE(P-40:7)	772.5280	772.5278	**-0.2569**	C41H69O7NP

Table 6. PG lipid species identified in HC11 cells.

Lipid Species (C:N)	Calculated m/z	Observed m/z	Error (ppm)	Fatty acyl chains (C:N)	Formula
PG(30:0)	693.4707	693.4713	**0.8541**	**PG(12:0/18:0)**	C36H70O10P
PG(30:1)	691.4550	691.4547	**-0.4247**	**PG(14:1/16:0)**	C36H68O10P
PG(32:0)	721.5020	721.5021	**0.0811**	**PG(16:0/16:0)**	C38H74O10P
PG(32:1)	719.4863	719.4862	**-0.1595**	**PG(16:0/16:1), PG(14:0/18:1)**	C38H72O10P
PG(32:2)	717.4707	717.4702	**-0.6701**	**PG(16:1/16:1)**	C38H70O10P
PG(34:1)	747.5176	747.5174	**-0.2724**		C40H76O10P
PG(34:2)	745.5020	745.5023	**0.3949**	**PG(16:1/18:1), PG(16:0/18:2)**	C40H74O10P
PG(34:3)	743.4863	743.4864	**0.1871**	**PG(16:2/18:1)**	C40H72O10P
PG(34:4)	741.4707	741.4691	**-2.2234**	**PG(16:2/18:2), PG(16:1/18:3)**	C40H70O10P
PG(36:1)	775.5489	775.5481	**-0.9745**	**PG(18:0/18:1)**	C42H80O10P
PG(36:2)	773.5333	773.5339	**0.7176**	**PG(18:0/18:2), PG(18:1/18:1), PG(16:0/20:2), PG(16:1/20:1)**	C42H78O10P
PG(36:3)	771.5176	771.5173	**-0.3700**	**PG(18:0/18:3), PG(18:1/18:2), PG(16:0/20:3), PG(16:1/20:2)**	C42H76O10P
PG(36:4)	769.5020	769.5018	**-0.2304**	**PG(18:1/18:3), PG(16:1/20:3)**	C42H74O10P
PG(36:5)	767.4863	767.4862	**-0.0682**	**PG(16:1/20:4), PG(16:2/20:3)**	C42H72O10P
PG(36:6)	765.4707	765.4709	**0.1999**	**PG(16:1/20:5)**	C42H70O10P
PG(38:2)	801.5646	801.5634	**-1.5296**		C44H82O10P
PG(38:3)	799.5489	799.5481	**-0.9921**		C44H80O10P

PG(38:4)	797.5333	797.5329	**-0.4693**		C44H78O10P
PG(38:5)	795.5176	795.5172	**-0.5402**	**PG(16:0/22:5), PG(16:1/22:4), PG(18:2/20:3), PG(18:1/20:4)**	C44H76O10P
PG(38:6)	793.5020	793.5011	**-1.1132**	**PG(16:0/22:6), PG(16:1/22:5)**	C44H74O10P
PG(38:7)	791.4863	791.4864	**0.1670**	**PG(16:1/22:6)**	C44H72O10P
PG(40:2)	829.5959	829.5954	**-0.5535**		C46H86O10P
PG(40:3)	827.5802	827.5795	**-0.8044**	**PG(18:0/22:3), PG(18:1/22:2)**	C46H84O10P
PG(40:4)	825.5646	825.5636	**-1.2167**	**PG(18:1/22:3), PG(18:2/22:2), PG(20:1/20:3)**	C46H82O10P
PG(40:5)	823.5489	823.5479	**-1.1620**		C46H80O10P
PG(40:6)	821.5333	821.5309	**-2.8769**		C46H78O10P
PG(40:7)	819.5176	819.5185	**1.0448**		C46H76O10P
PG(40:8)	817.5020	817.5027	**0.8702**		C46H74O10P
PG(42:7)	847.5489	847.5487	**-0.2132**	**PG(18:1/24:6), PG(20:2/22:5)**	C48H80O10P
PG(42:8)	845.5333	845.5348	**1.7998**		C48H78O10P
PG(42:9)	843.5176	843.5174	**-0.2172**	**PG(20:3/22:6), PG(20:4/22:5)**	C48H76O10P
PG(O-34:0)	735.5540	735.5524	**-2.1815**		C40H80O9P

Table 7. PS lipid species identified in HC11 cells.

Lipid Species (C:N)	Calculated m/z	Observed m/z	Error (ppm)	Fatty acyl chains (C:N)	Formula
PS(30:3)	700.4190	700.4173	**-2.4962**	**PS(14:2/16:1)**	C36H63NO10P
PS(32:1)	732.4816	732.4817	**0.1335**	**PS(16:0/16:1)**	C38H71NO10P
PS(34:1)	760.5129	760.5123	**-0.7580**	**PS(16:1/18:0)**	C40H75NO10P
PS(34:2)	758.4972	758.4968	**-0.5148**	**PS(16:1/18:1)**	C40H73NO10P
PS(36:2)	786.5285	786.5291	**0.7732**	**PS(18:1/18:1)**	C42H77NO10P
PS(36:3)	784.5129	784.5130	**0.1939**		C42H75NO10P
PS(36:4)	782.4972	782.4969	**-0.4423**		C42H73NO10P
PS(38:4)	810.5285	810.5281	**-0.5497**	**PS(18:0/20:4)**	C44H77NO10P
PS(40:5)	836.5442	836.5440	**-0.2912**	**PS(18:0/22:5)**	C46H79NO10P
PS(40:6)	834.5285	834.5286	**0.1038**	**PS(18:0/22:6)**	C46H77NO10P

Table 8. SM lipid species identified in HC11 cells.

Lipid Species (C:N)	Calculated m/z	Observed m/z	Error (ppm)	Fatty acyl chains (C:N)	Formula
SM(d30:1)	647.5128	647.5134	**0.8495**		C35H72N2O6P
SM(d32:0)	677.5598	677.5597	**-0.1234**		C37H78N2O6P

SM(d32:1)	675.5441	675.5441	**0.0036**	**SM(d18:1/14:0)**	C37H76N2O6P
SM(d34:0)	705.5911	705.5908	**-0.3191**		C39H82N2O6P
SM(d34:1)	703.5754	703.5753	**-0.1346**	**SM(d18:1/16:0)**	C39H80N2O6P
SM(d34:2)	701.5598	701.5586	**-1.6337**		C39H78N2O6P
SM(d36:0)	733.6224	733.6212	**-1.6145**		C41H86N2O6P
SM(d36:1)	731.6067	731.6061	**-0.8238**	**SM(d18:1/18:0)**	C41H84N2O6P
SM(d36:2)	729.5911	729.5909	**-0.1844**		C41H82N2O6P
SM(d36:3)	727.5754	727.5741	**-1.8374**		C41H80N2O6P
SM(d38:1)	759.6380	759.6375	**-0.6723**		C43H88N2O6P
SM(d38:2)	757.6224	757.6213	**-1.4512**	**SM(d18:1/20:1)**	C43H86N2O6P
SM(d40:1)	787.6693	787.6680	**-1.6157**	**SM(d18:1/18:2)**	C45H92N2O6P
SM(d40:2)	785.6537	785.6528	**-1.1254**		C45H90N2O6P
SM(d40:3)	783.6380	783.6358	**-2.7834**		C45H88N2O6P
SM(d42:1)	815.7006	815.7008	**0.2416**	**SM(d18:1/24:1)**	C47H96N2O6P
SM(d42:2)	813.6850	813.6835	**-1.8163**		C47H94N2O6P
SM(d42:3)	811.6693	811.6681	**-1.4619**		C47H92N2O6P
SM(d44:1)	843.7319	843.7303	**-1.9047**		C49H100N2O6P
SM(d44:2)	841.7163	841.7157	**-0.6204**		C49H98N2O6P

Table 9. Cer and HexCer lipid species identified in HC11 cells.

Lipid Species (C:N)	**Calculated m/z**	**Observed m/z**	**Error (ppm)**	**Fatty acyl chains (C:N)**	**Formula**
Cer(d34:1)	538.5199	538.5195	**-0.8540**	**Cer(d18:1/16:0)**	C34H68NO3
Cer(d34:2)	536.5043	536.5056	**2.4206**		C34H66NO3
Cer(d36:1)	566.5512	566.5516	**0.6251**		C36H72NO3
Cer(d38:1)	594.5825	594.5820	**-0.8365**		C38H76NO3
Cer(d40:1)	622.6138	622.6135	**-0.4582**	**Cer(d18:1/22:0)**	C40H80NO3
Cer(d40:2)	620.5982	620.5983	**0.1847**	**Cer(d18:2/22:0)**	C40H78NO3
Cer(d42:1)	650.6451	650.6448	**-0.4897**	**Cer(d18:1/24:0)**	C42H84NO3
Cer(d42:2)	648.6295	648.6291	**-0.5211**		C42H82NO3
Cer(d44:1)	678.6764	678.6759	**-0.7312**	**Cer(d18:1/26:0)**	C44H88NO3
Cer(d44:2)	676.6608	676.6609	**0.1448**		C44H86NO3
HexCer(d18:0/16:0)	702.5884	702.5870	**-1.9550**		C40H80NO8
GlcCer(d18:1/14:0)/GlcCer(d18:0/14:1)/GlcCer(d14:1/18:0)	672.5414	672.5406	**-1.2339**		C38H74NO8
HexCer(d18:1/16:0)/GlcCer(d14:1/20:0)/GlcCer(d16:1/18:0)	700.5727	700.5727	**-0.0676**	**HexCer(d18:1/16:0)**	C40H78NO8
HexCer(d18:1/18:0)/GlcCer(d18:0/18:1/GlcCer(d14:1/22:0)/GlcCer(d16:1/20:0)	728.6040	728.6025	**-2.1793**		C42H82NO8
HexCer(d18:1/20:0)/HexCer(d16:1/22:0)/GlcCer(d14:1/24:0)	756.6353	756.6354	**0.1367**		C44H86NO8

HexCer(d18:1/22:0)/GlcCer(d16:1/24:0)	784.6666	784.6660	**-0.8044**	**HexCer(d18:1/22:0)**	C46H90NO8
HexCer(d18:1/24:0)/GlcCer(d18:0/24:1)	812.6979	812.6964	**-1.8418**	**HexCer(d18:1/24:0)**	C48H94NO8
GlcCer(d18:1/24:1(15Z))/GalCer(d18:1/24:1)	810.6823	810.6812	**-1.3285**	**HexCer(d18:1/24:1)**	C48H92NO8
HexCer(d18:1/26:0)/HexCer(d18:0/26:1)	840.7292	840.7259	**-3.9368**	**HexCer(d18:1/26:0)**	C50H98NO8
HexCer(d18:1/26:1(17Z))	838.7136	838.7112	**-2.8569**		C50H96NO8
HexCer(d18:2/16:0)/GlcCer(d14:2/20:0)/GlcCer(d16:2/18:0)	698.5571	698.5574	**0.4201**		C40H76NO8
HexCer(d18:2/22:0)/GlcCer(d16:2/24:0)	782.6510	782.6504	**-0.7126**		C46H88NO8
LacCer(d18:1/24:0)/LacCer(d18:0/24:1)	974.7508	974.7505	**-0.2356**		C54H104NO13

Table 10. PI lipid species identified in HC11 cells.

Lipid Species (C:N)	Calculated m/z	Observed m/z	Error (ppm)	Fatty acyl chains (C:N)	Formula
PI(30:0)	781.4867	781.4863	**-0.5530**		C39H74O13P
PI(30:1)	779.4711	779.4698	**-1.6217**		C39H72O13P
PI(30:2)	777.4554	777.4555	**0.0964**		C39H70O13P
PI(32:1)	807.5024	807.5024	**-0.0518**	**PI(16:1/16:0)**	C41H76O13P
PI(32:2)	805.4867	805.4863	**-0.5047**	**PI(16:1/16:1)**	C41H74O13P
PI(34:1)	835.5337	835.5334	**-0.3490**	**PI(16:0/18:1), PI(16:1/18:0)**	C43H80O13P
PI(34:2)	833.5180	833.5181	**0.0797**	**PI(16:1/18:1)**	C43H78O13P
PI(34:3)	831.5024	831.5022	**-0.2206**	**PI(16:0/18:3), PI(16:1/18:2)**	C43H76O13P
PI(36:1)	863.5650	863.5637	**-1.5553**	**PI(18:1/18:0)**	C45H84O13P
PI(36:2)	861.5493	861.5488	**-0.6218**	**PI(18:1/18:1)**	C45H82O13P
PI(36:3)	859.5337	859.5332	**-0.6329**	**PI(16:0/20:3), PI(18:1/18:2), PI(18:0/18:3)**	C45H80O13P
PI(36:4)	857.5180	857.5171	**-1.0355**	**PI(16:0/20:4), PI(18:1/18:3)**	C45H78O13P
PI(36:5)	855.5024	855.5025	**0.0839**	**PI(16:0/20:5), PI(16:1/20:4), PI(18:3/18:2), PI(18:1/18:4)**	C45H76O13P
PI(38:2)	889.5806	889.5774	**-3.5986**		C47H86O13P
PI(38:3)	887.5650	887.5636	**-1.5226**	**PI(18:0/20:3)**	C47H84O13P
PI(38:4)	885.5493	885.5487	**-0.6362**	**PI(18:0/20:4), PI(18:1/20:3)**	C47H82O13P

PI(38:5)	883.5337	883.5332	**-0.5278**	**PI(18:0/20:5), PI(18:1/20:4)**	C47H80O13P
PI(38:6)	881.5180	881.5173	**-0.7839**	**PI(16:0/22:6), PI(18:1/20:5), PI(18:2/20:4)**	C47H78O13P
PI(40:2)	917.6119	917.6080	**-4.1988**	**PI(18:1/22:1), PI(18:0/22:2)**	C49H90O13P
PI(40:3)	915.5963	915.5964	**0.1078**	**PI(18:1/22:2), PI(18:0/22:3)**	C49H88O13P
PI(40:4)	913.5806	913.5789	**-1.8141**		C49H86O13P
PI(40:5)	911.5650	911.5639	**-1.1592**		C49H84O13P
PI(40:6)	909.5493	909.5484	**-1.0371**		C49H82O13P
PI(40:7)	907.5337	907.5337	**-0.0033**		C49H80O13P

Table 11. CL lipid species identified in HC11 cells.

Lipid Species (C:N)	Calculated m/z	Observed m/z	Error (ppm)	Fatty acyl chains (C:N)	Formula
CL(66:2)	1375.9640	1375.9587	**-3.8874**	**CL(16:1/16:0/16:0/18:1)**	C75H141O17P2
CL(68:1)	1406.0110	1406.0069	**-2.9302**		C77H147O17P2
CL(68:2)	1403.9960	1403.9946	**-1.0240**		C77H145O17P2
CL(68:3)	1401.9800	1401.9758	**-2.9950**	**CL(16:1/18:1/16:1/18:0)**	C77H143O17P2
CL(68:4)	1399.9640	1399.9616	**-1.7119**	**CL(16:1/18:1/16:1/18:1**	C77H141O17P2
CL(70:3)	1430.0110	1430.0065	**-3.1792**	**CL(18:0/18:1/16:1/18:1)**	C79H147O17P2
CL(70:4)	1427.9960	1427.9928	**-2.2618**	**CL(18:0/18:2/16:1/18:1)**	C79H145O17P2
CL(70:5)	1425.9800	1425.9764	**-2.5546**	**CL(18:1/18:2/16:1/18:1)**	C79H143O17P2
CL(70:6)	1423.9640	1423.9635	**-0.3427**	**CL(18:1/18:2/16:1/18:2)**	C79H141O17P2
CL(72:4)	1456.0270	1456.0265	**-0.3684**	**CL(18:1/18:1/18:1/18:1)**	C81H149O17P2
CL(72:5)	1454.0110	1454.0130	**1.3549**	**CL(18:2/18:1/18:1/18:1)**	C81H147O17P2
CL(72:6)	1451.9960	1451.9900	**-4.1647**	**CL(18:2/18:1/18:2/18:1)**	C81H145O17P2
CL(72:7)	1449.9800	1449.9750	**-3.4460**	**CL(18:2/18:1/18:2/18:2)**	C81H143O17P2
CL(72:8)	1447.9640	1447.9597	**-2.9849**		C81H141O17P2
CL(74:7)	1478.0110	1478.0081	**-1.9733**	**CL(20:2/18:2/18:1/18:2)**	C83H147O17P2
CL(74:8)	1475.9960	1475.9915	**-3.0378**		C83H145O17P2
CL(74:9)	1473.9800	1473.9748	**-3.5553**		C83H143O17P2

3.1.4 Changes in the phospholipidome of HC11 cells during differentiation

After the identification of all lipid species, peak integration and normalization to the internal standard added per class was performed. This allowed the relative quantitation of the lipid abundances in the different cell differentiation stages. Data obtained from the HILIC-MS

analysis showed an evolution of the phospholipidome of these cells throughout the differentiation process. Firstly, the number of total carbons on the fatty acid chains of the quantified phospholipids (calculated by the sum of the lipid species with the same number of carbons) seemed to slightly increase with differentiation. Even though no significant differences between carbon numbers were found using the applied statistical methods, these results are in agreement with our previous study in the same cell stages but without DMSO[17]. A tendency to increase is visible, particularly in PL containing 36 carbons (Figure 32).

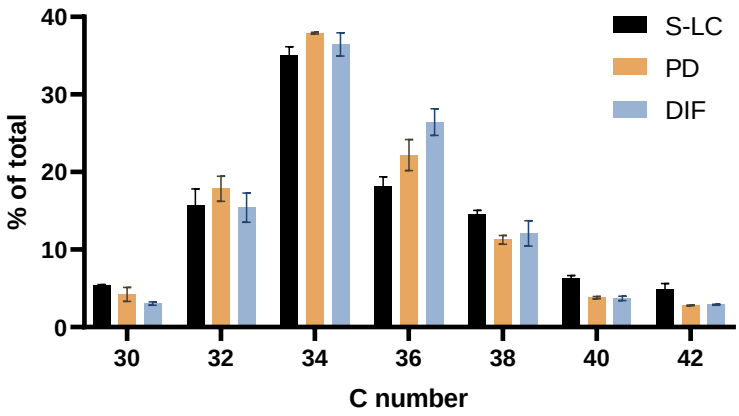

Figure 32. Carbon (C) numbers in the fatty acid chains of detected phospholipid species using HILIC-MS, in the differentiation states of HC11 cells treated with DMSO for 24h (black: stem-like cells; brown: pre-differentiated cells; blue: differentiated cells). Error bars represented as mean±SD. (n=2)

It was interesting to observe that in PC, for example, the most abundant species were PC(32:1) and PC(34:1) in the S-LC state, while in the differentiated state, PC(O-32:1) and PC(O-34:1) were the most abundant. A broad overview of all analysed classes showed that the relative amount of plasmanyl/plasmenyl PL species tends to increase with differentiation (Figure 33), peaking at nearly 45% of the total PL in differentiated cells.

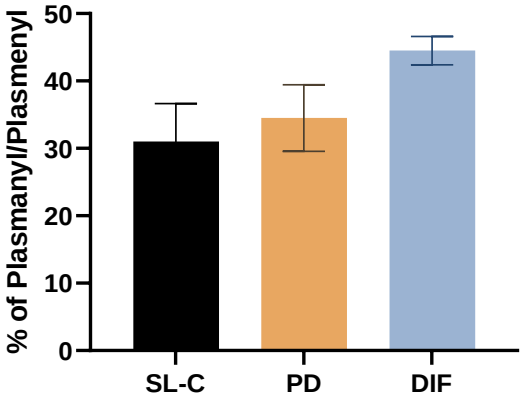

Figure 33. Relative amount of plasmanyl/plasmenyl PL, across differentiation states of HC11 cells treated with DMSO for 24h (black: stem-like cells; brown: pre-differentiated cells; blue: differentiated cells). Error bars represented as mean±SD. (n=2)

The sum of the lipid species with the same number of double bonds (from none to 7) showed that the total number of double bonds seemed to increase in differentiated cells, despite no significant differences (Figure 34). A tendency to increase the 2 and 3 double bond-containing PL and lower the monounsaturated chains seems to be present, which was also in agreement with our previous study[17].

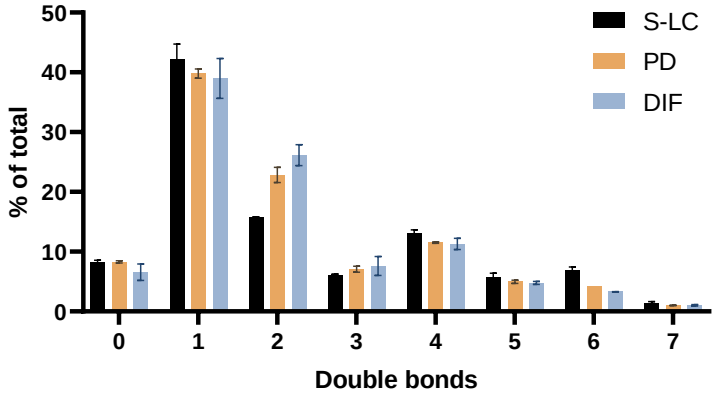

Figure 34. Sum of the lipid species with the same number of double bonds (from 0 to 7) of detected lipid species using HILIC-MS, across differentiation states of HC11 cells treated with DMSO for 24h (black: stem-like cells; brown: pre-differentiated cells; blue: differentiated cells). Error bars represented as mean±SD. (n=2)

The profile of the most abundant (>1%) PE, PC and SM is presented in Figure 35 to Figure 37. The full quantified profiles can be found in Supplementary Figures 1 to 12. Clear changes are noticeable on almost every lipid species. This demonstrates the continuous changing occurs on the lipidome of these cells during differentiation, shaping it according to the cellular needs and characteristics.

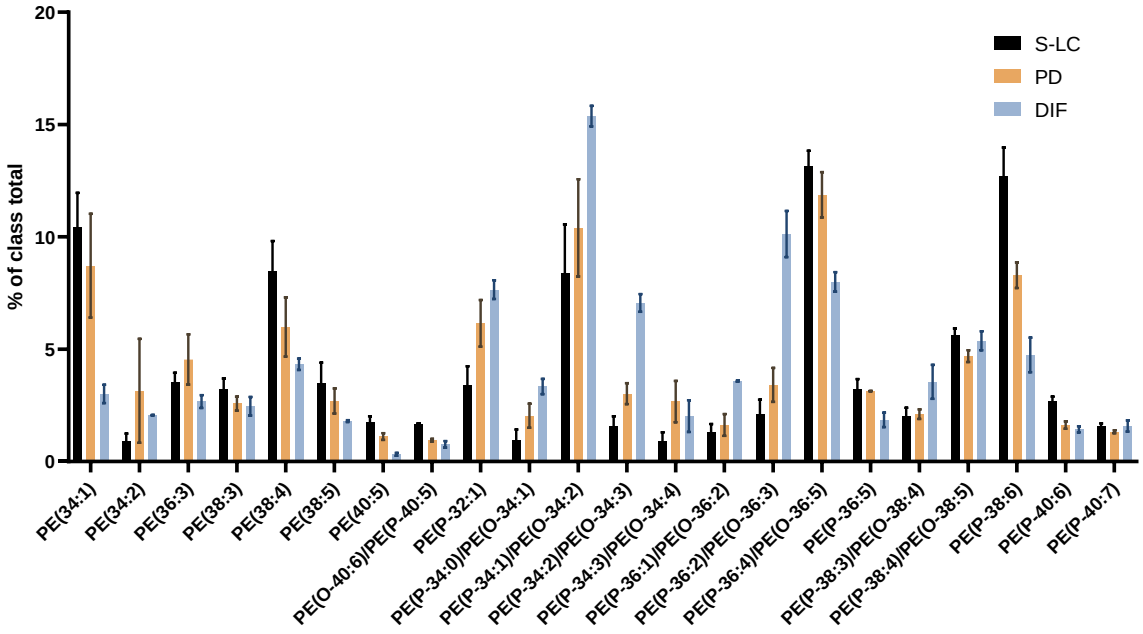

Figure 35. Phosphatidylethanolamine profile of HC11 cells treated with DMSO for 24h (only PE representing >1% of total PE are shown. Black: stem-like cells; brown: pre-differentiated cells; blue: differentiated cells). Error bars represented as mean±SD. (n=2)

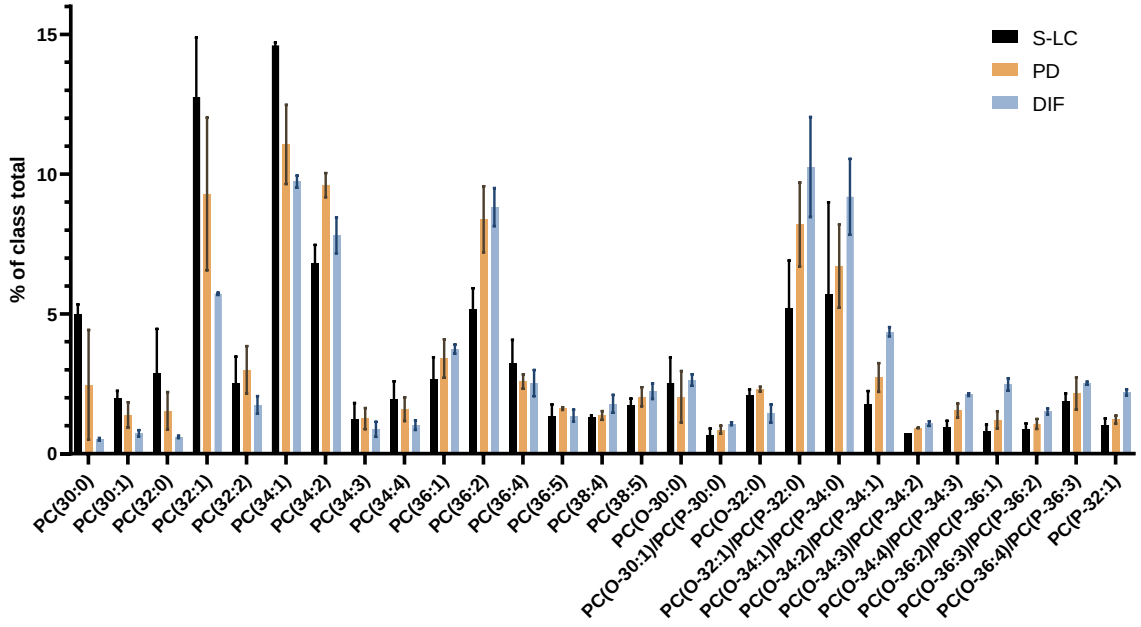

Figure 36. Phosphatidylcholine profile of HC11 cells treated with DMSO for 24h (only PC representing >1% of total PC are shown. Black: stem-like cells; brown: pre-differentiated cells; blue: differentiated cells). Error bars represented as mean±SD. (n=2)

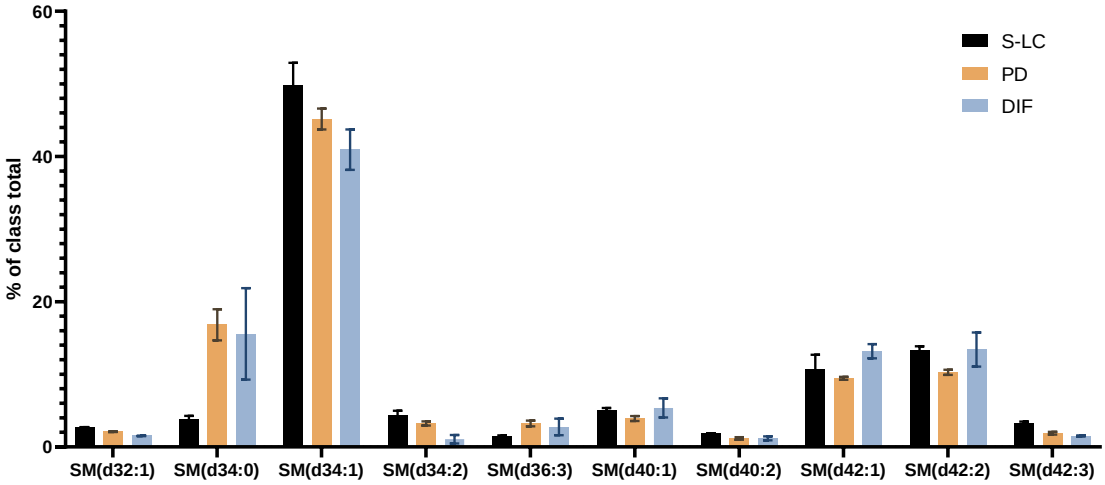

Figure 37. Sphingomyelin profile of HC11 cells treated with DMSO for 24h (Black: stem-like cells; brown: pre-differentiated cells; blue: differentiated cells). Error bars represented as mean±SD. (n=2)

3.1.5 Fatty acid profile

With the intent to further analyse the differences on the PL profile, specifically the variations on the fatty acid chains of the PL from differentiating HC11 cells, GC-MS was used to separate, identify, and quantify FA after alkaline hydrolysis of the lipid extracts. As observed previously, as cells differentiate, the number of double bonds on FA seems to increase. Accordingly, the relative amount of C14:0, C16:0 and C18:0 tends to decrease with differentiation, and monounsaturated fatty acids tend to increase, particularly C18:1 (Figures Figure 38 and Figure 39). This is in line with the previous observation on the increase on 36-carbon PL, since most of these are composed of C16 and C18 fatty acids.

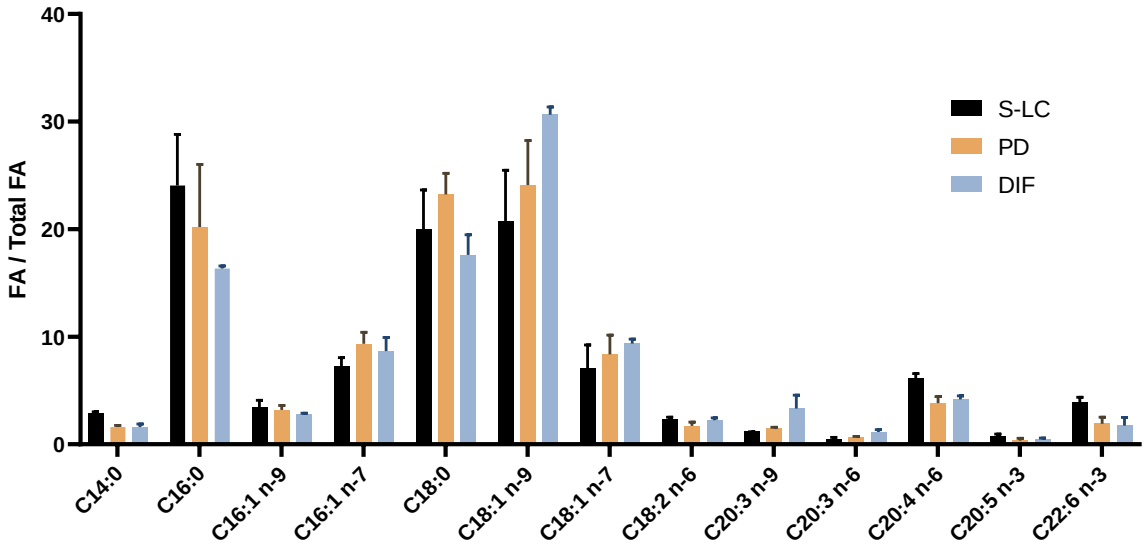

Figure 38. Fatty acid profile of HC11 cells treated with DMSO for 24h (Black: stem-like cells; brown: pre-differentiated cells; blue: differentiated cells). Error bars represented as mean±SD. (n=2)

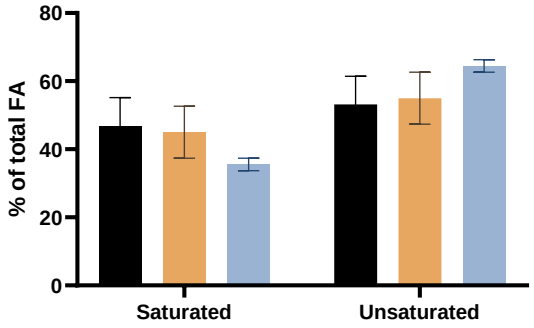

Figure 39. Variation of FA saturation/unsaturation during the differentiation of HC11 cells (Black: stem-like cells; brown: pre-differentiated cells; blue: differentiated cells). Error bars represented as mean±SD. (n=2)

3.2 Effects of SETD7 catalytic inhibition on the Lipidome of HC11 Cells after a 24-hour treatment with (R)-PFI-2

3.2.1 Phospholipid Classes

A screening of the lipidome of HC11 cells (S-LC, PD and DIF) was performed on the lipid extracts of cells treated with (R)-PFI-2 for 24 hours, with the goal of assessing the changes induced by the inhibition of SETD7 activity. To study this effect on the PL classes, TLC was performed (Figure 40). The catalytic inhibition of SETD7 after 24-hour treatment with (R)-PFI-2 led to a significant increase of PC and decrease in PA and PS in S-LC. Differentiated cells showed no remarkable changes.

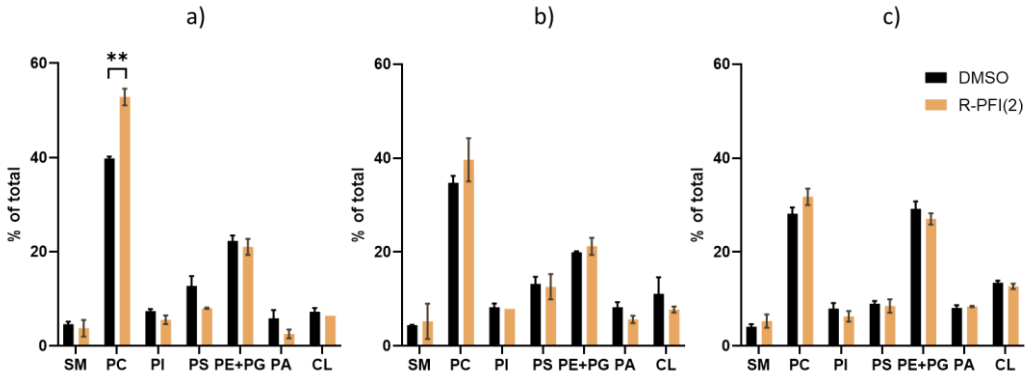

Figure 40. Lipid class profile of HC11 cells, quantified by thin layer chromatography, after 24-hour treatment with DMSO (black) or R-PFI(2) (brown) on a) stem-like cells, b) pre-differentiated cells and c) differentiated cells. ** statistical significance ($p<0.01$) after t-test. Error bars represented as mean±SD. (n=2)

The PC/PE (cylindrical/conic-shaped) ratio, which was progressively lowered during differentiation, seems to be increased with the (R)-PFI-2 treatment, in proliferative S-LC (Figure 41). This suggests an enhancing effect of SETD7 inhibition on the synthesis of PC, important constituent of membrane structures. As proliferative cells, S-LC are expected to present a high cylindrical/conic-shaped ratio, which then lowers with the increment on secretory function.

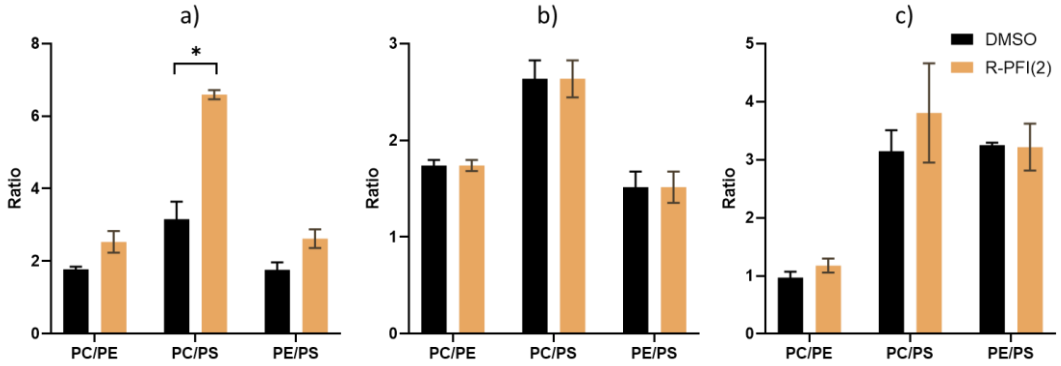

Figure 41. Ratio between PL species known to be in high proportion in the plasma membrane and metabolically interconverted, after 24-hour treatment with DMSO (black) or R-PFI(2) (brown) on a) stem-like cells, b) pre-differentiated cells and c) differentiated cells. * statistical significance ($p<0.05$) after t-test. Error bars represented as mean±SD. (n=2)

3.2.2 Lipidomics analysis with LC-MS

The analysis on the changes inducted by the inhibition of SETD7 activity on the profile of lipid species of MECs was performed following the previously described methods. After quantification and normalization by the internal standards, no significant differences were found between the control and treatment groups using univariate statistical analysis regarding the number of carbons (Figure 42) and double bonds (Figure 43). 34 and 36-carbon containing PL remained the most abundant, as well as the monounsaturated species, which were increased with differentiation, as previously determined.

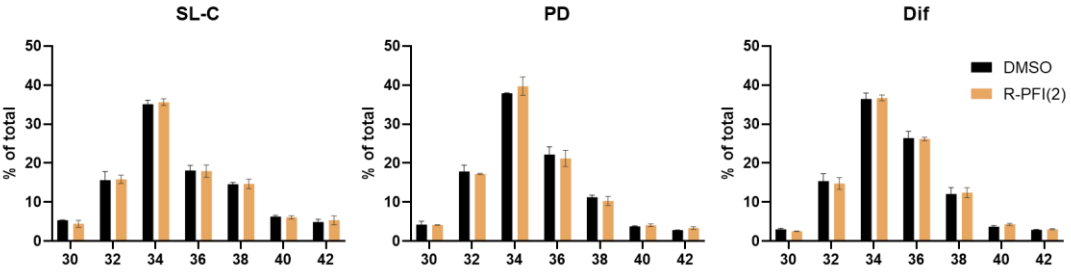

Figure 42. Sum of the lipid species with the same carbon number on detected lipid species using HILIC-MS, across differentiation states of HC11 cells after 24-hour treatment with DMSO (black) or R-PFI(2) (brown). Differences between groups non-significant after t-test. Error bars represented as mean±SD. (n=2)

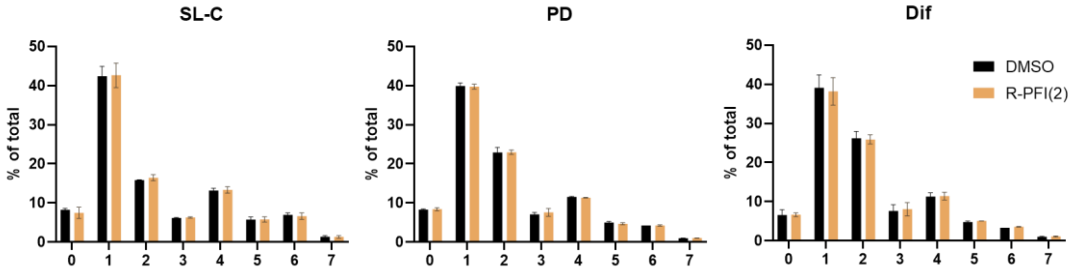

Figure 43. Sum of the lipid species with the same number of double bonds on detected lipid species using HILIC-MS, across differentiation states of HC11 cells after 24-hour treatment with DMSO (black) or R-PFI(2) (brown). Differences between groups non-significant t-test. Error bars represented as mean±SD. (n=2)

No significant differences were found between the control and treatment groups regarding the relative amount of lipid species for each studied class, as the tendencies observed with differentiation were unaffected. Figure 44 to Figure 46 illustrate the profile of PE, PC and SM, after the 24h treatment, as example. No significant changes were detected in any class, which was unexpected considering previous evidence. We next focused on the fatty acid profile and the gene expression, to further assess the impact of the inhibition of the catalytic activity of SETD7.

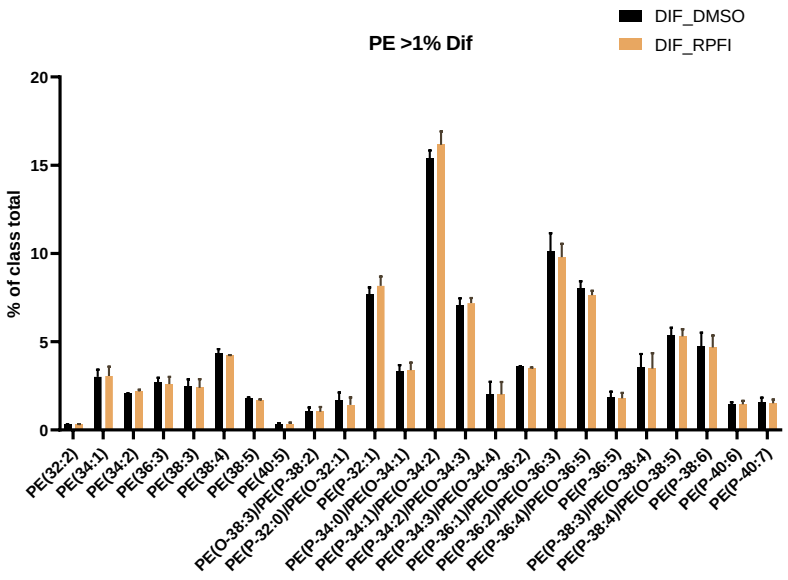

Figure 44. Phosphatidylethanolamine profile of differentiated HC11 cells treated with DMSO (black) and (R)-PFI-2 (brown) for 24h (only PE representing >1% of total PE are shown). Differences between groups non-significant after Mann-Whitney non-parametric t-test. Error bars represented as mean±SD. (n=2)

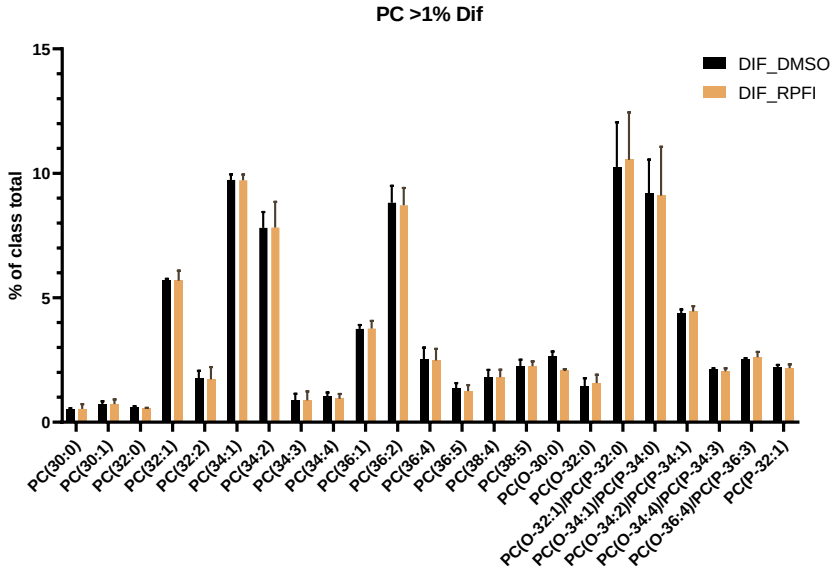

Figure 45. Phosphatidylcholine profile of differentiated HC11 cells treated with DMSO (black) and (R)-PFI-2 (brown) for 24h (only PC representing >1% of total PE are shown). Differences between groups non-significant after Mann-Whitney non-parametric t-test. Error bars represented as mean±SD. (n=2)

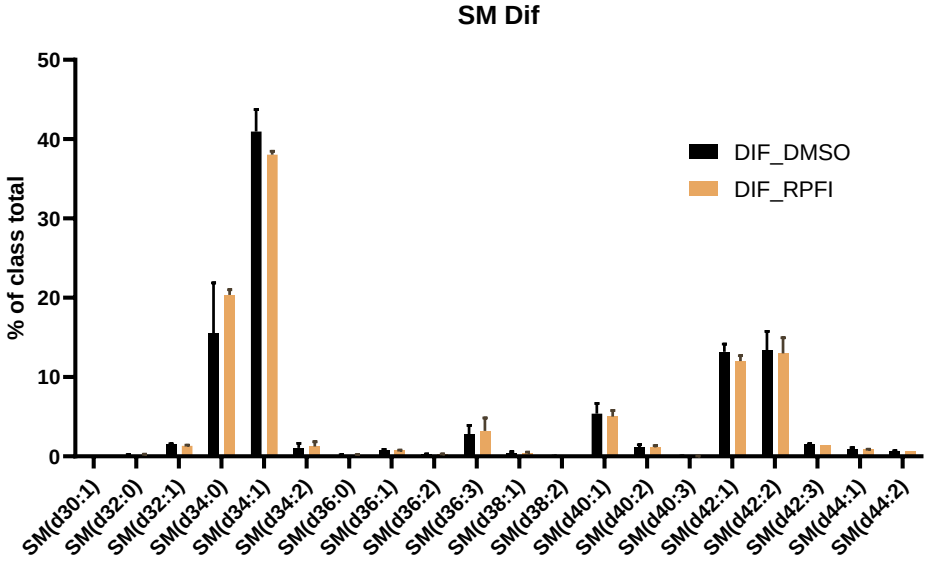

Figure 46. Sphingomyelin profile of differentiated HC11 cells treated with DMSO (black) and (R)-PFI-2 (brown) for 24h. Differences between groups non-significant after Mann-Whitney non-parametric t-test. Error bars represented as mean±SD. (n=2)

3.2.3 Fatty acid profile

To finalize the analysis on the 24-hour treatment, GC-MS was used to assess the fatty acid profile of the lipid extracts (Figure 47 to Figure 49). The differentiation state presenting the most changes after SETD7 inhibition was PD, with a significant decrease on C18:0, and a tendency to increase in monounsaturated fatty acids C18:1 ω7 and ω9 (Figure 48). No remarkable differences were found on either S-LC or Dif cells, suggesting no significant effect of SETD7 inhibition on FA metabolism after 24-h treatment with (R)-PFI-2. The tendencies verified during differentiation were maintained, with a reduction on C16 and C18, and an increase on C18:1 ω9, que most abundant fatty acid in differentiated cells.

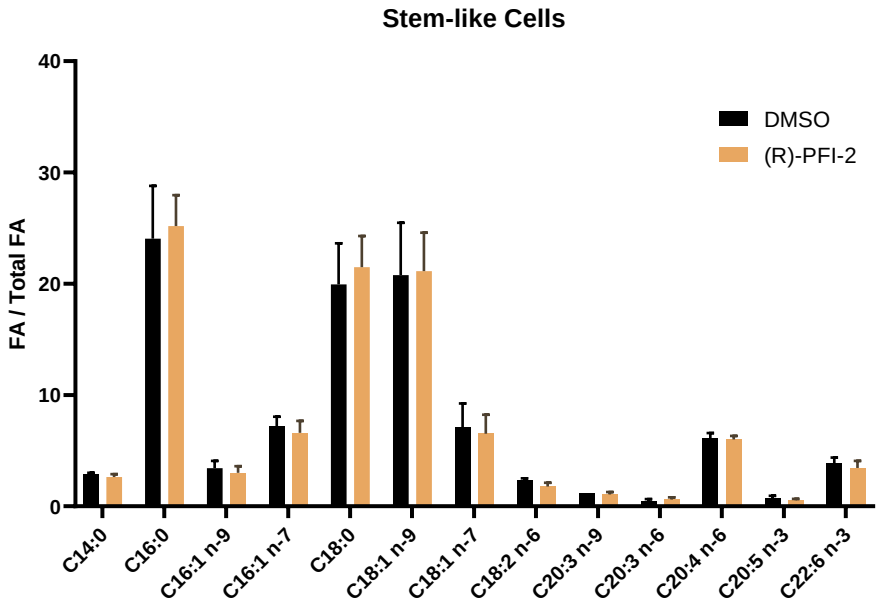

Figure 47. Fatty acid profile of stem-like HC11 cells treated with DMSO (black) or (R)-PFI-2 (brown) for 24h. Differences non-significant after t-test. Error bars represented as mean±SD. (n=2)

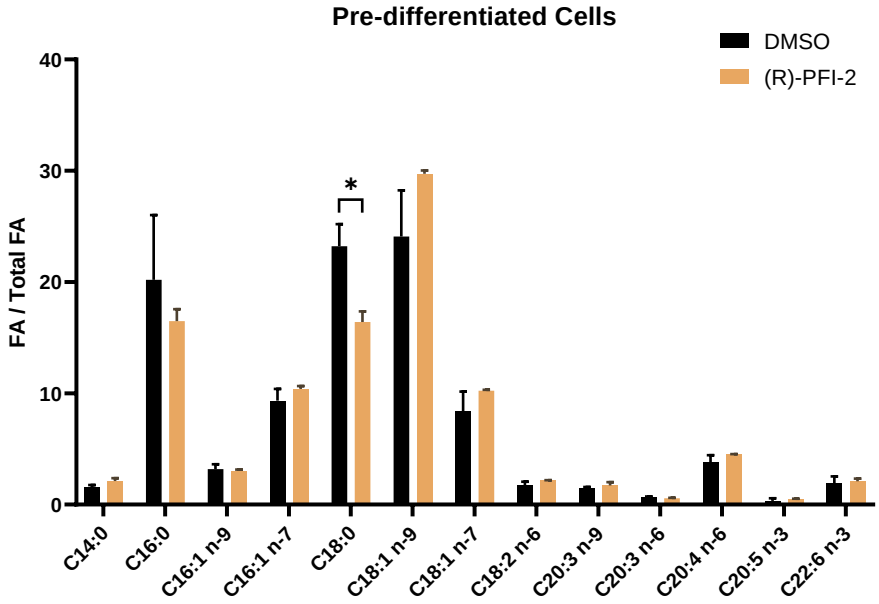

Figure 48. Fatty acid profile of pre-differentiated HC11 cells treated with DMSO (black) or (R)-PFI-2 (brown) for 24h. * $p < 0.05$ after t-test. Error bars represented as mean±SD. (n=2)

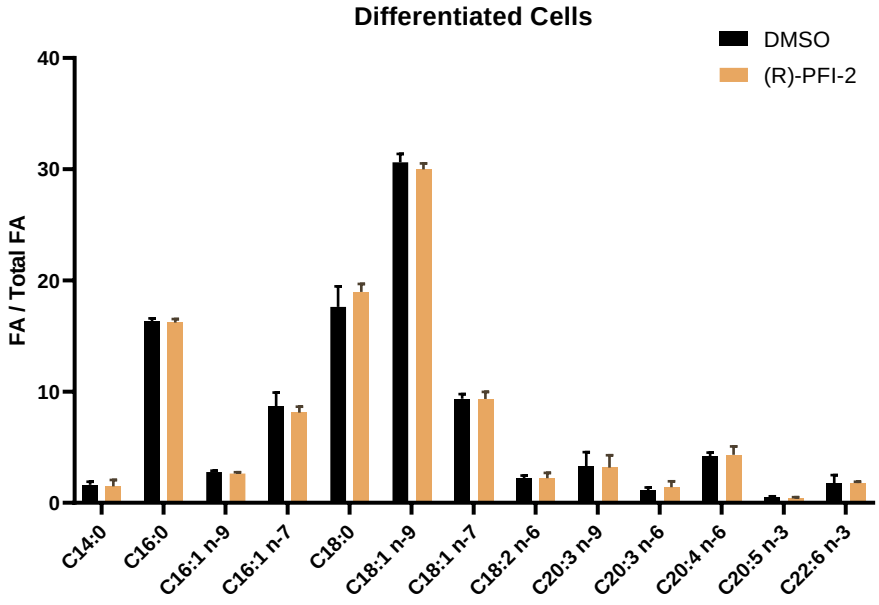

Figure 49. Fatty acid profile of differentiated HC11 cells treated with DMSO (black) or (R)-PFI-2 (brown) for 24h. Differences non-significant after t-test. Error bars represented as mean±SD. (n=2)

3.2.4 The effects of SETD7 inhibition on gene expression

In order to assess the effect of SETD7 inhibition on the gene expression of certain key players of lipid metabolism, particularly, genes involved in fatty acid synthesis, RT-PCR was used to study the relative changes in expression of lipid metabolism genes. The results were normalized using the ribosomal protein S18 mRNA as housekeeping gene. It was found that with differentiation, the expression of elongases Elovl5/6 increases, which may be related to the increase in C18 and C20:3ω6 (Figure 50). The oxygenases Acox1/3 increase as well. The expression of desaturase Fads1 increases on PD cells but was reduced in differentiated cells, which is possibly connected to the decrease C20:4ω6 and C20:5ω3. Additionally, FA synthase (Fasn) increased as well, in line with the decrease in C14:0. The inhibition of SETD7 activity, however, had a variable effect on these expression levels (Figure 51). Despite no significant changes, the expression of Elovl5/6 tended to decrease, particularly on S-LC, which would impair the synthesis of longer FA in this state. Expression of Fads remained relatively unaltered, and Acox1/3 tended to increase on S-LC and PD cells but lowered on fully differentiated cells, also affecting the synthesis of LC-FA. FASN followed a similar tendency and was decreased on PD and DIF cells. Previous results from our group showed an increase in Chpt1 and Pcyt2 during differentiation (unpublished work). However, the inhibition of SETD7 led to a decrease in the expression of Pcyt2 in differentiated cells, and a further increase in the expression of Chpt1. These can be found in Supplementary Figure 13.

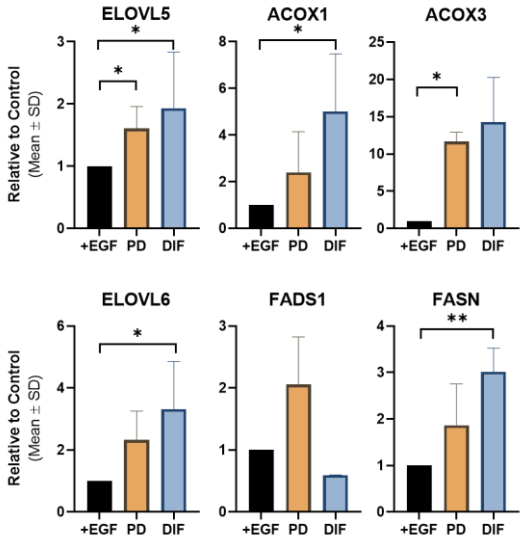

Figure 50. Expression of genes involved in fatty acid synthesis, throughout differentiation of HC11 mammary epithelial stem-cells. *, ** statistical significance ($p<0.05$, $p<0.01$, respectively). n=4

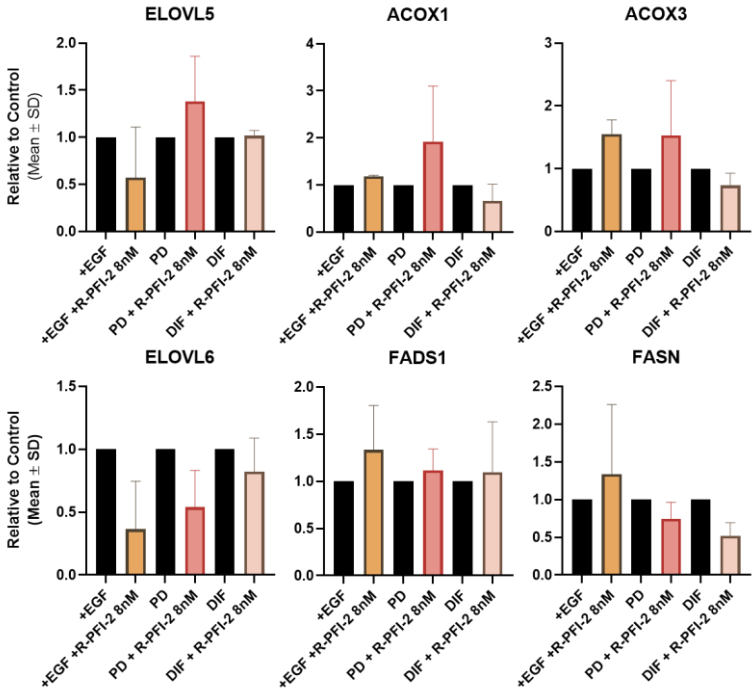

Figure 51. Expression of genes involved in fatty acid synthesis on HC11 mammary epithelial stem-cells, after treatment with DMSO (control) and (R)-PFI-2. n=4

3.3 The effects of SETD7 catalytic inhibition on the Lipidome of Differentiated HC11 cells after a 48-hour treatment with (R)-PFI-2

Previous evidence from our lab supported an important effect of SETD7 inhibition for 24h in HC11 mammary epithelial cells, particularly on the differentiated cells. However, the 24-hour treatment applied did not lead to significant changes. To further investigate this matter, and to enhance possible effects of SETD7 inhibition on functionally differentiated cells, a prolonged treating period with (R)-PFI-2 was used. Differentiated cells were studied due to the significance of their lipidome, and the importance of maintaining the integrity of their function, as well as the previous evidence supporting the loss of lactating phenotype, and its link to a worse prognosis in the event of BC.

3.3.1 Phospholipid Classes

To study the effect of SETD7 inhibition after the 48-hour treatment period on the PL classes, TLC was applied (Figure 52). The TLC separation was improved by removing the use of boric acid, which allowed for an enhanced partitioning of the PE and PG spots and benefited the overall analysis.

The 48-hour treatment with (R)-PFI-2 led to an increase of PC and decrease of SM (Figure 53). Although the differences were not significant, an increase in the ratio of cylindrical/conic species (PC/PE) was observed, which opposes the previous observations on the outcomes of differentiation (Figure 54). Multivariate analysis (Figure 55) showed a good group separation, further cementing the effects of SETD7 inhibition on PL metabolism on these cells. However, the Q^2 value of 0.20 suggests the model is not very robust, likely due to the low number of replicates. Significant correlations were observed between PC-PS ($r = -0.867$, $p = 0.025$), and between CL-PG ($r = -0.873$, $p = 0.023$). Albeit not significant, positive correlations between PI-PG and PI-PS were detected (0.80 and 0.74, respectively), as well as negative correlations between CL-PS, and PC-SM (-0.77 and -0.73, respectively), with p values < 0.10.

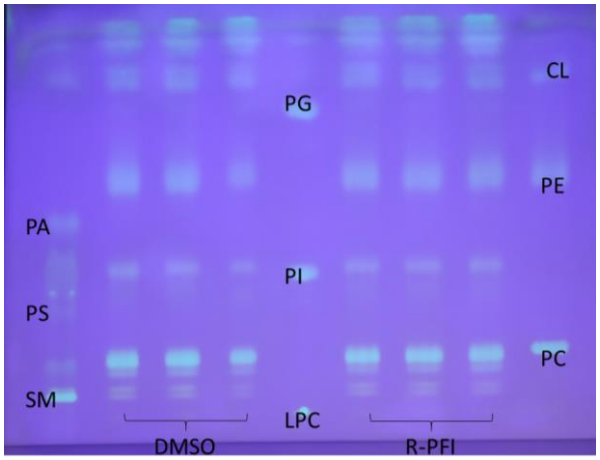

Figure 52. Thin layer chromatography plate of the lipid extract of HC11 cells. On the left, lipid extracts from differentiated cells treated with DMSO for 48 hours and on the right, that of HC11 differentiated cells treated with (R)-PFI-2 for 48 hours.

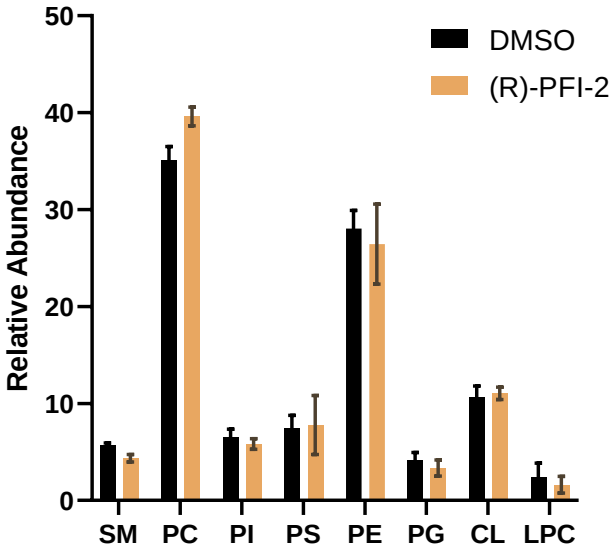

Figure 53. Variation of the relative amount of lipid classes under a 48-hour treatment of differentiated cells with DMSO (black) or (R)-PFI-2 (brown). Error bars represented as mean±SD. (n=3)

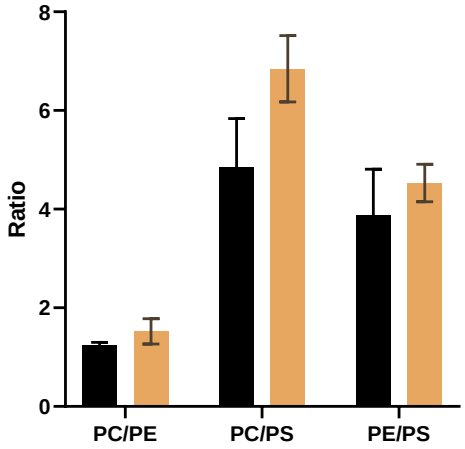

Figure 54. Ratio between PL classes known to be in high proportion in the plasma membrane and metabolically interconverted on differentiated cells. (black: differentiated cells treated with DMSO for a 48-hour period; brown: differentiated cells treated with (R)-PFI-2 for a 48-hour period). Error bars represented as mean±SD. (n=3)

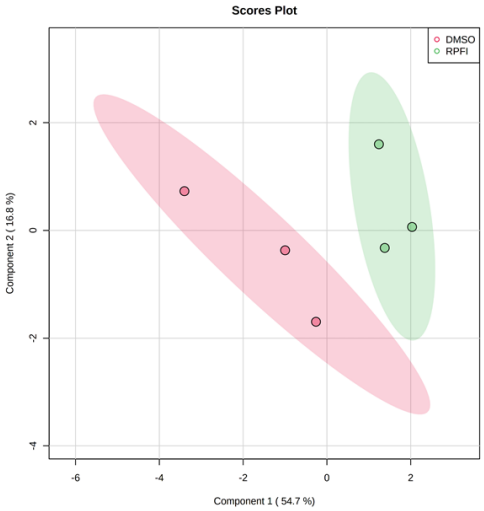

Figure 55. Multivariate analysis of PL classes profile assigned by TLC data collected for HC11 cells. PLS DA scores scatter plot, comparing cells treated with SETD7 specific inhibitor (R)-PFI-2 (green) and DMSO-treated controls (red).

3.3.2 Lipidomics analysis with LC-MS

As previously, mass spectrometry was used to identify and quantify lipid species. However, to better characterize the effects of SETD7 catalytic inhibition on the lipidome of

differentiated cells, a C18-MS approach was applied. C18 columns separate species depending on their acyl chain, and thus the quantification of individual molecular species is possible. Figure 56 shows a TIC from an LC-MS of the lipid extract.

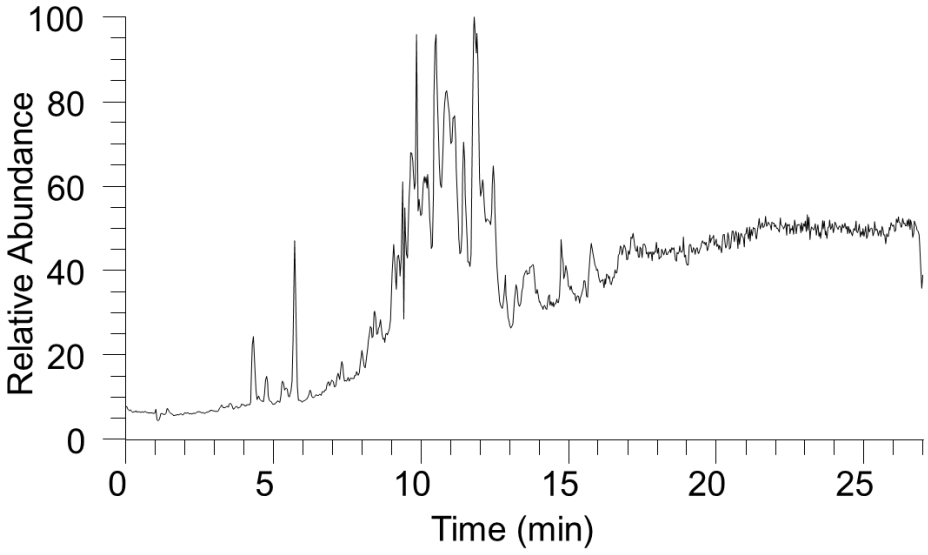

Figure 56. C18 negative mode total ion chromatogram of DMSO-treated (48h) (control) HC11 cells at the differentiated cell state.

3.3.3 Class Identification on C18-MS

Given the previously observed results from the TLC, the C18-MS analysis was focused solely on PC, PE, and SM classes. As mentioned previously, a reverse-phase C18 column separates the sample analytes according to polarity, primarily of their acyl chains. As such, longer acyl chains (N) from the same PL class eluted at higher retention time, and a higher number of unsaturations results in a lower RT, for the same carbon number. Despite the impossibility of assigning one single peak on the total ion chromatogram to a single class as was possible using HILIC, a C18 approach has the advantage of being able to quantify separate molecular species of the same lipid species. Using the previous HILIC technique, lipid species were quantified as a whole, and no distinction between separate molecular species with varying acyl chains was possible. The identification of all PL classes was performed according to the methods described for HILIC. However, given the use of

different mobile phases, PC and SM were detected as formate adducts in the negative mode, rather than acetate adducts.

Phosphatidylethanolamines were identified in positive ion mode as [M+H]+ ions and in the negative mode as [M-H]- ions. MS/MS data presented the typical neutral loss of 141, due to the loss of the polar head group. Moreover, negative ion mode MS/MS data allowed for the identification of the fatty acyl chains, which were quantified individually.

Sphingomyelins and phosphatidylcholines were identified as [M+H]+ ions in positive ion mode and [M+HCOO]- in the negative ion mode. Positive mode MS/MS spectra of both PC and SM were similar as the one reported previously and showed the typical fragment ion at *m/z* 184 and fragment ions of sphingoid bases in the SM spectral data. MS/MS data of PC in the negative mode contained the carboxylate anion of fatty acyl chains and allowed their identification as well. All the detected molecular species are presented in tables Table 12Table 14.

Table 12. PC and LPC molecular species identified in HC11 cells using C18-MS.

Lipid Species (C:N)	Calculated m/z	Observed m/z	Error (ppm)	Formula
LPC(16:0)	540.3301	**540.3320**	**3.3537**	C25H51NO9P
LPC(18:0)	568.3614	**568.3633**	**3.2175**	C27H55NO9P
LPC(18:1)	566.3458	**566.3477**	**3.3515**	C27H53NO9P
PC(30:0)	750.5285	**750.5281**	**-0.6065**	C39H77NO10P
PC(30:1)	748.5129	**748.5139**	**1.3229**	C39H75NO10P
PC(32:1)	776.5441	**776.5445**	**0.5373**	C41H79NO10P
PC(34:1)	804.5755	**804.5771**	**2.0134**	C43H83NO10P
PC(34:2)	802.5598	**802.5609**	**1.3927**	C43H81NO10P
PC(34:3)	800.5442	**800.5440**	**-0.1862**	C43H79NO10P
PC(36:1)	832.6068	**832.6089**	**2.5519**	C45H87NO10P
PC(36:2)	830.5911	**830.5926**	**1.8400**	C45H85NO10P
PC(36:3)	828.5755	**828.5768**	**1.6737**	C45H83NO10P
PC(36:4)	826.5598	**826.5610**	**1.4530**	C45H81NO10P
PC(38:2)	858.6224	**858.6236**	**1.4126**	C47H89NO10P
PC(38:3)	856.6068	**856.6098**	**3.6042**	C47H87NO10P
PC(38:4)	854.5911	**854.5925**	**1.5871**	C47H85NO10P
PC(38:5)	852.5755	**852.5762**	**0.8651**	C47H83NO10P
PC(O-30:0)	736.5492	**736.5500**	**1.0598**	C39H79NO9P
PC(O-30:1)/PC(P-30:0)	734.5336	**734.5353**	**2.3645**	C39H77NO9P
PC(O-32:0)	764.5805	**764.5830**	**3.1677**	C41H83NO9P

PC(O-32:1)/PC(P-32:0)	762.5649	**762.5660**	**1.4843**	C41H81NO9P
PC(O-32:2)/PC(P-32:1)	760.5492	**760.5522**	**3.8462**	C41H79NO9P
PC(O-34:1)/PC(P-34:0)	790.5962	**790.5975**	**1.6281**	C43H85NO9P
PC(O-34:2)/PC(P-34:1)	788.5805	**788.5803**	**-0.3412**	C43H83NO9P
PC(O-34:2)/PC(P-34:1)	788.5805	**788.5803**	**-0.2674**	C43H83NO9P
PC(O-34:3)/PC(P-34:2)	786.5649	**786.5680**	**3.9680**	C43H81NO9P
PC(O-34:4)/PC(P-34:3)	784.5492	**784.5505**	**1.5989**	C43H79NO9P
PC(O-36:1)/PC(P-36:0)	818.6275	**818.6299**	**2.8941**	C45H89NO9P
PC(O-36:2)/PC(P-36:1)	816.6118	**816.6132**	**1.6884**	C45H87NO9P
PC(O-36:3)/PC(P-36:2)	814.5962	**814.5973**	**1.3248**	C45H85NO9P
PC(O-36:4)/PC(P-36:3)	812.5805	**812.5836**	**3.8137**	C45H83NO9P
PC(O-36:5)/PC(P-36:4)	810.5649	**810.5664**	**1.8723**	C45H81NO9P
PC(O-38:1)/PC(P-38:0)	846.6588	**846.6609**	**2.4968**	C47H93NO9P
PC(O-38:2)/PC(P-38:1)	844.6431	**844.6453**	**2.6045**	C47H91NO9P
PC(O-38:5)/PC(P-38:4)	838.5962	**838.5968**	**0.6881**	C47H85NO9P

Table 13. PE and LPE molecular species identified in HC11 cells using C18-MS

Lipid Species (C:N)	**Calculated m/z**	**Observed m/z**	**Error (ppm)**	**Formula**
LPE(18:0)	480.3090	**480.3106**	**3.3122**	C23H47NO7P
LPE(18:1)	478.2934	**478.2950**	**3.3147**	C23H45NO7P
LPE(O-16:1)/LPE(P-16:0)	436.2828	**436.2841**	**3.0625**	C21H43NO6P
LPE(O-18:1)/LPE(P-18:0)	464.3141	**464.3144**	**0.6636**	C23H47NO6P
PE(32:0)	690.5074	**690.5092**	**2.6003**	C37H73NO8P
PE(32:1)	688.4917	**688.4931**	**2.0478**	C37H71NO8P
PE(32:2)	686.4760	**686.4776**	**2.3794**	C37H69O8NP
PE(34:0)	718.5387	**718.5399**	**1.6339**	C39H77NO8P
PE(34:1)	716.5230	**716.5235**	**0.6338**	C39H75NO8P
PE(34:2)	714.5070	**714.5076**	**0.8187**	C39H73NO8P
PE(36:1)	744.5543	**744.5539**	**-0.5965**	C41H79NO8P
PE(36:2)	742.5387	**742.5389**	**0.2808**	C41H77NO8P
PE(36:4)	738.5074	**738.5070**	**-0.5703**	C41H73NO8P
PE(38:2)	770.57	**770.5711**	**1.3901**	C43H81NO8P
PE(38:3)	768.5540	**768.5566**	**3.3709**	C43H79NO8P
PE(38:4)	766.5390	**766.5399**	**1.1637**	C43H77O8NP
PE(38:5)	764.5230	**764.5242**	**1.6247**	C43H75NO8P
PE(38:5)	764.5230	**764.5236**	**0.7790**	C43H75NO8P
PE(38:6)	762.5074	**762.5105**	**4.0793**	C43H73NO8P
PE(40:3)	796.5856	**796.5888**	**3.9623**	C45H83NO8P
PE(40:5)	792.5540	**792.5539**	**-0.1057**	C45H79O8NP
PE(40:6)	790.5387	**790.5387**	**0.0677**	C45H77NO8P
PE(40:7)	788.5230	**788.5226**	**-0.4656**	C45H75NO8P
PE(O-30:2)/PE(P-30:1)	644.4660	**644.4668**	**1.3054**	C35H67NO7P
PE(O-32:1)/PE(P-32:0)	674.5130	**674.5143**	**1.9297**	C37H73NO7P

PE(O-32:2)/PE(P-32:1)	672.4970	**672.4985**	**2.2415**	C37H71NO7P
PE(O-34:1)/PE(P-34:0)	702.5440	**702.5469**	**4.0844**	C39H77NO7P
PE(O-34:1)/PE(P-34:0)	702.5440	**702.5425**	**-2.1432**	C39H77NO7P
PE(O-34:2)/PE(P-34:1)	700.5280	**700.5303**	**3.2294**	C39H75NO7P
PE(O-34:3)/PE(P-34:2)	698.5130	**698.5158**	**3.9843**	C39H73NO7P
PE(O-34:4)/PE(P-34:3)	696.4970	**696.4979**	**1.3358**	C39H71NO7P
PE(O-34:4)/PE(P-34:3)	696.4970	**696.4980**	**1.3956**	C39H71NO7P
PE(O-34:5)/PE(P-34:4)	694.4810	**694.4806**	**-0.5532**	C39H69NO7P
PE(O-36:1)/PE(P-36:0)	730.5750	**730.5765**	**2.1205**	C41H81NO7P
PE(O-36:2)/PE(P-36:1)	728.5590	**728.5588**	**-0.2568**	C41H79NO7P
PE(O-36:3)/PE(P-36:2)	726.5440	**726.5446**	**0.8717**	C41H77NO7P
PE(O-36:4)/PE(P-36:3)	724.5281	**724.5284**	**0.4261**	C41H75NO7P
PE(O-36:4)/PE(P-36:3)	724.5281	**724.5285**	**0.4836**	C41H75NO7P
PE(O-36:5)/PE(P-36:4)	722.5130	**722.5134**	**0.5766**	C41H73NO7P
PE(O-36:6)/PE(P-36:5)	720.4970	**720.4974**	**0.5366**	C41H71NO7P
PE(O-38:2)/PE(P-38:1)	756.5910	**756.5922**	**1.5410**	C43H83NO7P
PE(O-38:3)/PE(P-38:2)	754.5750	**754.5754**	**0.5897**	C43H81NO7P
PE(O-38:3)/PE(P-38:2)	754.5750	**754.5756**	**0.7368**	C43H81NO7P
PE(O-38:3)/PE(P-38:2)	754.5750	**754.5757**	**0.9464**	C43H81NO7P
PE(O-38:4)/PE(P-38:3)	752.5590	**752.5597**	**0.9163**	C43H79NO7P
PE(O-38:4)/PE(P-38:3)	752.5590	**752.5597**	**0.9864**	C43H79NO7P
PE(O-38:5)/PE(P-38:4)	750.5440	**750.5439**	**-0.1106**	C43H77NO7P
PE(O-38:6)/PE(P-38:5)	748.5281	**748.5278**	**-0.4585**	C43H75NO7P
PE(O-38:6)/PE(P-38:5)	748.5281	**748.5278**	**-0.4363**	C43H75NO7P
PE(O-38:7)/PE(P-38:6)	746.5130	**746.5126**	**-0.5494**	C43H73NO7P
PE(O-38:7)/PE(P-38:6)	746.5130	**746.5122**	**-1.1217**	C43H73NO7P
PE(O-38:8)/PE(P-38:7)	744.4968	**744.4992**	**3.2096**	C43H71NO7P
PE(O-40:3)/PE(P-40:2)	782.6060	**782.6082**	**2.7491**	C45H85NO7P
PE(O-40:4)/PE(P-40:3)	780.5910	**780.5933**	**2.8938**	C45H83NO7P
PE(O-40:5)/PE(P-40:4)	778.5750	**778.5743**	**-0.9393**	C45H81NO7P
PE(O-40:6)/PE(P-40:5)	776.5594	**776.5592**	**-0.3371**	C45H79NO7P
PE(O-40:7)/PE(P-40:6)	774.5440	**774.5449**	**1.1400**	C45H77NO7P
PE(O-40:8)/PE(P-40:7)	772.5280	**772.5292**	**1.5638**	C45H75NO7P

Table 14. SM molecular species identified in HC11 cells using C18-MS

Lipid Species (C:N)	Calculated m/z	Observed m/z	Error (ppm)	Formula
SM(d32:1)	675.5441	**675.5470**	**4.2295**	C37H76N2O6P
SM(d34:0)	705.5911	**705.5928**	**2.4968**	C39H82N2O6P
SM(d34:1)	703.5754	**703.5754**	**-0.0399**	C39H80N2O6P
SM(d36:1)	731.6067	**731.6071**	**0.5682**	C41H84N2O6P
SM(d40:1)	787.6693	**787.6703**	**1.2179**	C45H92N2O6P
SM(d42:1)	815.7006	**815.7011**	**0.5536**	C47H96N2O6P
SM(d42:2)	813.6850	**813.6858**	**1.0596**	C47H94N2O6P

3.3.4 Effects of SETD7 catalytic Inhibition on Differentiated HC11 Cells

SETD7 inhibition after a longer treatment led to differences in the lipidome of differentiated cells. Particularly, a decrease was verified on PC(18:0/18:1), PC(18:1/20:4), PE(18:0/22:3), PE(O-18:2/22:6), PE(O-18:2/20:5), PE(O-16:1/20:1) and SM(d36:1) (Figure 60). In all cases, the inhibition led to a decrease in the number of molecular species, and not a single increase was verified, which suggests an involvement of SETD7 on the synthesis of PL, as shown in figures Figure 57 to Figure 59. The effect size of most lipid species was not significant. However, 26 molecular species presented an ES>1, despite a considerable error (>1.2 in all cases). All of these were negative, thus indicating a negative change after SETD7 inhibition.

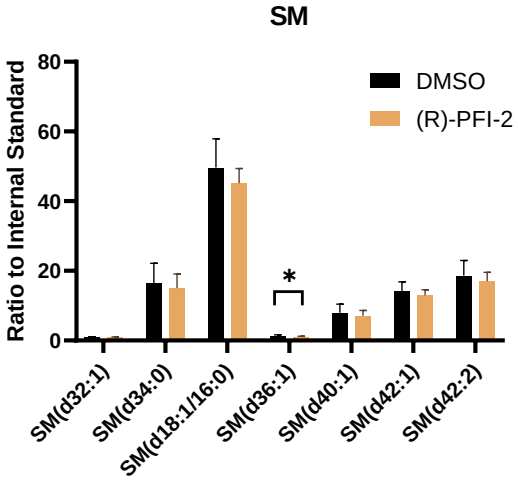

Figure 57. Sphingomyelin profile of differentiated HC11 cells treated with DMSO (black) and (R)-PFI-2 (brown) for 48h. * statistical significance ($p<0.05$) after t-test. Error bars represented as mean±SD. (n=3)

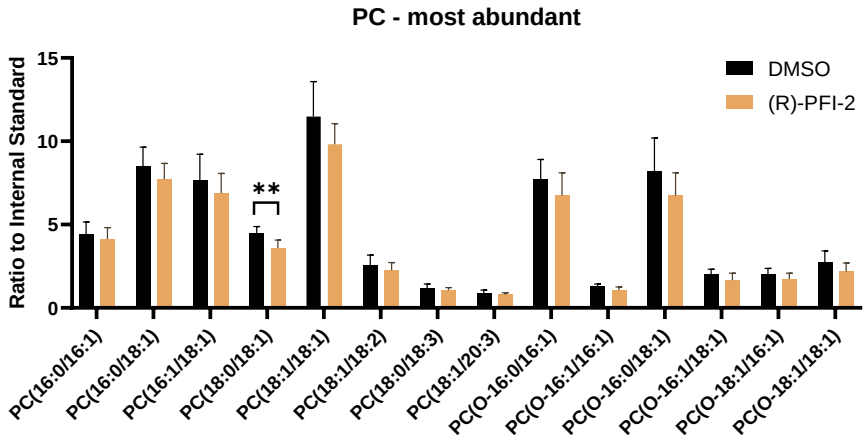

Figure 58. Most abundant phosphatidylcholine profile of differentiated HC11 cells treated with DMSO (black) and (R)-PFI-2 (brown) for 48h (only PC representing >1%). ** statistical significance ($p<0.01$) after t-test. Error bars represented as mean±SD. (n=3)

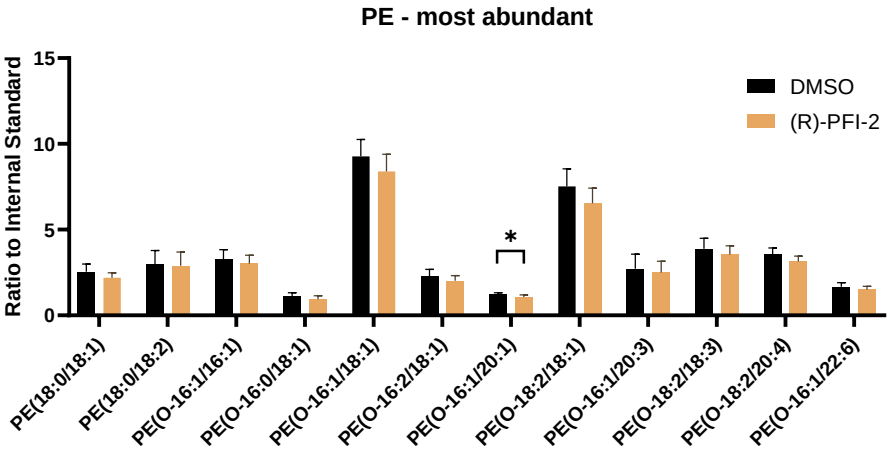

Figure 59. Most abundant phosphatidylethanolamine profile of differentiated HC11 cells treated with DMSO (black) and (R)-PFI-2 (brown) for 48h (only PE representing >1%). * statistical significance ($p<0.05$) after t-test. Error bars represented as mean±SD. (n=3)

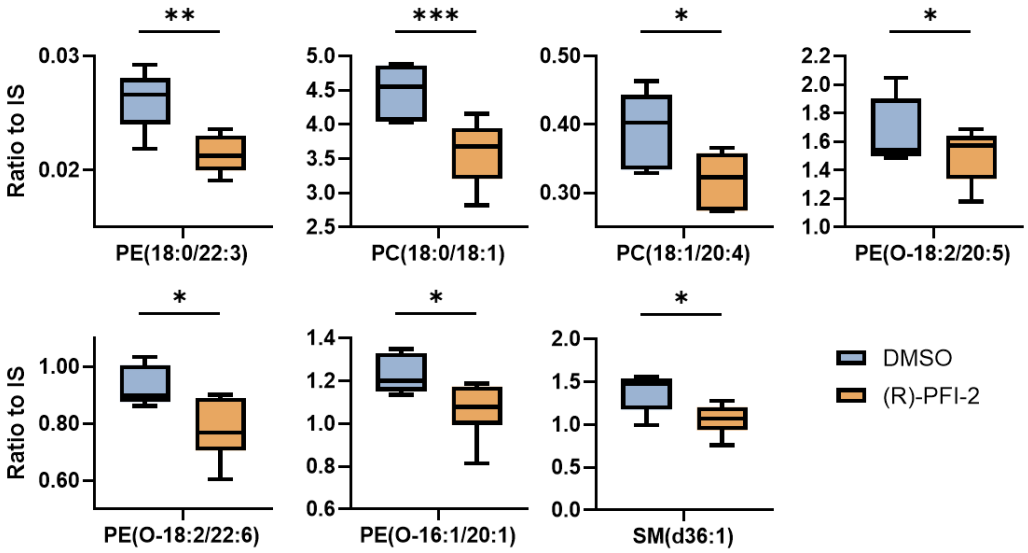

Figure 60. Boxplots showing the varying PL species after SETD7 inhibition, presented as ratio to the respective' s class internal standard (IS). (Blue: DMSO, brown: (R)-PFI-2). *, **, *** statistical significance ($p<0.05$, $p<0.01$, $p<0.001$, respectively). n=6.

Multivariate analysis, however, did not return a good separation between groups on principal component analysis (PCA) nor in Partial Least Squares Discriminant Analysis (PLS-DA), which would suggest a non-significant overall effect of SETD7 inhibition (Supplementary Figure 14). However, hierarchical clustering dendrogram and heatmap (Figure 61) resulted in a relatively good separation of samples from the 2 groups, although imperfect.

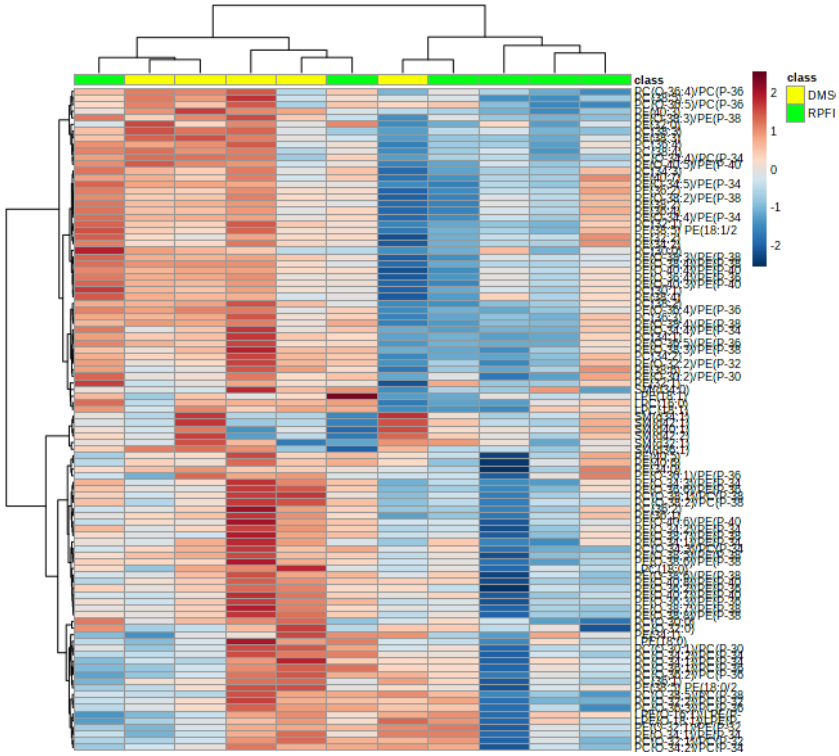

Figure 61. Condensed heatmap of data obtained from the C18-MS analysis of lipid extract from differentiated HC11 MEC treated with DMSO (yellow) and (R)-PFI-2 (green) for 48h.

4 Discussion

With the purpose of assessing the evolution of phospholipid class metabolism throughout differentiation, thin layer chromatography was first employed. The phospholipid class variations observed during differentiation were consistent with previous observations in HC11 cells by Dória et al.[17]. Namely, an upregulation on PE biosynthesis appears highly likely, which was related in the previous study from this group to the increased expression of genes Etnk1, Pcyt2 and Chka[17]. A reduction on PC was also observed, and previous observations reported a similar occurrence, although not statistically significant. Yet, this is conflicting with the previous observation by Dória et al. of an increase in the expression of Chpt1. The decrease in PC could therefore be related to its conversion to SM, which was increased in the study by Dória et al., but not in the present experiment. As major constituents of cell membranes, the levels of PC are expected to be higher on stages of increased proliferation[61,62]. As functional differentiation progresses, proliferative behaviour decreases[62], and so does the synthesis of PC, as was observed. The same could be thought to PE. However, evidence from this study, as well as previous observations, support an upregulation of PE synthesis in differentiated mammary epithelial cells. CL were increased in differentiated cells, which may be correlated to an increase in Gpdl1 and Cds1. PS were also lower on differentiated cells, possibly a result of the increase in PE, and the activity of Pisd, which catalyses the decarboxylation reaction. With differentiation, the cylindrical/conic-shaped PL ratio (PC/PE ratio) lowers, which suggests the promotion of membrane curvature and fluidity, consistent with the secretory demands of fully differentiated mammary epithelial cells[63,64]. This was also observed by Dória et al[17]. During lactation, lipid droplets (LD) originate from the ER and store and transport neutral lipids. These LD then fuse with the cell membrane and are secreted intact to the mammary gland lumen[65]. A large amount of lipids is secreted into milk, and thus lipogenesis and biogenesis of LD are activated during the functional differentiation of MEC[65]. Therefore, the observed modifications to the lipidome can be understood in this context. It is important to note that the study by Dória et al.[17] was performed on a cell culture grown in complete medium with EGF for the maintenance of S-LC, and dexamethasone and prolactin in an EGF-depleted medium to induce the functional differentiation of HC11 cells, as in this study. An important difference, however, is the absence of DMSO, which was used in our culture as a negative

control for (R)-PFI-2, as it was used as solvent for this compound, and at a low concentration (0.1%). At doses above 10%, DMSO has been shown to reduce lipid content in adipocytes by impairing their differentiation, reduce cell viability and accelerate apoptosis and necrosis[66]. A concentration of 1% led to a decrease in intracellular TG content likely through suppression of lipogenesis, and increase in the expression of genes involved in glucose metabolism[67]. At ≥ 0.1%, the concentration used in this study, DMSO increased mitochondrial membrane potential, and at 0.01%, attenuated free fatty acid-induced TG accumulation in hepatocytes[68], improved glutathione and presented minimal effects on cell viability in adipocytes[66]. The results found in this study were close to those observed by Dória et al.[17], suggesting the effect of DMSO under these conditions is not significant, although it shouldn't be overlooked.

The lipidomics analysis using HILIC led to good results, successfully screening the lipidome. A total of 317 lipid species belonging to 10 classes of PL were identified, significantly more than previously identified by Dória et al (117 species)[17], since a less sensitive ion trap system was used in that study, as opposed to the Orbitrap applied in the present study[69]. There was a noticeable variation on the relative amount of lipid species with the course of differentiation. The impossibility to apply ANOVA or multivariate analysis due to the low number of samples, however, hindered proper statistical analysis. Nonetheless, general comparisons, such as the number of carbons or double bonds on the fatty acid chains of PL demonstrated an evolution towards a lipidome containing more 36-carbon PL, and species with a total of two double bonds distributed in variable combinations on the fatty acid chains, and a higher degree of plasmanyl/plasmenyl PL. The study of fatty acids supported these observations, considering the increasing amount of monounsaturated C16 and C18 fatty acids, common constituents of lipid species containing 36 carbons. Furthermore, the amount of saturated FA declined with the progression of differentiation. On previous observations, differentiated HC11 cells presented lower amounts of essential FA (C20:5ω3 and C18:2ω6) and increased C20:4ω6 (ARA), C16:1 and C18:1, the most abundant FA in human milk[65]. Accordingly, and although ARA wasn't increased in this study, C16:1 and C18:1 were more abundant in differentiated cells. Lipogenesis is induced during pregnancy and lactation by the activity of regulatory factors of gene expression. Particularly, a switch occurs from PPARγ/XRX-induced fatty acid β-oxidation to

lipogenesis, controlled by LXR/RXR dimerization[70,71], leading to synthesis of long-chain (LC) MUFA, LC-PUFA, and secretion of neutral lipids, specifically TAG. Ether lipids were increased as well. Since plasmalogens have been related to the regulation of membrane fluidity, fusion and fission[70], this increase may be a result of the cell directing its lipidic phenotype towards the optimization of secretory function.

The PCR analysis revealed an increase in all studied genes related to fatty acid synthesis. Dória et al.[17] had already reported an increase in Scd1, Elovl6, and Fads2 with differentiation. The increase in Fasn shown herein may be responsible for the decrease in C14:0, which is then converted to C16:0 by this enzyme. The increased elongase Elovl6 led to the formation of C18:0, and desaturases to the formation of the corresponding C16:1ω9, C16:1ω7, C18:1ω9 and C18:1ω7. The increase in C20:3ω6 can also be related to the increase in Elovl5, and the reduction on C20:4ω6 and C20:5ω3 to the lower expression of desaturase Fads1 on differentiated cells. Interestingly, although a marginally lower amount of C22:6ω3 was found in differentiated cells, the expression of Acox1/3 was increased. Altogether, these results illustrate an adaptation of the lipidome of HC11 cells to functional differentiation. Longer and more unsaturated fatty acids, abundance of PE and the adoption of a phenotype that facilitates secretion of lipid droplets are hallmarks of these adaptations. Figure 62 and Figure 63 sum the observed tendencies on the expression of genes from FA synthetic pathways during differentiation.

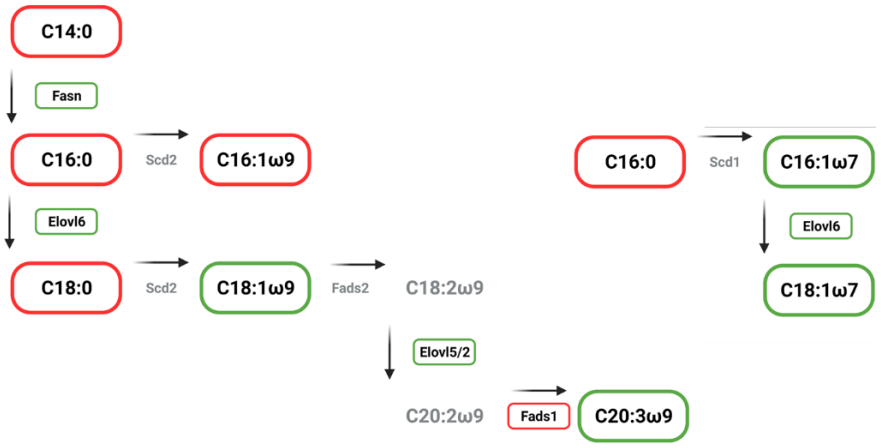

Figure 62. Schematic representation of tendencies in gene expression and fatty acid profile changes of ω7 and ω9 fatty acid synthesis during the differentiation of HC11 cells. (Red, decreased in Dif in relation to S-LC; green, increased in Dif in relation to S-LC; grey, not identified/not analysed)

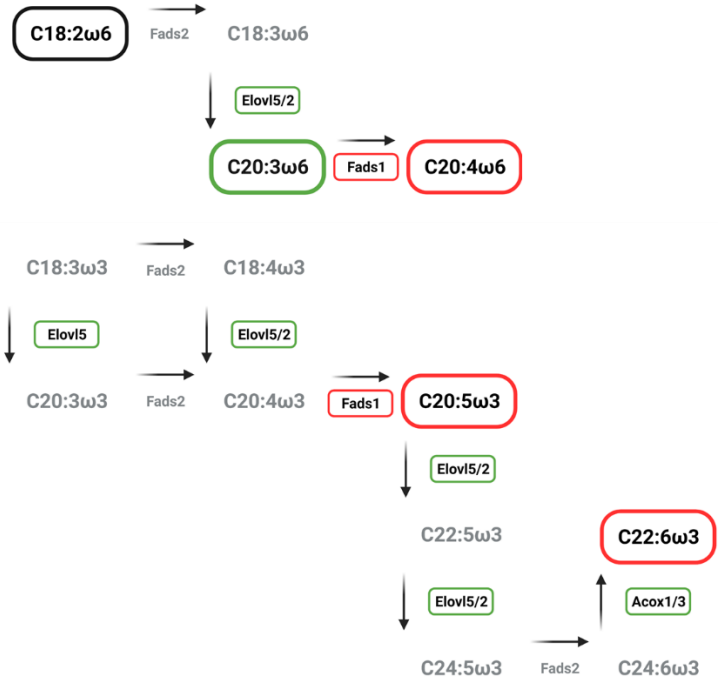

Figure 63. Schematic representation of tendencies of gene expression and fatty acid profile changes of ω6 and ω3 fatty acid synthesis during the differentiation of HC11 cells. (Red, decreased in Dif in relation to S-LC; green, increased in Dif in relation to S-LC; black, same amount in Dif in relation to S-LC; grey, not identified/not analysed)

These results present an indication of the performance of these cells under their normal differentiation process, and all observations are in line with others previously reported. Considering the adaptations of the lipidome to functional differentiation, an impairment of these could compromise lactation. SETD7 has been established in previous studies from our group as a regulator of MEC proliferation and differentiation[72], as its expression increases throughout development[31]. In this sense and considering the adaptation of the lipidome of MEC to functional differentiation, a link between SETD7 and the lipidome is possible. Therefore, the inhibition of SETD7's catalytic activity is expected to affect the lipidomic variations occurring during differentiation. Particularly, changes which may lead to a less fluid cell membrane, and thus impair vesicle budding and lipid droplet secretion, for instance, would indicate an important role for SETD7 in this process.

This association was studied by treating HC11 cells with the selective SETD7 inhibitor (R)-PFI-2 for 24 hours and studying the evolution of the lipidome in all stages of differentiation. At S-LC stage, an increase in PC and decrease in PS and PA were observed, leading to an increase in the cylindrical/conic-shaped ratio. As S-LC are highly proliferative, the synthesis of membrane constituents is expected to be increased. Particularly, PC, which were progressively lowered during differentiation, were increased at this stage, which may suggest an effect of SETD7, further promoting a proliferative phenotype. In S-LC, the inhibition of SETD7 also led to a decrease of Elovl5/6, and increase in Fads1, Fasn and Acox1/3. This would imply an allocation of FA synthesis towards shorter FA in the absence of the catalytic activity of SETD7, although no differences were observed on the FA profile or lipidomics analysis. At PD stage, similar outcomes were observed, with no remarkable differences in TLC, FA or lipidomics analysis after the inhibition of SETD7. However, gene expression of Elovl5 and Acox1/3 was increased, and Fasn and Elovl6 were lower. As these cells are transitioning towards a differentiated and secretory state, these switches possibly indicate an impairment of the synthesis of longer fatty acids. Acox1/3, Elovl6 and Fasn were lower on DIF cells, also suggesting a hindering of the synthesis of LC-PUFA. However, once more no notable changes were observed on the lipidome, despite the variation on gene expression. The small variations on the lipidome after the treatment with (R)-PFI-2 could suggest an insufficient period for the inhibition effects on gene expression to be translated and detectable on the lipidome. Previous observations from our group report an increase in

SETD7 expression throughout differentiation, which may illustrate its connection to the adaptation to secretory function. These also report a decrease on the synthesis of β-casein and lactoferrin on differentiated HC11 cells and increase of proliferation after treatment with (R)-PFI-2 after 24h (Supplementary Figure 16). This would suggest the inhibition of the catalytic activity of SETD7 deeply affects the lactogenic differentiation of HC11 cells, as these tend to stay away from the functional secretory function, and acquire a proliferative character, abnormal in this stage and that might predispose to neoplastic transformation. Considering these observations, a role for SETD7 on the lipidome was expected to some extent. Since lipogenesis is one of the main features of lactogenic differentiation of MECs and is reproduced by HC11 cells[17,73], any disturbance caused to lipid metabolism at this stage may impair lactation considering the functional role of differentiated mammary epithelial cells.

To assess the possibility of an insufficient inhibition within 24-hours, a longer treatment (48h) was applied, which would enhance the possible outcomes. Since the lipidome is being used as a tool to assess the role of SETD7 on lipid metabolism, it could be possible that the effects of SETD7 inhibition did not translate to the molecular fingerprint. The 24 hours may in fact have been enough to lower SETD7 expression, but this time may have not been enough for these modifications to translate into the profile of lipids within the cell. Thus, HC11 cells were cultured in a medium containing (R)-PFI-2 8nM during the last 48 hours corresponding to the transition into differentiated lactogenic cells, in the presence of lactogenic hormones. A different lipidomics analysis was performed on these cell's lipid extract, resorting to C18-LC-MS, as this approach would allow for the identification and quantification of individual molecular species, yielding a more detailed profiling of the lipidome. Select PL classes, PC, PE, and SM were analysed, as these were of the most interest considering all the observations to date. A total of 35 molecular species of PC, 58 PE and 7 SM were identified and quantified. Of these, 9 PE molecular species were not identified previously in the HILIC analysis, likely due to a lower abundance.

The lipid class composition on these cells was first analysed by TLC for PL class profiling. The TLC separation was improved in comparison to the first application, by removing the use of boric acid. This allowed for an enhanced partitioning of the PE and PG spots, which benefited the overall analysis. Boric acid forms complexes with compounds

containing vicinal hydroxyl groups, slowing their migration[74]. Such is the case of PG and PI. A boric acid concentration of 1,8% or 2,3% was suggested by Vaden et al.[75] as an optimal concentration for the separation of PL. However, possibly due to differences on the properties of the silica plates used in this study, this led to the coelution of PE and PG. Not using boric acid allowed for a good separation of all classes. Multivariate analysis of data from TLC of lipid extracts from cells treated for 48h revealed a poor group separation on PLS DA scores scatter plot, with Q^2 was under 0.2. Observations were made of a direct effect on the amount of SM (decreased) and PC (increased), and this was accompanied by a negative correlation between the two (borderline non-significant, $p < 0.10$), suggesting SETD7 may affect this synthetic pathway. SM are synthesized through the enzymatic transfer of a phosphocholine from phosphatidylcholine to a ceramide, by sphingomyelin synthase, Sgms2[76]. Therefore, an effect of SETD7 on this enzyme cannot be discarded. A significant correlation between PC and PS was found ($p < 0.05$). Together with the increase in PC, this may indicate that the PC to PS conversion, via Ptdss1, needs SETD7 in order to fully progress. The negative CL-PG correlation was also significant ($p < 0.05$). These PL classes are biosynthetically connected, since CL are formed by the binding of a CDP-DAG molecule to PG, by cardiolipin synthase (Crls1)[77]. Cardiolipins increased with differentiation, thus the effect of SETD7 on their synthesis may also be relevant. PI were positively correlated to PS and PG, as well as PS-CL, and as most of these classes are biosynthetically related, this association is expected. The association between these classes and PS is surprising, since no direct link between CDP-DG (their main substrate) and PS has been reported in mammals. PS are synthesized by the replacement of the polar head groups of pre-existing PE and PC by serine. However, in prokaryotes and yeast, CDP-diacylglycerol-serine O-phosphatidyltransferase is able to perform this transformation directly from CDP-DG[78].

Considering these observations, it can be proposed that SETD7 plays a role in the regulation of glycerophospholipid metabolism. A schematic representation of the pathways possibly influenced by the inhibition of the catalytic activity of SETD7 is presented in Figure 64. This effect can perhaps be implemented by the regulation of gene expression, possibly of genes coding enzymes involved in PL synthesis, since a longer treatment period led to a heightened effect on the relative abundance of PL classes. Genes that are possibly influenced

by SETD7 are thus Ptdss1, Sgms2, Cdipt, Crls1 and Pgs1, as well as the previously established Pcyt2 and Chpt1, acting towards a decrease in PC synthesis, and increase in SM, PS, and PL derived from CDP-DG.

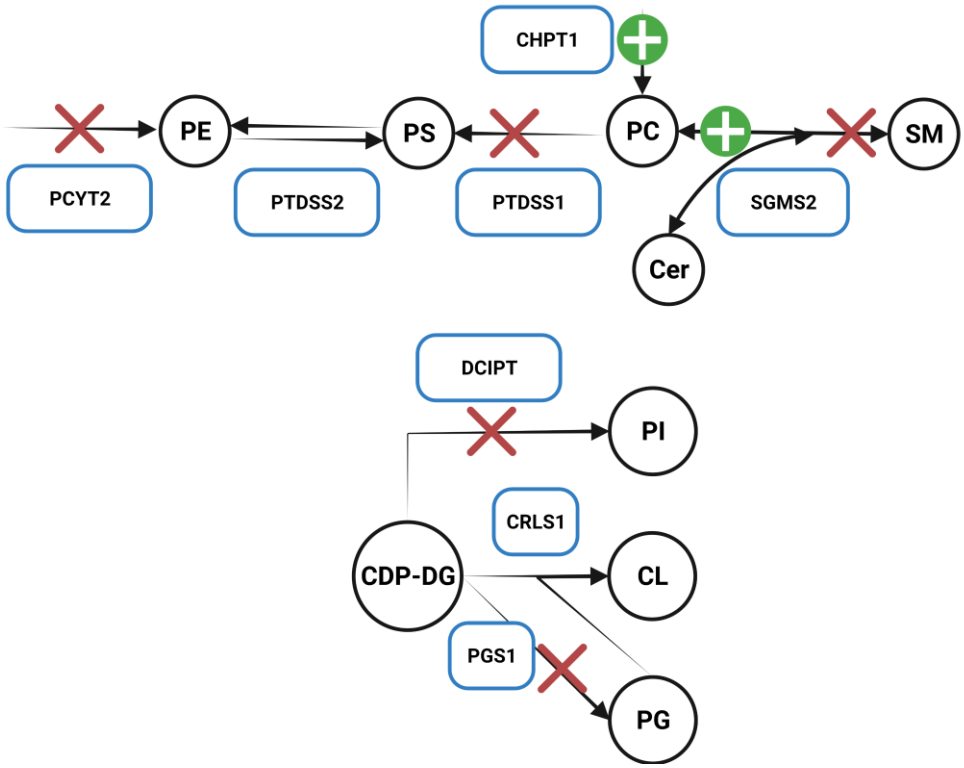

Figure 64. Schematic representation of phospholipid biosynthetic pathways possibly influenced by the inhibition of the catalytic activity of SETD7 in differentiated HC11 cells. P*tdss*1, phosphatidylserine synthase 1; P*tdss*2, phosphatidylserine synthase 2; S*gms*2, phosphatidylcholine:ceramide cholinephosphotransferase 2; C*dipt*, CDP-diacylglycerol-inositol 3-phosphatidyltransferase; C*rls*1, cardiolipin synthase 1; P*gs*1, phosphatidylglycerophosphate synthase 1; *Pcyt2*, phosphate cytidylyltransferase 2, ethanolamine; *Chpt1*, choline phosphotransferase 1; Green, possibly enhanced by SETD7 activity; Red, possibly impaired by SETD7 activity. (Adapted from Kyoto Encyclopedia of Genes and Genomes (KEGG) and Dória et al.[17])

No previous studies suggested a direct link between SETD7 and PL synthesis. However, known SETD7 substrates like Xbp1 and Rorα2 may comprise a link to these processes. For instance, although cardiolipins were not increased, their metabolic connection to PG seemed to be affected. Cardiolipins are a marker of mitochondrial stress, which may be caused due to leakage of calcium from the ER and its resulting uptake by mitochondria, ultimately resulting in the generation of ROS[79]. Considering the important role played by Xbp1 during

ER stress and the UPR, it is not improbable that SETD7 inhibition may impact Xbp1 in some way. Sgms2 regulates ceramide and sphingomyelin homeostasis, and its enhanced expression has been related to BC metastasis[80]. A primary study by Zheng et al.[80] suggested aberrant Sgms2 expression may inhibit apoptosis, by the suppression of Cer synthesis, promoting cancer cell proliferation. It may also promote invasiveness by the enhancement of EMT, by promoting SM synthesis, which enhances the secretion of TGF-β1, and in turn activates the TGF-β/Smad signalling pathway. The observations made in the present study, including a decrease on SM and the effect of SETD7 activity on the PC-SM conversion, could indicate a role for SETD7 in this mechanism. However, the inhibition of SETD7 activity increases the EMT[31]. For this reason and considering the reduction on SM, it's not likely that a connection between the inhibition of SETD7 and the Sgms2-mediated increase of the EMT takes place.

The inhibition of SETD7 led to the statistically significant decrease of four PE species (PE(18:0/22:3), PE(O-18:2/20:5), PE(O-18:2/22:6) and PE(O-16:1/20:1)), two PC species (PC(18:0/18:1) and PC(18:1/20:4)) and SM(d36:1). Overall, the identified molecular species of both PE and PC were mostly lower after the treatment. This contrasts with the increase on the relative amount of PC, suggested by the TLC results, which was suggestive of increased proliferative activity upon inhibition of SETD7 in differentiated cells. It can be proposed that an allocation towards PC synthesis occurs, although the net amount of these species is lower, possibly due to lower amount of overall PL content. This decrease in total lipid content and allocation towards PC, important components of membranes, is noteworthy if we consider a possible impairment of secretory phenotype provoked by SETD7 inhibition. In differentiated cells, as XBP-1 activation occurs in the onset of lactogenesis, lipogenesis is triggered to prepare cells for secretory activation. As SETD7 is associated to XBP-1 activation, perhaps it is possible for an impairment of lipid synthesis to occur upon SETD7 inhibition, and the shift towards a proliferative phenotype to occur, particularly promoting the synthesis of PC. This hypothesis is further supported by the previous observation by our group of an increase in Chpt1 expression and decrease in Pcyt2 upon SETD7 inhibition (Supplementary Figure 13). The effect size of 26 molecular species was above 1, and all of these indicated a decrease after the inhibition of SETD7. However, these could not be considered significant, as the ES error remained above 1.2 in all species. Nonetheless, they

present a reasonable suggestion that SETD7 inhibition may affect the levels of these lipids. Finally, heatmaps showed a good separation of the DMSO and (R)-PFI-2 treatment groups, although not perfect. The correlation tables demonstrated a strong association between biosynthetically related molecular lipid species (Supplementary Figure 15). SM species were strongly correlated between themselves, and species of PE and PC seemed to be clustered according to their fatty acid chain composition more often than according to their polar head group.

Overall, these finding suggest that SETD7 has a role in maintaining the lipidome of mammary epithelial cells, and the inhibition of its activity is associated to changes that impair lactogenic differentiation needed to cope with the lipid demands of lactation. Together with previous observations from our group, these results illustrate that SETD7 may have a function on the homeostasis of mammary epithelial cells, by regulating lipid metabolism, particularly directing lipid synthesis towards conical-shaped PL species which promote membrane fluidity, proper for secretory function, instead of PC, structural cylindrical components of membranes, which are more abundant in a proliferative S-LC state.

5 Conclusion and Future Perspectives

In this study, we successfully analysed the lipidome of HC11 MEC throughout functional differentiation, having firstly corroborated previous observations. The lipidome adapts progressively to the demands of lactation, promoting the synthesis of longer fatty acids, as well as PL components of the cell membrane which increase its fluidity. Particularly, PL containing 36 carbon, a total of two double bonds, and a higher degree of plasmanyl/plasmenyl PL seemed to be the main features promoted throughout differentiation. A decrease in PC accompanied this development, and thus the synthesis of PL from this class was associated to a higher proliferative potential. Accordingly, the cylindrical/conic-shaped PL ratio was decreased in later stages of differentiation, suggesting higher membrane curvature and fluidity. Together, these modifications facilitate the secretion of lipid droplets and milk proteins, and thus ensure a functional mammary gland *in vivo*.

The expression of the methyltransferase SETD7 is known to be increased during differentiation, and its connection to this process has been established. It was known that the inhibition of the catalytic activity of SETD7 led to the partial loss of lactogenic phenotype, with impairment of the synthesis of milk proteins, and an increase in proliferation. Having determined the lipid hallmarks of HC11 cell differentiation, the role of SETD7 was studied in this process. As was expected, it was found that SETD7 inhibition led to the loss of lipid profile traits typical of lactogenic cells. It seems that SETD7 acts upon the regulation of the expression of genes responsible for some of the main steps of PL synthesis, particularly PC, SM and PS. New and previous observations also support an effect on the synthesis of PE, which was increased in lactogenic cells and seemed to be decreased by the inhibition of SETD7. The phenotype conferred by this inhibition is resemblant to undifferentiated stem-like cells, which share features of cancer cells with metastatic potential. In this sense, the role played by SETD7 in promoting or maintaining the differentiation of MEC through targeting the lipidome is of the utmost importance. This is because the lipid profile of tumoral cells is distinctive, and thus the results presented support studying SETD7 in cancer, to investigates if it could possibly aid in patient stratification and management. For example, the lack of SETD7 catalytic activity would imply not only a less functional mammary gland,

since milk production is impaired, but also the susceptibility to a more aggressive/less differentiated form of breast cancer, with the increase of the epithelial to mesenchymal transition and metastatic potential of BC cells.

The limitations of this study, however, reside on the still unclear mechanism through which SETD7 contributes to the modulation of MEC differentiation. The assessment of the level of gene expression and protein quantification of enzymes related to PL synthesis, as well as SETD7 targeting of their respective transcription factors would clarify some of the potential pathways regulated by SETD7 in MEC differentiation. Future studies could focus on this, as well as the assessment of the role of this enzyme in other tissues where its expression is also known to increase throughout differentiation, such as cardiomyocytes. Experiments *in vivo*, regarding the quality of the milk produced and the PL profile of MEC would also be important.

References

1. Inman, J. L., Robertson, C., Mott, J. D. & Bissell, M. J. Mammary gland development: Cell fate specification, stem cells and the microenvironment. *Dev.* **142**, 1028–1042 (2015).
2. Jena, M. K., Jaswal, S., Kumar, S. & Mohanty, A. K. Molecular mechanism of mammary gland involution: An update. *Dev. Biol.* **445**, 145–155 (2019).
3. Musumeci, G. *et al.* Mammary gland: From embryogenesis to adult life. *Acta Histochem.* **117**, 379–385 (2015).
4. Visvader, J. E. & Stingl, J. Mammary stem cells and the differentiation hierarchy: Current status and perspectives. *Genes Dev.* **28**, 1143–1158 (2014).
5. Macias, H. & Hinck, L. Mammary gland development. *Wiley Interdiscip. Rev. Dev. Biol.* **1**, 533–557 (2012).
6. Britt, K., Ashworth, A. & Smalley, M. Pregnancy and the risk of breast cancer. *Endocr. Relat. Cancer* **14**, 907–933 (2007).
7. Fu, N. Y., Nolan, E., Lindeman, G. J. & Visvader, J. E. Stem cells and the differentiation hierarchy in mammary gland development. *Physiol. Rev.* **100**, 489–523 (2020).
8. Williams, C., Helguero, L., Edvardsson, K., Haldosén, L. A. & Gustafsson, J. Å. Gene expression in murine mammary epithelial stem cell-like cells shows similarities to human breast cancer gene expression. *Breast Cancer Res.* **11**, 1–17 (2009).
9. Lim, E. *et al.* Aberrant luminal progenitors as the candidate target population for basal tumor development in BRCA1 mutation carriers. *Nat. Med.* **15**, 907–913 (2009).
10. Zhang, M., Lee, A. V. & Rosen, J. M. The cellular origin and evolution of breast cancer. *Cold Spring Harb. Perspect. Med.* **7**, 1–14 (2017).
11. Sørlie, T. *et al.* Gene expression patterns of breast carcinomas distinguish tumor subclasses with clinical implications. *Proc. Natl. Acad. Sci. U. S. A.* **98**, 10869–10874 (2001).
12. Lu, W. & Kang, Y. Cell lineage determinants as regulators of breast cancer metastasis. *Cancer Metastasis Rev.* **35**, 631–644 (2016).
13. Prat, A. & Perou, C. M. Mammary development meets cancer genomics. *Nat. Med.* **15**, 842–844 (2009).
14. Lodish, H. F. *et al. Molecular Cell Biology, 7th edition*. *Book* vol. 5 (2013).
15. Nelson, D. L. & Cox, M. M. Lehninger Principles of Biochemistry 7th. *W.H. Free. Co.* **2**, (2017).
16. Simons, K. & Sampaio, J. L. Membrane Organization and Lipid Rafts. *Cold Spring Harb Perspect Biol.* 1–17 (2011).
17. Dória, M. L. *et al.* Fatty acid and phospholipid biosynthetic pathways are regulated throughout mammary epithelial cell differentiation and correlate to breast cancer survival. *FASEB J.* **28**, 4247–4264 (2014).
18. Frolov, V. A., Shnyrova, A. V. & Zimmerberg, J. Lipid polymorphisms and membrane shape. *Cold Spring Harb. Perspect. Biol.* **3**, 1–14 (2011).
19. Van Meer, G. & De Kroon, A. I. P. M. Lipid map of the mammalian cell. *J. Cell Sci.* **124**, 5–8 (2011).
20. Argov-Argaman, N., Raz, C. & Roth, Z. Progesterone Regulation of Milk Fat Globule Size Is VLDL Dependent. *Front. Endocrinol. (Lausanne).* **11**, 1–13 (2020).

21. Neville, M. C., Morton, J. & Umemura, S. Lactogenesis: The transition from pregnancy to lactation. *Pediatr. Clin. North Am.* **48**, 35–52 (2001).

22. Rudolph, M. C. *et al.* Metabolic regulation in the lactating mammary gland: A lipid synthesizing machine. *Physiol. Genomics* **28**, 323–336 (2007).

23. McManaman, J. L. Lipid transport in the lactating mammary gland. *J. Mammary Gland Biol. Neoplasia* **19**, 35–42 (2014).

24. McManaman, J. L., Russell, T. D., Schaack, J., Orlicky, D. J. & Robenek, H. Molecular determinants of milk lipid secretion. *J. Mammary Gland Biol. Neoplasia* **12**, 259–268 (2007).

25. Mohammad, M. A. & Haymond, M. W. Regulation of lipid synthesis genes and milk fat production in human mammary epithelial cells during secretory activation. *Am. J. Physiol. - Endocrinol. Metab.* **305**, 700–716 (2013).

26. Rudolph, M. C. *et al.* Sterol regulatory element binding protein and dietary lipid regulation of fatty acid synthesis in the mammary epithelium. *Am. J. Physiol. - Endocrinol. Metab.* **299**, 918–927 (2010).

27. Suburu, J. *et al.* Fatty acid synthase is required for mammary gland development and milk production during lactation. *Am. J. Physiol. - Endocrinol. Metab.* **306**, 1132–1143 (2014).

28. Liga Portuguesa Contra o Cancro. Programa de Rastreio de Cancro da Mama. https://www.ligacontracancro.pt/servicos/detalhe/url/programa-de-rastreio-de-cancro-da-mama/ (2021).

29. Dória, M. L. *et al.* Lipidomic analysis of phospholipids from human mammary epithelial and breast cancer cell lines. *J. Cell. Physiol.* **228**, 457–468 (2013).

30. Dória, M. L. *et al.* Lipidomic approach to identify patterns in phospholipid profiles and define class differences in mammary epithelial and breast cancer cells. *Breast Cancer Res. Treat.* **133**, 635–648 (2012).

31. Batista, I. de A. A. & Helguero, L. A. Biological processes and signal transduction pathways regulated by the protein methyltransferase SETD7 and their significance in cancer. *Signal Transduct. Target. Ther.* **3**, 1–14 (2018).

32. Lee, J. *et al.* SETD7 Drives Cardiac Lineage Commitment through Stage-Specific Transcriptional Activation. *Cell Stem Cell* (2018) doi:10.1016/j.stem.2018.02.005.

33. Nayak, A. *et al.* Regulation of SETD7 Methyltransferase by SENP3 Is Crucial for Sarcomere Organization and Cachexia. *Cell Rep.* **27**, 2725-2736.e4 (2019).

34. Shen, Y. *et al.* SETD7 mediates spinal microgliosis and neuropathic pain in a rat model of peripheral nerve injury. *Brain. Behav. Immun.* **82**, 382–395 (2019).

35. He, S., Owen, D. R., Jelinsky, S. A. & Lin, L. L. Lysine methyltransferase SETD7 (SET7/9) regulates ROS signaling through mitochondria and NFE2L2/ARE pathway. *Sci. Rep.* **5**, 1–14 (2015).

36. Bultman, S. J. SETD7 interacts with other chromatin-modifying factors to regulate cardiac development. *Stem Cell Investigation* vol. 6 (2019).

37. Castaño, J. *et al.* SETD7 Regulates the Differentiation of Human Embryonic Stem Cells. *PLoS One* **11**, e0149502 (2016).

38. Tuano, N. K., Okabe, J., Ziemann, M., Cooper, M. E. & El-Osta, A. Set7 mediated interactions regulate transcriptional networks in embryonic stem cells. *Nucleic Acids Res.* **44**, 9206–9217 (2016).

39. Barsyte-Lovejoy, D. *et al.* (R)-PFI-2 is a potent and selective inhibitor of SETD7 methyltransferase activity in cells. *Proc. Natl. Acad. Sci. U. S. A.* **111**, 12853–12858 (2014).

40. Montenegro, M. F. *et al.* Tumor suppressor SET9 guides the epigenetic plasticity of breast cancer cells and serves as an early-stage biomarker for predicting metastasis. *Oncogene* **35**, 6143–6152 (2016).

41. Song, Y. *et al.* SET7/9 inhibits oncogenic activities through regulation of Gli-1 expression in breast cancer. *Tumor Biol.* **37**, 9311–9322 (2016).

42. Huang, R. *et al.* SETD7 is a prognosis predicting factor of breast cancer and regulates redox homeostasis. *Oncotarget* **8**, 94080–94090 (2017).

43. Han, J. & Kaufman, R. J. The role of ER stress in lipid metabolism and lipotoxicity. *J. Lipid Res.* **57**, 1329–1338 (2016).

44. Chen, J. *et al.* ER stress triggers MCP-1 expression through SET7/9-induced histone methylation in the kidneys of db/db mice. *Am. J. Physiol. - Ren. Physiol.* **306**, 20–26 (2014).

45. Song, H. *et al.* Isoform-specific lysine methylation of RORα2 by SETD7 is required for association of the TIP60 coactivator complex in prostate cancer progression. *Int. J. Mol. Sci.* **21**, (2020).

46. Kim, K. *et al.* RORα controls hepatic lipid homeostasis via negative regulation of PPARγ transcriptional network. *Nat. Commun.* **8**, (2017).

47. Lau, P., Nixon, S. J., Parton, R. G. & Muscat, G. E. O. RORα regulates the expression of genes involved in lipid homeostasis in skeletal muscle cells: Caveolin-3 and CPT-1 are direct targets of ROR. *J. Biol. Chem.* **279**, 36828–36840 (2004).

48. Coskun, O. Separation Tecniques: Chromatography. *North. Clin. Istanbul* **3**, 156–160 (2016).

49. Buszewski, B. & Noga, S. Hydrophilic interaction liquid chromatography (HILIC)-a powerful separation technique. *Anal. Bioanal. Chem.* **402**, 231–247 (2012).

50. Guo, R. *et al.* The Function and Mechanism of Lipid Molecules and Their Roles in The Diagnosis and Prognosis of Breast Cancer. *Molecules* **25**, 4864 (2020).

51. Fichtali, K., Bititi, A., Elghanmi, A. & Ghazi, B. Serum Lipidomic Profiling in Breast Cancer to Identify Screening, Diagnostic, and Prognostic Biomarkers. *Biores. Open Access* **9**, 1–6 (2020).

52. Sevinsky, C. J. *et al.* NDRG1 regulates neutral lipid metabolism in breast cancer cells. *Breast Cancer Res.* **20**, 55 (2018).

53. Kus, K. *et al.* Alterations in arginine and energy metabolism, structural and signalling lipids in metastatic breast cancer in mice detected in plasma by targeted metabolomics and lipidomics. *Breast Cancer Res.* **20**, 148 (2018).

54. Chagovets, V. V *et al.* Validation of Breast Cancer Margins by Tissue Spray Mass Spectrometry.

55. Wolrab, D. *et al.* Plasma lipidomic profiles of kidney , breast and prostate cancer patients differ from healthy controls. *Sci. Rep.* 1–14 (2021) doi:10.1038/s41598-021-99586-1.

56. Chen, X. *et al.* Plasma lipidomics profiling identified lipid biomarkers in distinguishing early-stage breast cancer from benign lesions. *Oncotarget* **7**, 36622–36631 (2016).

57. Bligh, E. G. & Dyer, W. J. A rapid method for total lipid extraction. *Biochem. Cell Biol.* (1959) doi:10.1139/o59-099.

58. Bartlett, E. M. & Lewis, D. H. Spectrophotometric determination of phosphate esters in the

presence and absence of orthophosphate. *Anal. Biochem.* (1970) doi:10.1016/0003-2697(70)90343-X.

59. Pluskal, T., Castillo, S., Villar-Briones, A. & Orešič, M. MZmine 2: Modular framework for processing, visualizing, and analyzing mass spectrometry-based molecular profile data. *BMC Bioinformatics* (2010) doi:10.1186/1471-2105-11-395.

60. Tsugawa, H. *et al.* A lipidome atlas in MS-DIAL 4. *Nat. Biotechnol.* **38**, 1159–1163 (2020).

61. Ridgway, N. D. The role of phosphatidylcholine and choline metabolites to cell proliferation and survival. *Crit. Rev. Biochem. Mol. Biol.* **48**, 20–38 (2013).

62. Szlasa, W., Zendran, I., Zalesińska, A., Tarek, M. & Kulbacka, J. Lipid composition of the cancer cell membrane. *J. Bioenerg. Biomembr.* **52**, 321–342 (2020).

63. Van Meer, G., Voelker, D. R. & Feigenson, G. W. Membrane lipids: Where they are and how they behave. *Nat. Rev. Mol. Cell Biol.* **9**, 112–124 (2008).

64. Lipowsky, R. Remodeling of membrane compartments: Some consequences of membrane fluidity. *Biol. Chem.* **395**, 253–274 (2014).

65. Ladinsky, M. S., Mardones, G. A., Orlicky, D. J., Howell, K. E. & McManaman, J. L. Electron Tomography Revels that Milk Lipids Originate from Endoplasmic Reticulum Domains with Novel Structural Features. *J. Mammary Gland Biol. Neoplasia* **24**, 293–304 (2019).

66. Dludla, P. V. *et al.* A dose-dependent effect of dimethyl sulfoxide on lipid content, cell viability and oxidative stress in 3T3-L1 adipocytes. *Toxicol. Reports* **5**, 1014–1020 (2018).

67. Nikolaou, N., Green, C. J., Gunn, P. J., Hodson, L. & Tomlinson, J. W. Optimizing human hepatocyte models for metabolic phenotype and function: Effects of treatment with dimethyl sulfoxide (DMSO). *Physiol. Rep.* **4**, 1–11 (2016).

68. Song, Y. M. *et al.* Dimethyl sulfoxide reduces hepatocellular lipid accumulation through autophagy induction. *Autophagy* **8**, 1085–1097 (2012).

69. Köfeler, H. C., Fauland, A., Rechberger, G. N. & Trötzmüller, M. Mass spectrometry based lipidomics: An overview of technological platforms. *Metabolites* **2**, 19–38 (2012).

70. Jump, D. B. *et al.* Fatty acid regulation of hepatic gene transcription. *J. Nutr.* **135**, 2503–2506 (2005).

71. Ide, T. *et al.* Cross-talk between peroxisome proliferator-activated receptor (PPAR) α and liver X receptor (LXR) in nutritional regulation of fatty acid metabolism. II. LXRs suppress lipid degradation gene promoters through inhibition of PPAR signaling. *Mol. Endocrinol.* **17**, 1255–1267 (2003).

72. Batista, I. de A. A. & Helguero, L. Contribution of SETD7 methyltransferase to cell proliferation and differentiation. (Universidade de Aveiro, 2016).

73. Rijnkels, M. *et al.* The epigenetic landscape of mammary gland development and functional differentiation. *J. Mammary Gland Biol. Neoplasia* **15**, 85–100 (2010).

74. Fuchs, B., Süß, R., Teuber, K., Eibisch, M. & Schiller, J. Lipid analysis by thin-layer chromatography-A review of the current state. *J. Chromatogr. A* **1218**, 2754–2774 (2011).

75. Vaden, D. L., Gohil, V. M., Gu, Z. & Greenberg, M. L. Separation of yeast phospholipids using one-dimensional thin-layer chromatography. *Anal. Biochem.* **338**, 162–164 (2005).

76. Tafesse, F. G., Ternes, P. & Holthuis, J. C. M. The multigenic sphingomyelin synthase family. *J. Biol. Chem.* **281**, 29421–29425 (2006).

77. Houtkooper, R. H. & Vaz, F. M. Cardiolipin, the heart of mitochondrial metabolism. *Cell. Mol. Life Sci.* **65**, 2493–2506 (2008).

78. Vance, J. E. Phosphatidylserine and phosphatidylethanolamine in mammalian cells : two metabolically related aminophospholipids. *J. Lipid Res.* **49**, 1377–1387 (2008).

79. Bhardwaj, A., Bhardwaj, R., Dhawan, D. K. & Kaur, T. Exploring the Effect of Endoplasmic Reticulum Stress Inhibition by 4-Phenylbutyric Acid on AMPA-Induced Hippocampal Excitotoxicity in Rat Brain. *Neurotox. Res.* **35**, 83–91 (2019).

80. Zheng, K. *et al.* Sphingomyelin synthase 2 promotes an aggressive breast cancer phenotype by disrupting the homoeostasis of ceramide and sphingomyelin. *Cell Death Dis.* **10**, (2019).

Supplementary Figures

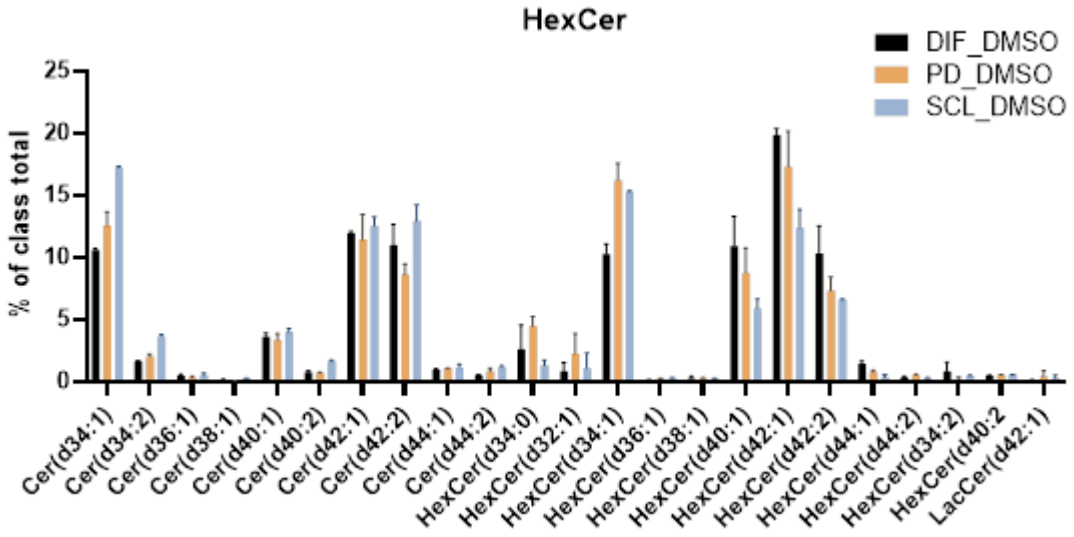

Supplementary Figure 1. Cer profile of HC11 cells treated with DMSO for 24h.

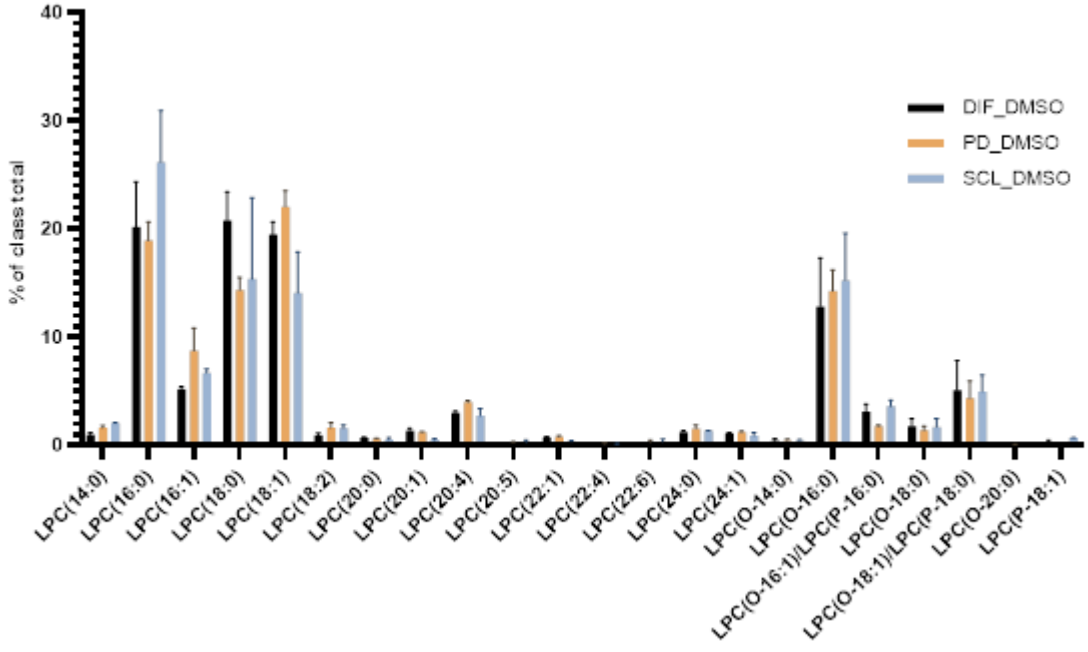

Supplementary Figure 2. LPC profile of HC11 cells treated with DMSO for 24h.

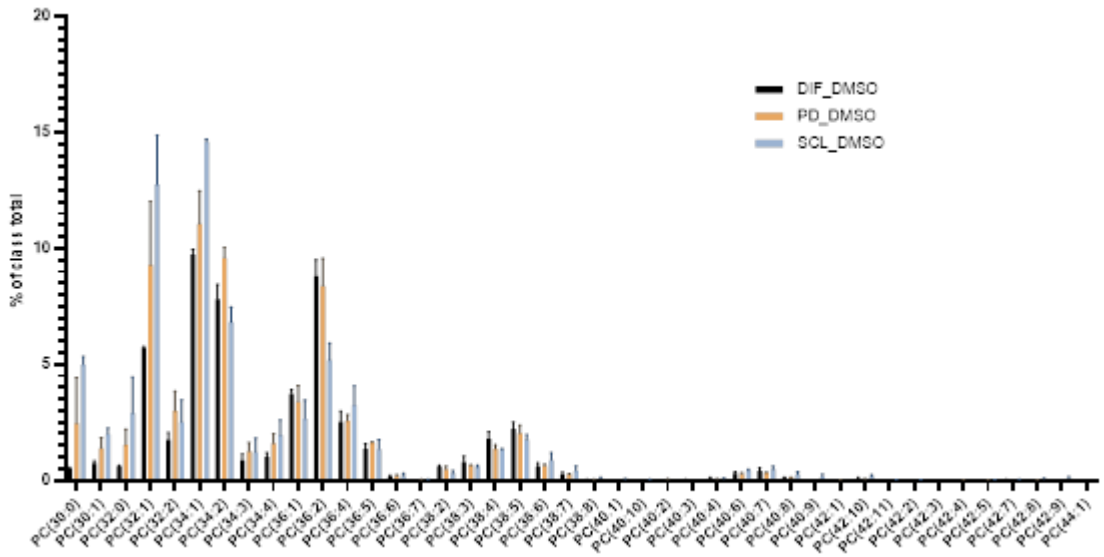

Supplementary Figure 3. PC profile of HC11 cells treated with DMSO for 24h (part 1).

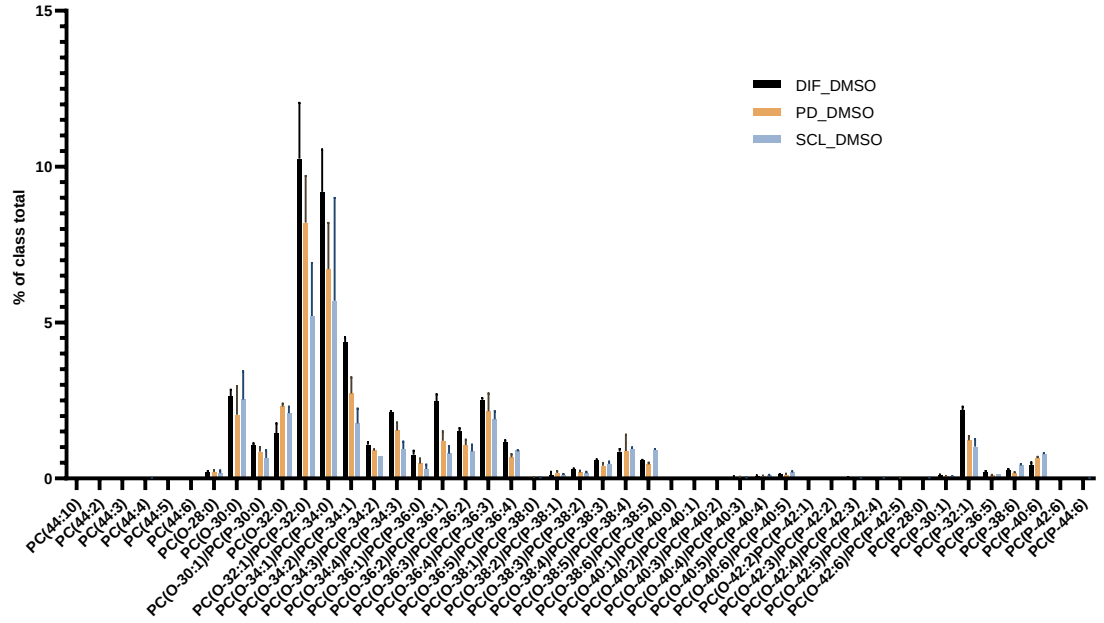

Supplementary Figure 4. PC profile of HC11 cells treated with DMSO for 24h (part 2).

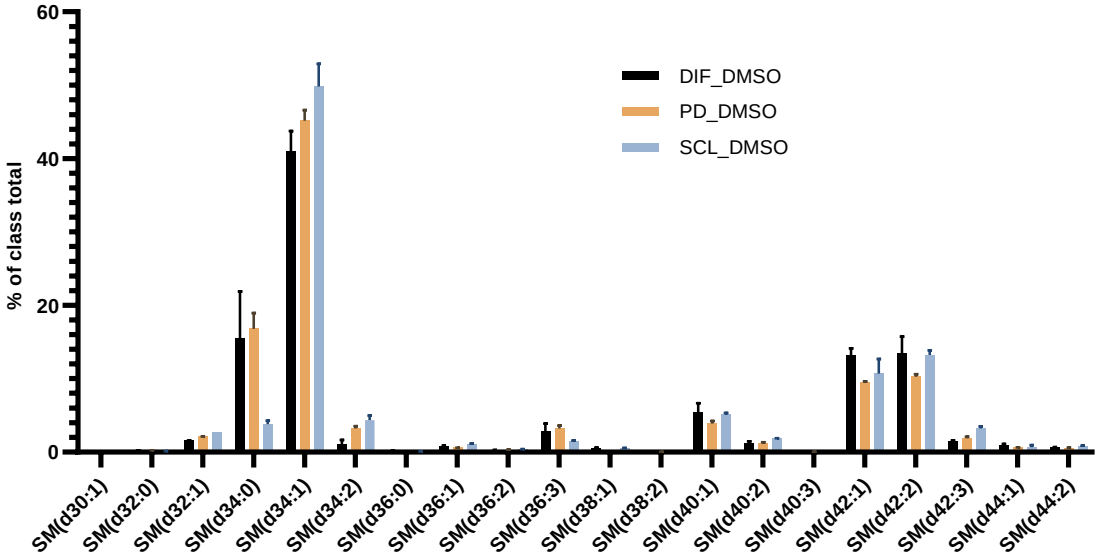

Supplementary Figure 5. SM profile of HC11 cells treated with DMSO for 24h.

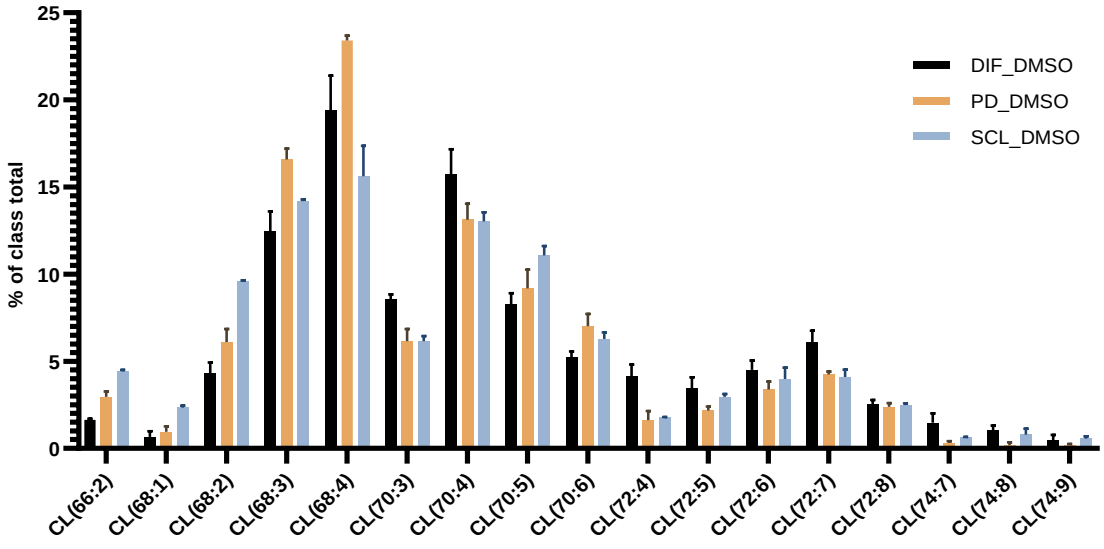

Supplementary Figure 6. CL profile of HC11 cells treated with DMSO for 24h.

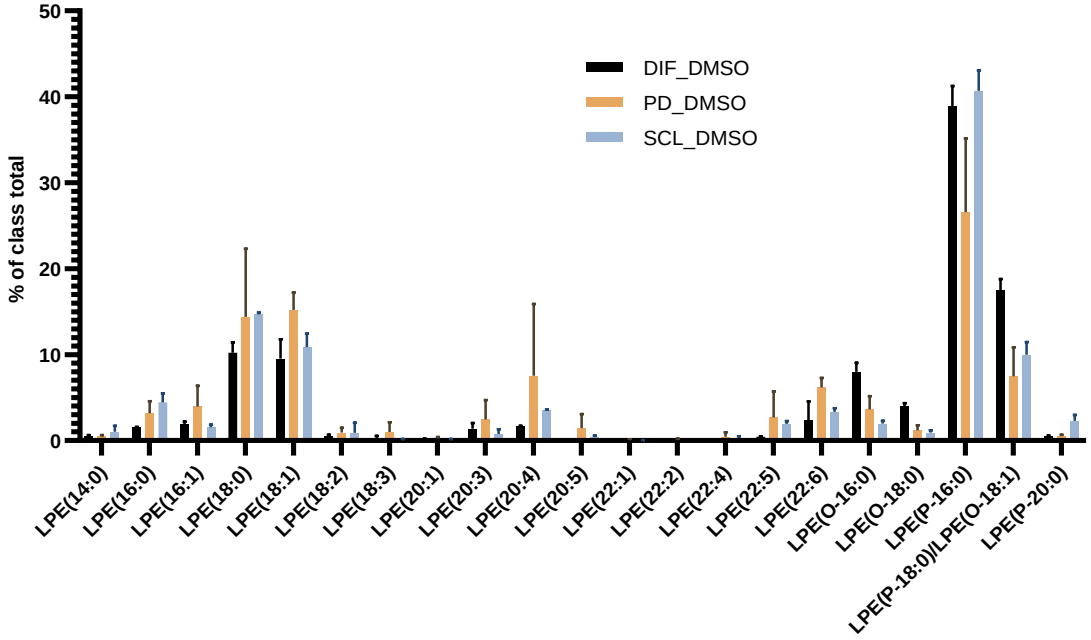

Supplementary Figure 7. LPE profile of HC11 cells treated with DMSO for 24h.

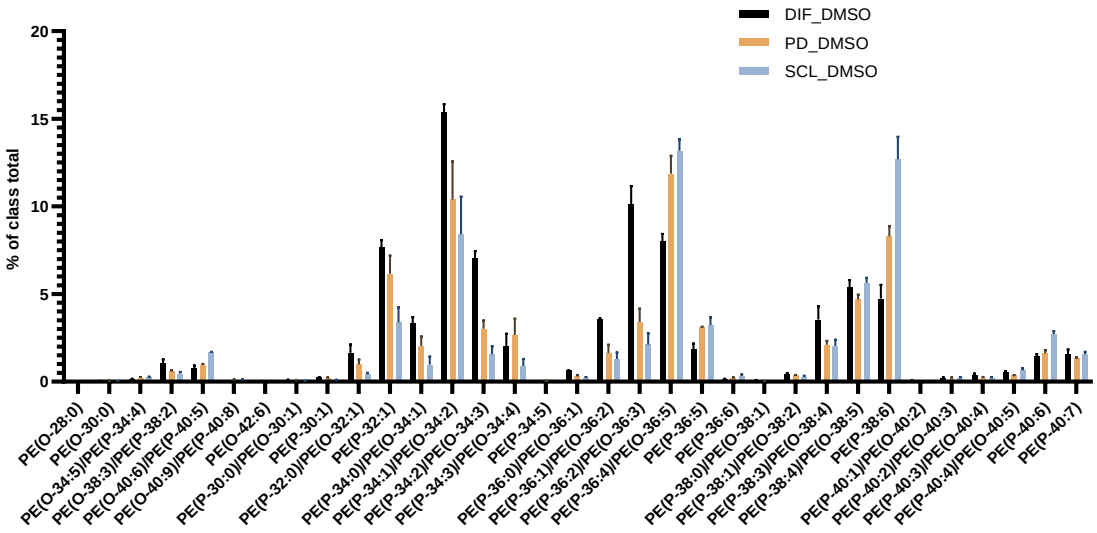

Supplementary Figure 8. PE profile of HC11 cells treated with DMSO for 24h.

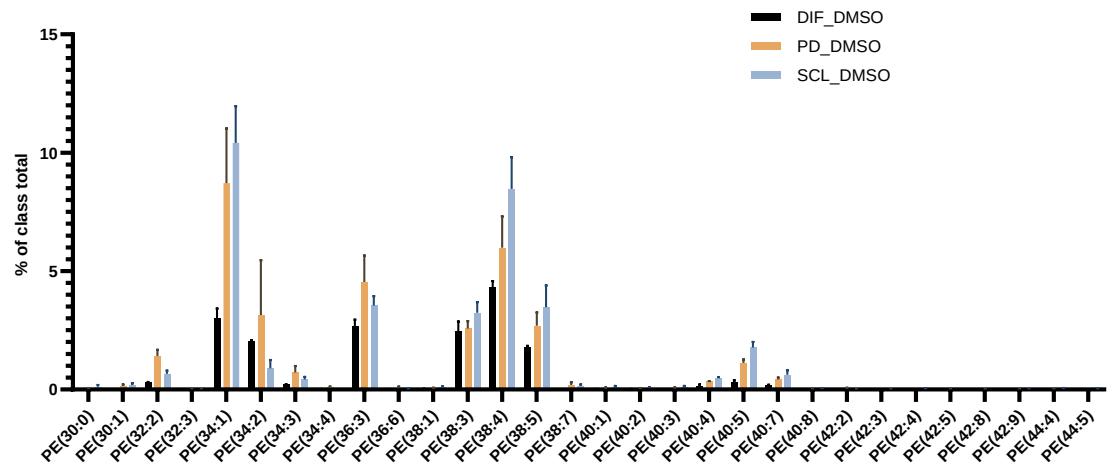

Supplementary Figure 9. PE profile of HC11 cells treated with DMSO for 24h.

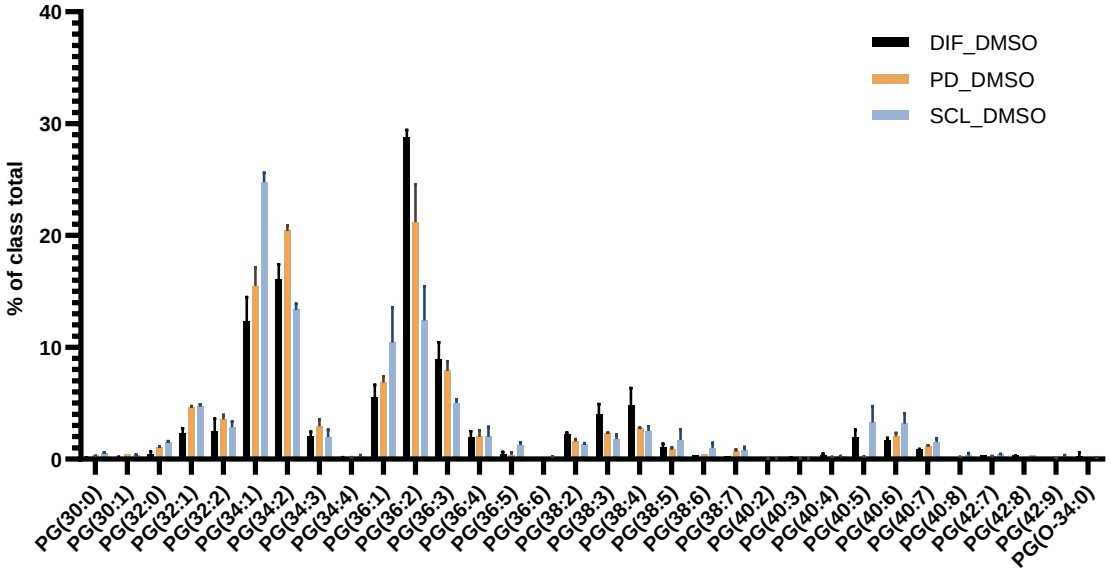

Supplementary Figure 10. PG profile of HC11 cells treated with DMSO for 24h.

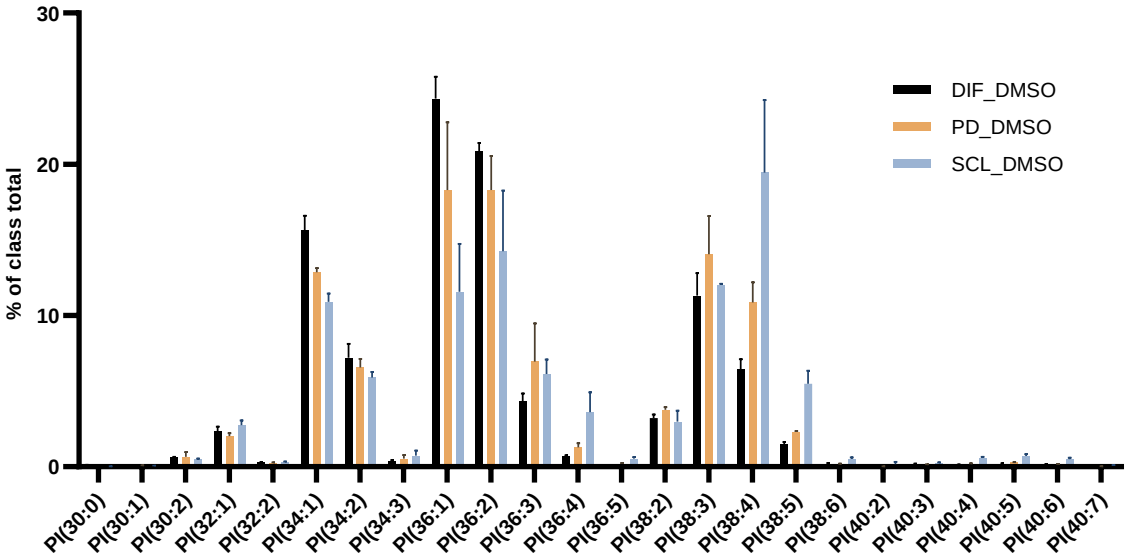

Supplementary Figure 11. PI profile of HC11 cells treated with DMSO for 24h.

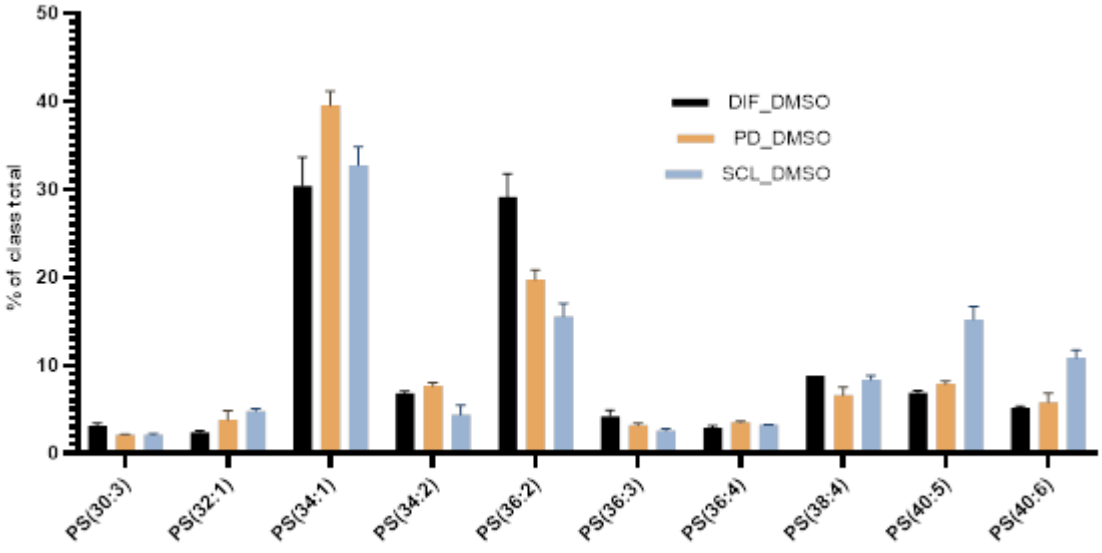

Supplementary Figure 12. PS profile of HC11 cells treated with DMSO for 24h.

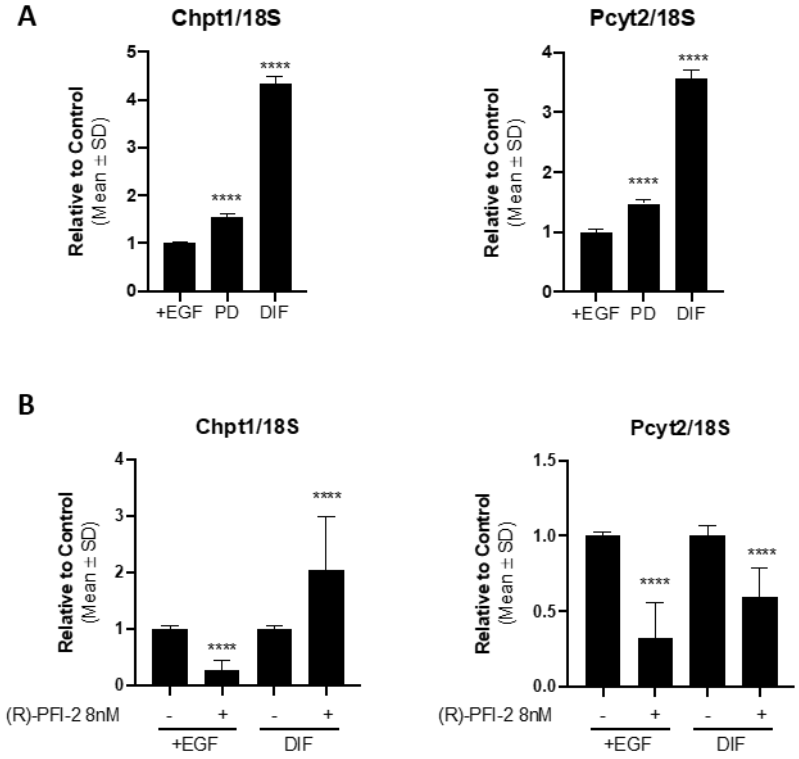

Supplementary Figure 13. A) Expression of Chpt1 and Pcyt2 throughout differentiation in HC11 cells; B) Effect of treatment with R-PFI-2 8nM on the expression of Chpt1 and Pcyt2. One-way ANOVA, relative to +EGF (SLC): ****<0.0001

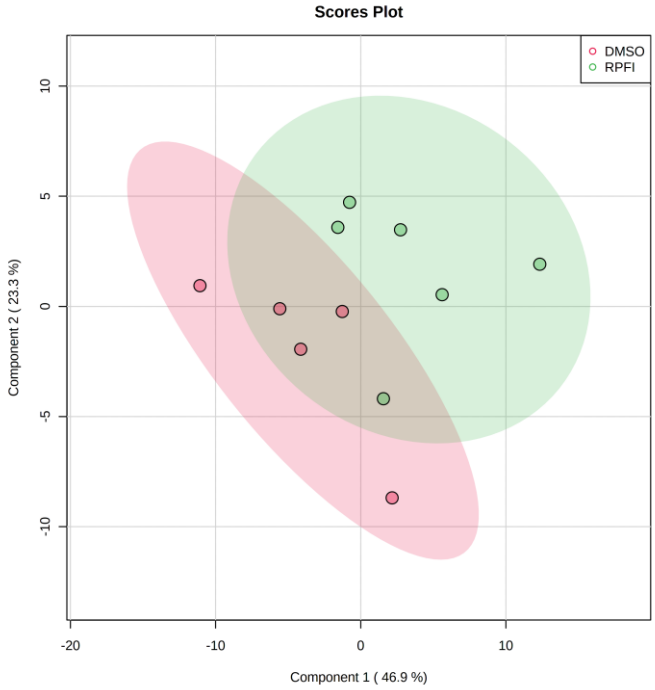

Supplementary Figure 14. Multivariate analysis of PL classes profile assigned by TLC data collected for HC11 cells. PLS DA scores scatter plot, comparing cells treated with SETD7 specific inhibitor (R)-PFI-2 (green) and DMSO-treated controls (red).

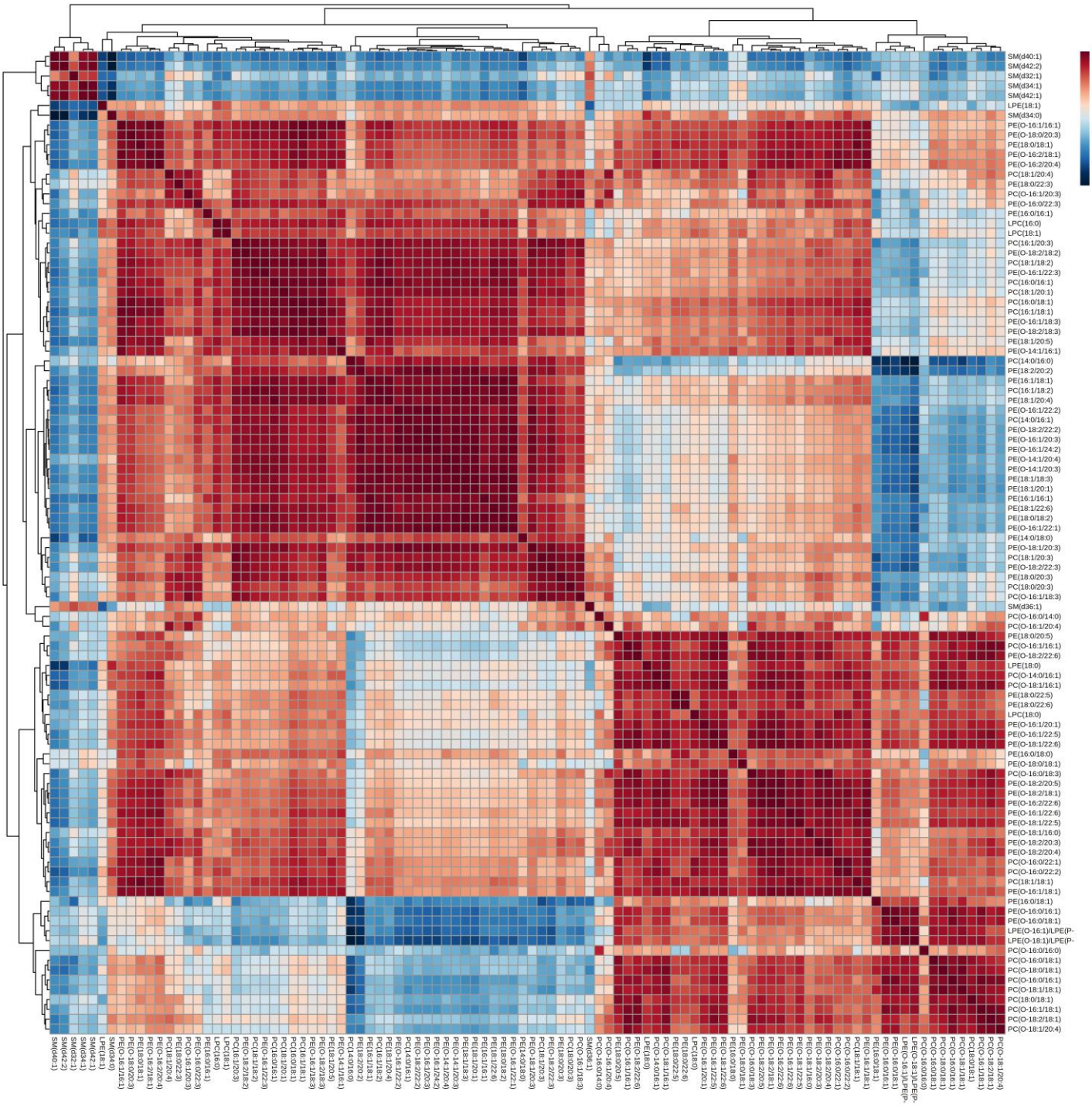

Supplementary Figure 15. Correlation table of molecular species identified by C18-MS.

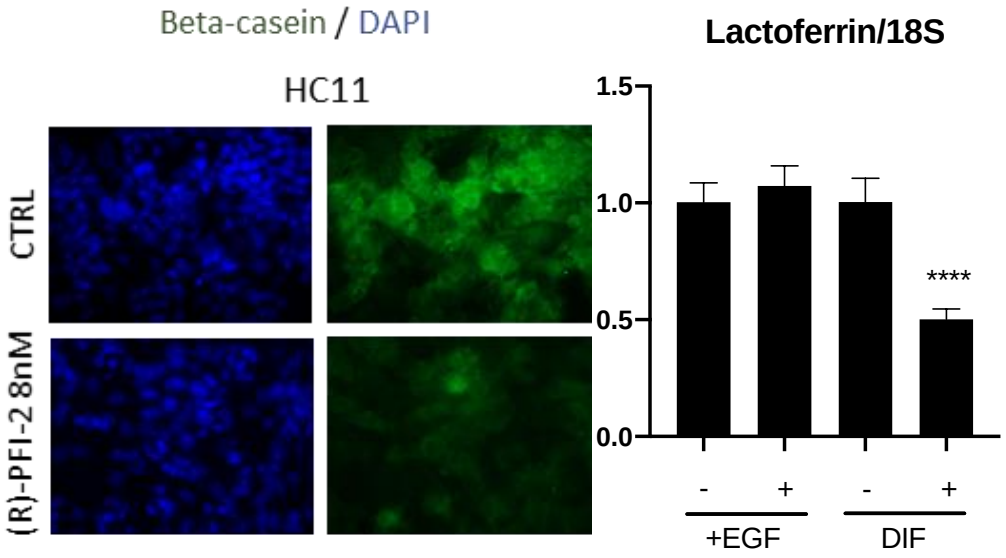

Supplementary Figure 16. SETD7 inhibition with (R)-PFI-2 leads to the decrease in Beta-casein protein levels and lactoferrin expression in differentiated HC11 cells.